

Nonlinear Robustness Analysis Tools for Flight Control Law  
Validation & Verification

A DISSERTATION  
SUBMITTED TO THE FACULTY OF THE GRADUATE SCHOOL  
OF THE UNIVERSITY OF MINNESOTA  
BY

Abhijit Chakraborty

IN PARTIAL FULFILLMENT OF THE REQUIREMENTS  
FOR THE DEGREE OF  
DOCTOR OF PHILOSOPHY

Gary J. Balas, Adviser  
Peter Seiler, Adviser

September 2012

© Abhijit Chakraborty  
September 2012

# Acknowledgements

“In every conceivable manner, the family is link to our past, bridge to our future.”

I want to thank my advisors Professor Gary Balas and Professor Peter Seiler for their guidance and support throughout my graduate career. I am blessed to have the opportunity to work with them. They have acted as the “adaptive controller” of my research. Their guidance has been the perfect “feedback measurement” to my research. I can’t stress enough how important their contribution is. I also thank Professor Yiyuan Zhao, Professor Murli Salapaka and Professor William Garrard for serving on my examination committee and providing me with valuable feedback. I am also grateful to Dr. Ufuk Topcu at Caltech and Prof. Andrew Packard at University of California at Berkley for useful discussions on numerous aspects of my research. I would also like to thank Dr. Demoz Gebre-Egziabher for useful discussion.

I would like to provide a very special thanks to all my lab mates and colleagues: Paw, Rohit, Arnar, Andrei, Paul, Arda, Hamid, David, Claudia and Austin. They have been the source of my productivity. Their advice has been very helpful. I will definitely miss our Friday group lunch!!! I want to thank my coffee partner Arnar. I will never forget my badminton partners Paw and Rohit. I also to express my gratitude to the young and cool folks of the lab: Andrei, Arda, Paul, David and Claudia. Their presence has been the source of my inspiration to graduate on time. I want to specially thank my friend Aman with whom I have shared countless hours of random ‘non-technical’ discussion.

Finally, I would like to acknowledge my gratitude to the technical monitor Dr. Christine Belcastro and NASA Langley for supporting our work. I would also like to thank you University of Minnesota for providing me with the Doctoral Dissertation Fellowship to continue and finish my research.

**Dedicated**

*To My Parents*

*&*

*To My Family*

# Abstract

Loss of control in flight is among the highest aviation accident categories for both the number of accidents and the number of fatalities. The flight controls community is seeking an improved validation tools for safety critical flight control systems. Current validation tools rely heavily on linear analysis, which ignore the inherent nonlinear nature of the aircraft dynamics and flight control system. Specifically, current practices in validating the flight control system involve gridding the flight envelope and checking various criteria based on linear analysis to ensure safety of the flight control system. The analysis and certification methods currently applied assume the aircrafts' dynamics is linear. In reality, the behavior of the aircraft is always nonlinear due to its aerodynamic characteristics and physical limitations imposed by the actuators. This thesis develops nonlinear analysis tools capable of certifying flight control laws for nonlinear aircraft dynamics. The proposed analysis tools can handle both the aerodynamic nonlinearities and the physical limitations imposed by the actuators in the aircrafts' dynamics. This proposed validation technique will extend and enrich the predictive capability of existing flight control law validation methods to analyze nonlinearities. The objective of this thesis is to provide the flight control community with an advanced set of analysis tools to reduce aviation fatalities and accidents rate.

# Contents

<b>List of Tables</b>	<b>viii</b>
<b>List of Figures</b>	<b>ix</b>
<b>Chapter 1 Introduction</b>	<b>1</b>
1.1 Motivation . . . . .	1
1.2 Thesis Contributions . . . . .	3
<b>Chapter 2 Preliminaries and Notations</b>	<b>7</b>
2.1 Notations . . . . .	7
2.2 Stability and Performance of Nonlinear Systems . . . . .	8
2.2.1 Region-of-Attraction . . . . .	8
2.2.2 Dissipation Inequality . . . . .	10
2.3 Sum of Squares (SOS) Optimization . . . . .	12
2.3.1 Connections Between SOS Polynomials and Semidefinite Matrices	12
2.3.2 Connection Between SOS Polynomials and ROA/Dissipation Inequality . . . . .	14
2.3.3 Software for SOS Optimizations . . . . .	15
2.4 Generalized S-Procedure . . . . .	16
2.5 Summary . . . . .	17

<b>Chapter 3</b>	<b>Polynomial Modeling of Aircraft Dynamics</b>	<b>18</b>
3.1	Motivation . . . . .	18
3.2	Polynomial Model Formulation of Generic Transport Model (GTM) Aircraft . . . . .	19
3.2.1	Longitudinal Dynamics of GTM . . . . .	19
3.2.2	Approach to Polynomial Model Formulation . . . . .	21
3.3	Polynomial Model Validation . . . . .	24
3.3.1	Comparisons of Trim Conditions & Simulation Responses . . . . .	25
3.4	Summary . . . . .	26
<b>Chapter 4</b>	<b>Local Stability and Performance Analysis of Polynomial Systems</b>	<b>28</b>
4.1	Technical Approach to the Region-of-Attraction (ROA) Estimation . . . . .	29
4.1.1	Upper Bound Computation . . . . .	30
4.1.2	Lower Bound Computation . . . . .	31
4.1.3	ROA Analysis of 4-State Longitudinal GTM Model . . . . .	37
4.2	Induced $L_2$ ( $L_2 \rightarrow L_2$ ) Gain Estimation . . . . .	42
4.2.1	Induced $L_2$ Gain Analysis of 4-State Longitudinal GTM Model . . . . .	45
4.3	Summary . . . . .	47
<b>Chapter 5</b>	<b>Local Performance Analysis of Polynomial Systems with Actuator Saturation</b>	<b>48</b>
5.1	Problem Formulation . . . . .	49
5.2	Induced $L_2$ Gain Analysis . . . . .	50
5.2.1	Review of IQCs . . . . .	50

5.2.1.1	IQC Modeling of Saturation . . . . .	52
5.2.2	Local Dissipation Inequality Formulation . . . . .	54
5.2.3	$L_2 \rightarrow L_2$ Gain Computation . . . . .	57
5.2.4	Guaranteed SOS Feasibility . . . . .	58
5.3	Applications . . . . .	60
5.3.1	Amplitude Saturation . . . . .	60
5.3.2	GTM Short Period Control with Rate Saturation . . . . .	61
5.4	Connection Between Dissipation Inequality to Lyapunov Function . . . . .	65
5.4.1	Equivalence to Circle Criterion . . . . .	66
5.4.2	Application . . . . .	68
5.5	Summary . . . . .	69
 <b>Chapter 6 Local Stability Analysis of Polynomial Systems with Actuator Saturation</b>		<b>71</b>
6.1	Problem Formulation . . . . .	71
6.2	Polytopic Set Invariance Conditions . . . . .	73
6.3	Estimation of Region of Attraction . . . . .	75
6.3.1	SOS Iteration Algorithm . . . . .	77
6.4	Application: F/A-18 Longitudinal Flight Control System with Saturation	79
6.4.1	Analysis of Short Period Model . . . . .	80
6.4.2	ROA Analysis of 4-State Longitudinal F/A-18 Model . . . . .	82
6.5	Summary . . . . .	83
 <b>Chapter 7 Peak Gain Analysis</b>		<b>84</b>
7.1	$L_\infty$ Gain Function Estimation . . . . .	85

7.2	Application . . . . .	90
7.3	Summary . . . . .	92
<b>Chapter 8 Conclusion</b>		<b>93</b>
8.1	Contributions . . . . .	93
8.2	Future Research . . . . .	94
<b>Bibliography</b>		<b>96</b>
<b>Appendix A Polynomial Longitudinal GTM Model</b>		<b>102</b>
A.1	Physical Parameters of GTM . . . . .	102
A.2	Longitudinal Aerodynamic Model . . . . .	102
A.2.1	Lift Coefficient, $C_L$ . . . . .	103
A.2.2	Drag Coefficient, $C_D$ . . . . .	103
A.2.3	Pitching Moment Coefficient, $C_m$ . . . . .	104
A.3	Engine Model . . . . .	104
A.4	Polynomial Longitudinal Model Formulation . . . . .	105
<b>Appendix B Polynomial Longitudinal F/A-18 Model</b>		<b>106</b>
B.1	Physical Parameters of the F/A-18 . . . . .	106
B.2	Longitudinal Aerodynamic Model . . . . .	106
B.2.1	Lift Coefficient, $C_L$ . . . . .	107
B.2.2	Drag Coefficient, $C_D$ . . . . .	107
B.2.3	Pitching Moment Coefficient, $C_m$ . . . . .	107
B.3	Polynomial Longitudinal Model Formulation . . . . .	108

# List of Tables

3.1	Aircraft and Environment Parameters . . . . .	19
A.1	Aircraft and Environment Parameters . . . . .	102
B.1	Aircraft and Environment Parameters . . . . .	106

# List of Figures

1.1	Statistical Summary of Fatal Accidents: Worldwide Commercial Jet Fleet (2001 - 2009) . . . . .	2
2.1	Demonstration of $\nabla V(x)f(x) < 0$ on the Lyapunov sublevel set $\Omega(V, 5)$ . . . . . .	10
3.1	GTM Aircraft developed by NASA . . . . .	21
3.2	Look-up table data and polynomial fit for $C_{L,\alpha}$ , $C_{m,\alpha}$ , $C_{D,\alpha}$ . . . . .	24
3.3	Trim states and inputs vs. trim speed for both polynomial and original nonlinear model. . . . .	26
3.4	Simulation Comparison . . . . .	27
4.1	Upper Bound Estimate of ROA. Red (dashed) curves indicate unstable trajectories and blue (solid) curve indicate stable trajectories. . . . .	31
4.2	Lower Bound Estimate of ROA. The maroon ellipse $p(x) \leq \beta$ indicates the lower bound estimate of the invariant set $V(x) \leq \gamma$ . . . . .	33
4.3	Lower and Upper Bound Estimate of ROA for the GTM longitudinal model at $V = 150$ ft/s; the rectangular region defines the validity region of the model . . . . .	39
4.4	Lower and Upper Bound Estimate of ROA for the GTM longitudinal model at $V = 100$ ft/s; the rectangular region defines the validity region of the model . . . . .	41

4.5	Estimation of induced $L_2 - L_2$ gain bounds from $d_{elev}$ to $q$ for open-loop and closed-loop GTM model. The open-loop and the closed-loop system is found to be divergent with an input size of 0.08 and 0.11, respectively. . . . .	46
5.1	Feedback Interconnection of $G - sat(\cdot)$ . . . . .	49
5.2	Uncertainties or nonlinearities represented by $\Delta$ . . . . .	50
5.3	Time Domain Interpretation of IQCs . . . . .	51
5.4	Time Domain Interpretation of IQCs . . . . .	52
5.5	$\alpha$ and $\beta$ are the slopes of the straight lines. The nonlinearity (green curve) lies within these slopes and is known as sector bounded or slope-restricted nonlinearities. . . . .	53
5.6	Analysis Interconnection Structure . . . . .	54
5.7	$L_2$ gain bounds with quadratic storage function for different size of inputs and different values of $\alpha$ . . . . .	61
5.8	Feedback interconnection of GTM short period dynamics . . . . .	62
5.9	Feedback encapsulation of rate limit . . . . .	63
5.10	Estimation of induced $L_2 - L_2$ gain bounds for GTM short period under rate limit . . . . .	64
5.11	Feedback Interconnection of $G - sat(\cdot)$ . . . . .	65
5.12	Saturation nonlinearity is transformed from $[\alpha, \beta]$ sector to $[0, \infty]$ sector. . . . .	67
5.13	Region of attraction obtained by the Lyapunov function from Theorem 5.3. . . . .	70
6.1	Feedback Interconnection of $G - sat(\cdot)$ . . . . .	72
6.2	Feedback Interconnection of the F/A-18 Longitudinal Direction . . . . .	79

6.3	Phase plane simulation for polynomial short period model with lower bound estimation of ROA; Stable trajectories are denoted by solid and dashed denotes the unstable trajectories . . . . .	81
6.4	Lower and Upper Bound Estimate of ROA for the F/A-18 4-state longitudinal model with actuator saturation . . . . .	83
7.1	Estimation of peak gain function of the 4-state longitudinal GTM dynamics. . . . .	91

# Chapter 1

## Introduction

### 1.1 Motivation

Safety-critical aerospace systems require extensive validation to ensure safety prior to entry into service. NASA's Aviation Safety Program (AvSP) aims to reduce the fatality rate for commercial aircraft (e.g., large transports, general aviation, and rotorcraft) by 90% by 2022 [21]. A key challenge to achieving this goal is certifying safety and performance of the flight control systems. Loss of control during flight is among the highest accident categories across all vehicle classes for both the number of accidents and the number of fatalities [21]. Figure 1.1<sup>1</sup> shows loss-of-control (LOC) in flight is responsible for 35% of fatalities and 22% of accidents in the commercial fleet from 2001 through 2009. Hence, it is crucial to validate proper functionality of the flight control system throughout the flight envelope for both nominal and unusual conditions (e.g., inclement weather, physical damages in aircraft).

Current flight control system validation practices involve gridding the flight envelope and checking stability/performance criteria based on linear analysis to ensure the safety of the flight control system. Standard analysis and certification methods assume linear aircraft dynamics, yet the true behavior of the aircraft is nonlinear. To provide some confidence that the flight control system will perform properly in the presence of nonlinearities, exhaustive nonlinear Monte Carlo simulations and extensive flight tests are performed [21]. These two techniques, due to their random nature, offer no guarantees regarding the worst-case behavior of the flight control system. Additionally, software-in-the-loop and hardware-in-the-loop tests are also

---

<sup>1</sup>Taken from page 23 of <http://www.boeing.com/news/techissues/pdf/statsum.pdf>

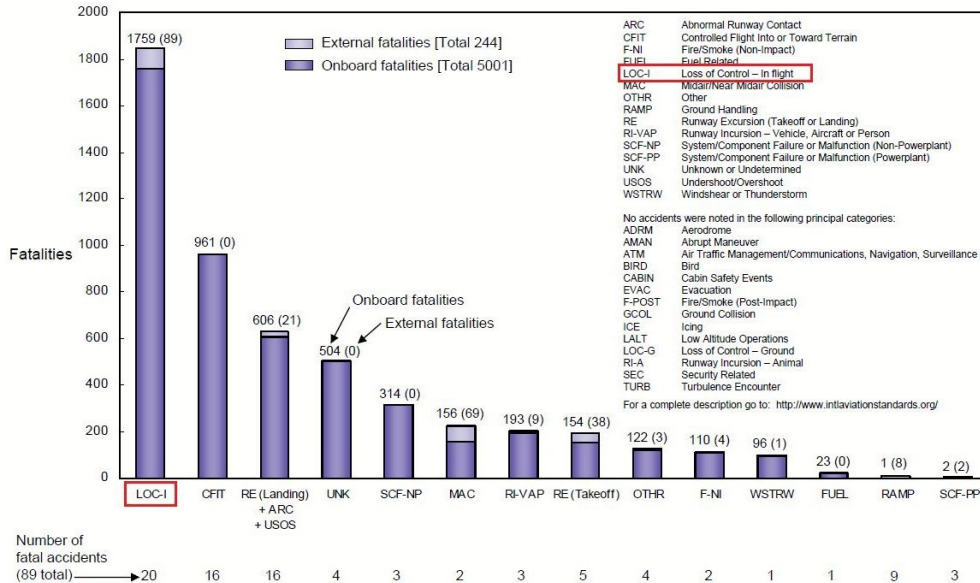


Figure 1.1: Statistical Summary of Fatal Accidents: Worldwide Commercial Jet Fleet (2001 - 2009)

performed to validate the flight control system. This validation process is extensive and has been successful in the past. It is, however, becoming increasingly challenging to validate due to the advent of complex nonlinear flight control algorithm in aircraft.

Two phenomena are primarily responsible for aircraft nonlinearities: (i) aerodynamic nonlinearities for operating in high angle-of-attack, and (ii) rate and/or magnitude saturation of flight control surfaces. Aerodynamic nonlinearities are inherent properties of the aircraft dynamics. The aerodynamics exhibit *strong* nonlinearities, especially when the aircraft is forced to operate at the boundary of or outside of the flight envelope due to inclement weather, physical damages or high angle maneuvers. The falling leaf mode in the F/A-18 aircraft is one such example. Several F/A-18 aircraft were lost due to the nonlinear loss-of-control departure phenomenon known as the falling leaf mode [19, 20, 25, 34]. The F/A-18 baseline flight control law underwent an extensive validation and verification process without detecting a susceptibility to the falling leaf motion. The failure to detect the falling leaf motion is not due to the lack of an accurate aerodynamic model. In fact, the nonlinear simulation model of the F/A-18 used in [6] is able to reproduce the falling leaf mode. Thus, the failure to detect this susceptibility should be attributed to the lack of appropriate analysis tools. The falling leaf motion is due to nonlinearities in the aircraft dynamics and cannot be replicated with linear models.

Rate and magnitude saturation in the control surfaces are other sources of nonlinearities in the flight control systems. Saturation nonlinearities come from the physical limitations imposed by the control surface actuators and makes the flight certification process challenging. Current practices in flight control law certification process typically involve analyzing the effect of rate/magnitude saturation assuming linear model of the flight control system. Unfortunately, the linearity assumption of the flight system is a restrictive modeling assumption. When the actuators are saturated, the aircraft is operating in the nonlinear regime and hence, in all likelihood, the linearity assumption is not valid. Two motivational examples are the crash of a Grippen at an air show [5] and the YF-22 crash landing [11]. Pilots of these two fighter aircraft lost control due to actuator saturation.

There is a need for improved validation tools to extend the existing flight control law verification and validation (V&V) methods. Nonlinear analysis methods capable of analyzing nonlinear aircraft behaviors can certainly enhance and complement the traditional V&V techniques. Unlike the traditional tools, which are only valid at the boundary of the operational limits, nonlinear techniques can guarantee that the worst-case behavior of the nonlinear flight control systems will be detected.

## 1.2 Thesis Contributions

Certification requirements for safety-critical aircraft come from the Federal Aviation Regulations (FARs) [21]. Demonstration of compliance to the requirements is nontrivial and involve analytical, simulation-based, and experimental methods. This thesis focuses primarily on analytical-based certification procedures.

Analytical certification methods typically rely on quantifying stability and performance metrics of the flight control systems. Two important, commonly used metrics for evaluating stability and performance of flight control systems are (i) size of the region-of-attraction (ROA), and (ii) induced input-output gain. Computational tools for estimating these metrics for linear systems, even under rate/magnitude saturation, are well-developed. Recently, significant research [48, 50, 55, 56] has been performed on the development of nonlinear analysis tools for computing robustness metrics such as ROA and input-output gains for nonlinear polynomial systems. These metrics are local properties of polynomial systems. In other words, ROA of a polynomial system is not guaranteed to be the whole state-space. These metrics are characterized in [48, 50, 55, 56] via conditions based on the Lyapunov/Storage function concept. The

conditions are then translated into optimization problems and solved via a polynomial sum-of-squares (SOS) optimization [38] framework.

Unfortunately, the SOS optimization framework has two major disadvantages

1. The computational requirements for sum-of-squares (SOS) optimizations grow rapidly with the number of variables and polynomial degree.
2. The polynomial SOS techniques can only be applied to the dynamics describable by a smooth polynomial vector field. Hence, dynamics describing hard nonlinearities like actuator saturation and/or rate limits can not be analyzed using SOS techniques.

The major contribution of this thesis is to address these disadvantages and thus enable the application of the SOS framework to flight control V&V.

One of the main contributions of this thesis is to demonstrate the application of SOS techniques to more realistic flight control problems of moderate complexity (4/5 states, up to degree 5 polynomial). In our previous work [6], we have successfully estimated ROA for a 7-state, cubic degree flight control problem using SOS techniques. Additionally, SOS techniques often suffer from dimensional scaling issues depending on the problem. This is particularly true for flight control problems mainly due to the presence of (i) both fast and slow modes in the dynamics, and (ii) nonhomogeneous units description of the states (e.g, velocity is in ft/s and pitch rate is in rad/s). This thesis provides insights on achieving numerical stability for solving large scale SOS optimization problem. The presentation of the thesis emphasizes the details that allow one to develop algorithms focusing on its practical implementation rather than on the theoretical aspects of SOS algorithm.

In addition to suffering from the numerical issues, the polynomial SOS techniques can only be applied to the dynamics describable by a smooth polynomial vector field. Hence, SOS techniques are not suitable for analyzing systems with rate/magnitude saturation. One of the main goals of this thesis is to analyze polynomial systems with saturation. Two approaches are proposed to model saturation. These approaches are such that the polynomial SOS optimization framework is retained as the computational tool. The first approach relies on a robustness analysis framework, known as integral quadratic constraints (IQCs). IQCs are capable of handling non-smooth nonlinearities, e.g. actuator saturation by treating the nonlinearities as a perturbation

to the linear dynamical system. SOS and IQC frameworks are utilized to formulate a dissipation inequality for analyzing induced  $L_2$  gain of the polynomial systems in feedback with saturation. The second approach models the saturation function as a convex combination of piecewise linear functions [12, 23, 24]. The results presented in [12, 23, 24] are extended in this thesis for saturated polynomial systems. SOS techniques are then applied for estimating region-of-attraction of such systems.

The content and the contributions of each chapter are outlined below.

**Chapter 2** provides a brief review of necessary background materials for developing subsequent chapters. This chapter presents introductory discussion on the following topics: (i) ROA and induced gain, (ii) SOS optimization, (iii) IQC framework, and (iv) S-procedure. The analysis framework in this thesis relies on making connections among these topics. This chapter presents a high-level discussion on these connections.

**Chapter 3** proposes a systematic approach to approximate nonlinear aircraft dynamics with polynomial vector fields. The longitudinal dynamics of NASA's Generic Transport Model (GTM) are used to demonstrate the approach. The approximated GTM polynomial model is analyzed extensively using SOS based techniques. Since the SOS based techniques are applicable only to polynomial systems, the polynomial approximation is an essential step of the analysis procedures. More importantly, a *sufficiently* accurate polynomial approximation is desirable. Several *ad-hoc* methods to validate the accuracy of the GTM polynomial approximations are also proposed.

In **Chapter 4**, the SOS based approaches for estimating the ROA and the local induced  $L_2$  gain of polynomial dynamics are presented. Unfortunately, the SOS optimization problems for moderately sized ( $\geq 4$ -5 states, more than cubic degree polynomial) problem is computationally challenging and often suffer from numerical scalability issues. Thus far the SOS techniques have not been applied to moderately sized, real engineering systems like flight control systems. The main contribution of this chapter is in successfully applying the proposed SOS approaches to estimate the ROA and the induced gain for a moderately sized (4-5 states), degree 5 polynomial GTM flight control example.

**Chapter 5** considers the local induced  $L_2$  gain analysis problem for polynomial systems in feedback with saturation. This chapter presents a dissipation inequality condition for estimating the induced  $L_2$  gain upper bound. The main contribution of this

chapter is in formulating the dissipation inequality that incorporates IQC framework to model the saturation. For polynomial systems, the dissipation inequality is verified using SOS optimizations. The effectiveness of the proposed method is demonstrated on two numerical examples, including the short period dynamics of the GTM model with rate limits.

**Chapter 6** presents an ROA estimation technique for polynomial systems with saturation. The saturation function is modeled as a convex combination of piecewise linear functions, as proposed in [13]. It has been shown that the set invariance conditions presented in [13] are readily extended for polynomial systems. An SOS based algorithm is proposed to estimate the region of attraction. Finally, the proposed method is verified on a simple 2-state polynomial system.

In **Chapter 7**, we analyze the performance of nonlinear systems in terms of  $L_\infty$  norm. In particular, the chapter computes the  $L_\infty$  gain function as a performance metric of the nonlinear systems. The technique relies on computing the reachable set for peak input gain and then maximizing the output direction in the estimated reachable set. The technique is then applied on the 4-state longitudinal GTM dynamics.

# Chapter 2

## Preliminaries and Notations

The thesis aims at developing computational tools for estimating local stability and performance properties of nonlinear flight control systems. The nonlinearities primarily arise from (i) aircraft dynamics: nonlinear equations of motion and aerodynamic characteristics, and (ii) hard nonlinearities like actuator saturation and/or rate limit. The thesis considers a polynomial description of the nonlinearities due to the aircraft dynamics. Stability and performance are characterized, respectively, by region-of-attraction (ROA) and induced input-output (I/O) gain of the systems. Appropriate set invariance conditions, based on Lyapunov/dissipation theory, are formulated to estimate the ROA and the induced I/O gain of the system. Finally, the invariance conditions are solved using freely available Sum-of-squares (SOS) optimization toolbox. This chapter presents a brief review of background materials needed to implement the above steps.

### 2.1 Notations

The set of real numbers, complex numbers and non-negative integers are denoted by  $\mathbb{R}$ ,  $\mathbb{C}$  and  $\mathbb{N}$ , respectively.  $\mathbb{R}^n$  denotes the set of all  $n \times 1$  column vectors with real number and  $\mathbb{R}^{n \times m}$  denotes the set of all  $n \times m$  matrices with real entries. If  $Q \in \mathbb{R}^{n \times m}$  then  $Q^T$  denotes the transpose of  $Q$ .  $Q$  is symmetric if  $Q = Q^T$ . The matrix  $Q$  is positive (negative) semidefinite, denoted as  $Q \succeq 0$  ( $\preceq 0$ ), if  $x^T Q x \geq 0$  ( $\leq 0$ ) for all  $x \in \mathbb{R}^n$ .  $Q$  is positive (negative) definite, denoted as  $Q \succ 0$  ( $\prec 0$ ), if  $x^T Q x > 0$  ( $< 0$ ) for all  $x \in \mathbb{R}^n$ . The notation  $a \in A$  is read as:  $a$  is an element of  $A$ .  $X \subset Y$  means that  $X$  is a subset of  $Y$ . The notation  $\Omega(V, c)$  denote the sublevel

set  $\{x \in \mathbb{R}^n : V(x) \leq c\}$ . Given  $V(x)$  and dynamics  $f(x)$ , define the notation  $D(V, f) := \{x \in \mathbb{R}^n : \nabla V(x)f(x) < 0\} \cup \{0\}$ . The binomial coefficient indexed by  $n$  and  $k$  is written as  $\binom{n}{k}$ .

## 2.2 Stability and Performance of Nonlinear Systems

This section briefly discusses the stability and performance metrics of nonlinear systems. Stability and performance metrics are characterized by the concept of ROA and dissipation inequality condition, respectively. Readers are encouraged to refer to standard nonlinear systems textbooks [31, 59] for a comprehensive treatment of the topics presented in this section.

### 2.2.1 Region-of-Attraction

Consider an autonomous nonlinear dynamical system of the form:

$$\dot{x} = f(x), \quad x(0) = x_0 \tag{2.1}$$

where  $x \in \mathbb{R}^n$  is the state vector and  $f : \mathbb{R}^n \rightarrow \mathbb{R}^n$  is a multivariable polynomial. Assume that  $x = 0$  is a locally asymptotically stable equilibrium point. This assumption is without loss of generality because state coordinates can always be redefined to shift an equilibrium point to the origin. For linear systems, asymptotic stability of an equilibrium point is a global property. In other words, if an equilibrium point is asymptotically stable then its state trajectory will converge back to the equilibrium when starting from any initial condition. For nonlinear systems, asymptotically stable equilibrium points are not necessarily globally asymptotically stable. Consequently, the state trajectory is not guaranteed to converge back to the equilibrium when starting from any initial condition. This fundamental difference between asymptotic stability for linear and nonlinear systems motivates the interest in estimating an invariant region around the equilibrium point. The ROA of an asymptotically stable equilibrium point provides an estimate to the invariant region. Roughly, the ROA is the set of initial conditions whose state trajectories converge back to the equilibrium [31]. Formally, the ROA is defined as:

$$\mathcal{R} = \left\{ x_0 \in \mathbb{R}^n : \text{If } x(0) = x_0 \text{ then } \lim_{t \rightarrow \infty} x(t) = 0 \right\} \tag{2.2}$$

If the ROA is small, then a disturbance can easily drive the system out of the ROA and the system will fail to return to the stable equilibrium point. Thus, the size of the ROA can be interpreted as a measure of the stability properties of a nonlinear system around an equilibrium point.

The invariant region of a system is usually characterized by Lyapunov theory [31,59]. Conditions provided by Lyapunov stability theory define the invariant region, specifically the ROA. For simplicity, assume we have a globally asymptotically stable (GAS) equilibrium (the case for locally stable equilibrium is considered in the following chapters). Proving stability of the equilibrium roughly amounts to searching for an energy-like function  $V(x) : \mathbb{R}^n \rightarrow \mathbb{R}$  with the following properties: (i)  $V(x)$  has to be positive definite, i.e.  $V(x) > 0$  and (ii) the gradient of  $V(x)$  has to decrease along the the flow of the system, i.e.  $\nabla V(x)f(x) < 0$  (except at origin). Roughly, a function  $V(x)$  satisfying these conditions is known as a *Lyapunov* function.

For a GAS equilibrium, one must obtain a Lyapunov function that satisfies the two conditions over the whole state space region. For a locally asymptotically stable equilibrium, the conditions need to be satisfied on a certain region of the state-space. The following chapter provides more detail on this issue. Here, we provide an interpretation of the condition  $\nabla V(x)f(x) < 0$ . The condition  $\nabla V(x)f(x) < 0$  indicates that the gradient of the  $V(x)$  and the flow of the system  $f(x)$  must have a negative inner product. This is possible only if the angle between the gradient of  $V(x)$  and  $f(x)$  is greater than 90 degree. The condition  $\nabla V(x)f(x) < 0$  also implies that when a trajectory crosses a Lyapunov surface  $V(x) = c$ , it permanently moves inside the sublevel set  $\Omega(V, c) := \{x \in \mathbb{R}^n : V(x) \leq c\}$ . Hence,  $\Omega(V, c)$  is an invariant region and an estimate to the ROA. Consider Figure 2.1. The trajectories of a globally stable plant are shown in (blue) solid line and the Lyapunov surfaces are shown in (red) dashed ellipses. Two sublevel sets,  $\Omega(V, 1)$  and  $\Omega(V, 5)$ , are shown in Figure 2.1. The condition  $\nabla V(x)f(x) < 0$  are demonstrated on the Lyapunov sublevel set  $\Omega(V, 5)$  at the point where the trajectory crosses the Lyapunov surface.

This thesis relies on estimating the ROA of the nonlinear systems to quantify the stability region. As discussed in this section, the stability region is characterized by appropriate Lyapunov function and its sublevel set.

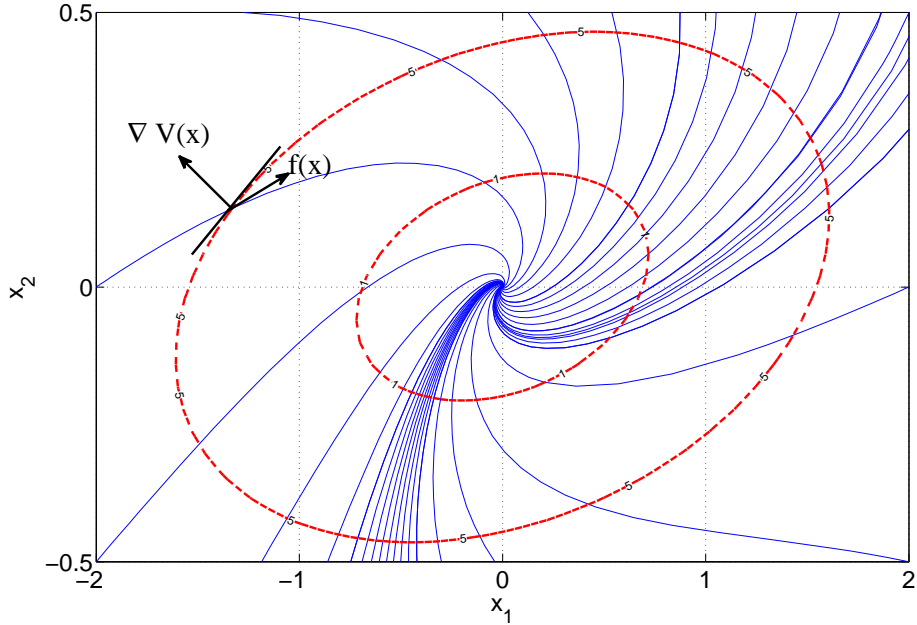


Figure 2.1: Demonstration of  $\nabla V(x)f(x) < 0$  on the Lyapunov sublevel set  $\Omega(V, 5)$ .

### 2.2.2 Dissipation Inequality

Input-output analysis plays a central role in performance assessments of dynamical systems. One way to characterize the performance of dynamical systems is to estimate the induced  $L_2$  gain.

Consider nonlinear dynamical systems of the form:

$$\dot{x} = f(x, u) \tag{2.3a}$$

$$y = h(x) \tag{2.3b}$$

where  $x \in \mathbb{R}^n$  is the state vector,  $u \in \mathbb{R}^m$  is the input, and  $y \in \mathbb{R}^p$  is the output. Assume that  $f$  is an  $n \times 1$  polynomial function of  $x$  and  $u$  such that  $f(0, 0) = 0$ . Also assume that  $h$  is an  $p \times 1$  polynomial function of  $x$  such that  $h(0) = 0$ . Denote this system by  $\mathcal{S}$ .

Now, define the  $L_2$  norm of a signal as:

$$\|u\|_2 = \sqrt{\int_0^\infty u^T(t)u(t)dt} \tag{2.4}$$

If the above integral is finite then  $u$  is called an  $L_2$  signal. The  $L_2$ - $L_2$  input-output

gain of  $\mathcal{S}$  is defined as:

$$\|\mathcal{S}\|_{L_2 \rightarrow L_2} := \sup_{\|u\|_2 \neq 0} \frac{\|y\|_2}{\|u\|_2} \quad (2.5)$$

The  $L_2$  gain is usually characterized by a storage function  $V$ .  $V : \mathbb{R}^n \rightarrow \mathbb{R}$ , is a continuously differentiable, positive definite function ( $V(0) = 0$  and  $V(x) \geq 0$ ). The connection between  $L_2$  gain and storage function of a system is described by a standard result in systems theory, known as dissipation inequality. Lemma 1 provides the standard dissipation inequality result which can be found in textbook [31].

**Lemma 1.** *If there exists a  $\gamma > 0$  and a continuously differentiable  $V : \mathbb{R}^n \rightarrow \mathbb{R}$  such that:*

$$V(0) = 0 \text{ and } V(x) \geq 0 \quad \forall x \in \mathbb{R}^n \quad (2.6)$$

$$\gamma^2 u^T u - y^T y - \frac{\partial V}{\partial x} f(x, u) \geq 0 \quad \forall x \in \mathbb{R}^m \text{ and } \forall u \in \mathbb{R}^m \quad (2.7)$$

then  $\|y\|_2^2 \leq V(x(0)) + \gamma^2 \|u\|_2^2$ . Moreover, if  $x(0) = 0$  then  $\|y\|_2 \leq \gamma \|u\|_2$ .

This is known as dissipation inequality with storage function  $V(x)$  and supply function  $s(u, y) = \gamma^2 u^T u - y^T y$ . The dissipation inequality in Equation 2.7 provides a sufficient condition for the  $L_2$ - $L_2$  input-output gain to be less than  $\gamma$ . This follows by integrating Equation 2.7 and using the fact that  $V(x)$  is positive definite. For a zero input ( $u = 0$ ) system, the storage function can also be shown to be a Lyapunov function of the system.

However, one issue is that the polynomial system will not, in general, be globally stable. If the system is only locally stable, then a sufficiently large disturbance can drive the state, and the output of the system will be unbounded. Hence, the notion of local  $L_2$  gain is introduced where attention is restricted to “local” inputs  $u$  that satisfy  $\|u\|_2 \leq R$  where  $R \in \mathbb{R}_+$ . The local  $L_2$  gain is formally defined in Equation 5.5.

$$\gamma_R := \sup_{\substack{d \in L_2, \|u\|_2 \leq R \\ x(0)=0}} \frac{\|e\|_2}{\|u\|_2} \quad (2.8)$$

Chapter 4 discusses the issue of estimating the local  $L_2$  gain,  $\gamma_R$ .

The Lyapunov and dissipation theory frameworks are standard tools in systems analysis. A direct application of Lyapunov and dissipation theory is to generate stability

and performance certificates of nonlinear systems by computing a Lyapunov or storage function. Unfortunately, it is difficult to generate any such certificates due to the lack of computational tools for nonlinear systems. However, we can restrict our search for Lyapunov or storage functions only to polynomial vector fields. With this restriction, one can utilize the SOS optimization framework to generate Lyapunov or Storage functions.

## 2.3 Sum of Squares (SOS) Optimization

This section provides a brief review of SOS optimizations. Additional details can be found in [33, 38, 39]. A polynomial  $p$  is a *sum of squares* (SOS) if there exist polynomials  $\{f_i\}_{i=1}^m$  such that  $p = \sum_{i=1}^m f_i^2$ . For example,  $p = x^2 - 4xy + 7y^2$  is a sum of squares since  $p = f_1^2 + f_2^2$  where  $f_1 = (x - 2y)^2$  and  $f_2 = 3y^2$ . Note that if  $p$  is a sum of squares then  $p(x) \geq 0 \forall x \in \mathbb{R}^n$ . Thus  $p \in \text{SOS}$  is a sufficient condition for a polynomial to be globally non-negative. Note that the converse is not true, i.e. non-negative polynomials are not necessarily SOS polynomials.

SOS optimization problems involve SOS polynomial constraints. Hence, problems with polynomial constraints can be posed within this optimization framework. The computational solutions to these problems rely on connections between semi-definite matrices and SOS polynomials [33, 38, 39]. Next section discusses the connections between semi-definite matrices and SOS polynomials. Software available to solve SOS optimization problems are also discussed.

### 2.3.1 Connections Between SOS Polynomials and Semidefinite Matrices

Theorem 2.1 below gives a concrete statement of the connection between sums of squares and positive semidefinite matrices. We require two facts that follow from [43] (refer to Theorem 1 and its preceding Lemma):

1. If  $p(x)$  is a sum of squares then  $p(x)$  must have even degree.
2. If  $p(x)$  is degree  $2d$  ( $d \in \mathbb{N}$ ) and  $p(x) = \sum_{i=1}^m f_i^2$  then  $\deg f_i \leq d \forall i$ .

Quadratic forms can be expressed as  $p(x) = x^T Q x$  where  $Q$  is a symmetric matrix. Similarly, polynomials of degree  $\leq 2d$  can be expressed as  $p(x) = z(x)^T Q z(x)$  where the vector  $z$  contains all monomials of degree  $\leq d$ . Define  $z$  as the column vector of

all monomials in variables  $\{x_1, \dots, x_n\}$  of degree  $\leq d$ :<sup>1</sup>

$$z \doteq \left[ 1, x_1, x_2, \dots, x_n, x_1^2, x_1x_2, \dots, x_n^2, \dots, x_n^d \right]^T \quad (2.9)$$

There are  $\binom{k+n-1}{k}$  monomials in  $n$  variables of degree  $k$ . Thus  $z$  is a column vector of length  $l_z \doteq \sum_{k=0}^d \binom{k+n-1}{k} = \binom{n+d}{d}$ . This is known as the *Gram matrix form*. An important fact is that  $p$  is SOS if and only if there exists  $Q \succeq 0$  such that  $p(x) = z(x)^T Q z(x)$ . Theorem 2.1 [8] provides a more formal description. Refer to [8] for proof and additional details. Theorem 2.1 provides a connection between SOS polynomials and positive semidefinite matrices.

**Theorem 2.1.** [8] Suppose  $p \in \mathbb{R}^n$  is a polynomial of degree  $2d$  and  $z$  is the  $l_z \times 1$  vector of monomials defined in Equation 2.9. Then  $p$  is a SOS if and only if there exists a symmetric matrix  $Q \in \mathbb{R}^{l_z \times l_z}$  such that  $Q \succeq 0$  and  $p(x) = z(x)^T Q z(x)$ .

The proof of this theorem can be found in [8].

**Remark 1:** If  $p(x)$  can be written as  $p(x) = z(x)^T Q z(x)$  with  $Q \succeq 0$ , then  $p(x)$  can be represented as a sum-of-squares polynomial. Specifically, there exist polynomials  $\{f_i(x)\}_{i=1}^m$  such that  $p(x) = \sum_{i=1}^m f_i(x)^2$ .

**Remark 2:** The Gram matrix  $Q$  is not necessarily unique. There may be multiple symmetric  $Q$  satisfying  $p(x) = z(x)^T Q z(x)$  and this fact is demonstrated by the following example [3]:

*Example:* The goal is to provide a Gram matrix representations of  $p(x) = 2x_1^4 + 2x_1^3x_2 - x_1^2x_2^2 + 5x_2^4$ . Notice  $p(x)$  can be represented as  $p(x) = z(x)^T Q_p z(x)$  where:

$$z(x) = \begin{bmatrix} x_1^2 \\ x_1x_2 \\ x_2^2 \end{bmatrix}, \quad Q_p = \begin{bmatrix} 2 & 1 & -0.5 \\ 1 & 0 & 0 \\ -0.5 & 0 & 5 \end{bmatrix}$$

Note that  $Q_p$  is not positive semi-definite, i.e., one of the eigenvalues of  $Q_p$  is negative. Using the fact  $(x_1x_2)^2 = (x_1)^2(x_2)^2$ , all possible Gram matrix representation of  $p(x)$

can be written as  $p(x) = z(x)^T (Q_p + \lambda N) z(x)$ , where  $\lambda \in \mathbb{R}$  and  $N = \begin{bmatrix} 0 & 0 & -1 \\ 0 & 2 & 0 \\ -1 & 0 & 0 \end{bmatrix}$ .

---

<sup>1</sup>Any ordering of the monomials can be used to form  $z$ .

Note that  $z(x)^T \lambda N z(x) = 0$ . The problem of finding an appropriate Gram matrix form reduces to finding the values of  $\lambda \in \mathbb{R}$  such that  $Q_p + \lambda N \succeq 0$ . It can be shown that  $\lambda = 1, 2$  are possible candidates satisfying  $Q_p + \lambda N \succeq 0$ .

### 2.3.2 Connection Between SOS Polynomials and ROA/Dissipation Inequality

This section demonstrates how SOS polynomials can be used to characterize the ROA and the dissipation inequality.

Assume that the Lyapunov or the storage function, in Section 2.2, is restricted to be a polynomial. Consequently, both stability and dissipation inequality conditions turn out to be polynomial non-negativity conditions given that the system dynamics is represented via polynomial vector fields. The non-negativity conditions are relaxed to be SOS polynomials. This SOS relaxation implies that the Lyapunov or the storage function can be found by searching over a class of polynomial functions of a specified degree satisfying the non-negativity constraints. The following example (taken from [31]. Ch. 4, Ex. 4.27) demonstrates the procedure:

*Example [31].* Consider the system:

$$\dot{x}_1 = -x_1 + x_2^2 \tag{2.10}$$

$$\dot{x}_2 = -x_2 \tag{2.11}$$

The system is globally asymptotically stable around the origin. The objective is to find a Lyapunov certificate proving global stability. In other words, we seek a Lyapunov function  $V(x)$  satisfying (i)  $V(x) \geq 0, \forall x \neq 0$ , and (ii)  $-\nabla V(x)f(x) > 0$  for all  $x \in \mathbb{R}^2 \cup \{0\}$ .

Assume the Lyapunov function to be of the following polynomial form,  $V(x) = \frac{1}{2}x_1^2 + a\frac{1}{4}x_2^4$ , where  $a > 0$  is to be determined. Define  $z(x) = \begin{bmatrix} x_1 \\ x_2^2 \end{bmatrix}$ . The condition  $-\nabla V(x)f(x) > 0$  is a polynomial constraint and can be rewritten as  $z(x)^T Q z(x) > 0$  with  $Q = \begin{bmatrix} 1 & \frac{1}{2} \\ \frac{1}{2} & a \end{bmatrix}$ . The inequality  $z(x)^T Q z(x) > 0$  can be relaxed to be an SOS constraint. According to Theorem 2.1,  $z(x)^T Q z(x)$  is SOS if we can find a value of  $a$  such that  $Q = Q^T \succeq 0$ .

The example provides insight on how SOS polynomials can be used to generate the

Lyapunov function. This is a contrived example whose analytical solution is easy to compute. Choosing  $a > \frac{1}{4}$  will satisfy the conditions. In general, it is not easy to compute the Gram matrix which proves non-negativity of a polynomial. Fortunately, computing Gram matrix can be automated by available softwares for SOS optimizations. The next section discusses details on the software that will be used as the primary computational tool in this thesis.

### 2.3.3 Software for SOS Optimizations

There are freely available MATLAB toolboxes for solving SOS optimizations, such as SOSTOOLS [41], Yalmip [35], and SOSOPT [3]. These packages allow the user to specify the polynomial constraints using a symbolic toolbox.

A SOS program is an optimization problem with a linear cost and SOS constraints on the decision variables [41]:

$$\begin{aligned} \min_{r \in \mathbb{R}^n} c^T u & \quad (2.12) \\ \text{subject to: } a_{k,0}(x) + a_{k,1}(x)r_1 + \cdots + a_{k,n}(x)r_n \in \text{SOS } (k = 1, \dots, N_s) \end{aligned}$$

The vector  $c \in \mathbb{R}^n$  and polynomials  $\{a_{k,j}\}$  are given as part of the optimization data, while  $r \in \mathbb{R}^n$  are decision variables. SOS programs can be converted to semidefinite programs (SDPs) using the connection between SOS polynomials and positive semidefinite matrices. SOSTOOLS [41], Yalmip [35], and SOSOPT [3] are freely available softwares which convert the SOS optimization into an SDP which is solved with SeDuMi [46, 47] or another freely available SDP solver. Finally the solution of the SDP is converted back to a polynomial solution.

A drawback of the SOS framework is that the size of the resulting SDP grows rapidly if the SOS optimization involves polynomials with many variables and/or high degree. For a generic degree  $2d$  polynomial  $p(x)$  in  $n$  variables, the Gram matrix representation involves  $\binom{n+d}{d}$  monomials. An SOS constraint on  $p(x)$  is enforced via a positive semidefinite constraint on the Gram matrix  $Q \succeq 0$  such that  $p(x) = z(x)^T Q z(x)$ . For example, for a generic degree  $2d = 8$  polynomial in  $n = 8$  variables the Gram matrix has dimension  $495 \times 495$ . The size of this positive semidefinite constraint is at or near the limits of current semidefinite programming solvers. While various techniques can be used to exploit the problem structure [15], this computational growth is a generic trend in SOS optimizations. For analysis of polynomial systems, this roughly lim-

its the approach to systems with fewer than 8-10 states and cubic degree models. Polynomial models of higher degree can be handled if there are fewer states.

Another drawback of the SOS framework is that it cannot handle hard (non-smooth) nonlinearities like actuator saturations or rate limits. These nonlinearities cannot be (globally) approximated by any polynomial function. Chapter 5 and 6 discusses how to handle these hard nonlinearities for estimating the ROA and the induced gain in terms of Lyapunov and storage function.

## 2.4 Generalized S-Procedure

This thesis analyzes stability and performance of the polynomial systems. The polynomial system will not, in general, be globally stable. Consequently, the stability and the dissipation inequality conditions will not hold globally, i.e., these conditions can not be satisfied on the entire state-space. In other words, these conditions are only valid within a certain region of the state-space. These conditions can be enforced to hold locally using set containment constraints. For example, a locally asymptotically stable system ( $\dot{x} = f(x)$ ) around the origin requires the condition  $\nabla V(x)f(x) < 0$  to hold within a sublevel set of Lyapunov function  $V(x)$ . In other words,  $\nabla V(x)f(x) < 0$  is true on  $\Omega(V, c)$ , where  $c \in \mathbb{R}$ . Set containment constraints provide a natural framework to formulate this kind of local conditions.

The S-procedure [4] is heavily used in robust control theory for proving set containments involving quadratic functions. For example, let  $F_i$  be of the quadratic form  $F_i(x) = \begin{bmatrix} x \\ 1 \end{bmatrix}^T Q_i \begin{bmatrix} x \\ 1 \end{bmatrix}$ ,  $\forall i = 0, 1, \dots, m$  with  $Q_i = Q_i^T \in R^{(n_x+1) \times (n_x+1)}$ . The S-procedure addresses if the following set containment constraint is satisfied.

$$\{x \in R^n : F_1(x) \geq 0, \dots, F_m(x) \geq 0\} \subseteq \{x \in R^n : F_0(x) \geq 0\} \quad (2.13)$$

The S-procedure states that if there exists  $\tau_i \geq 0 \forall j = 1, \dots, m$  such that  $F_0(x) - \sum_{i=1}^m \tau_i F_i(x) \geq 0 \forall x$ , then the set containment constraint in Equation 2.13 holds. The S-procedure can be generalized for higher order polynomials (not limited to quadratic polynomials). Theorem 2.2 [3] provides the generalized polynomial S-procedure. Refer to [3] for details on the proof.

**Theorem 2.2.** [3] Let  $g_1$  and  $g_2$  be given polynomials. Define sets  $S_1$  and  $S_2$ :

$$S_1 = \{x \in \mathbb{R}^n : g_1(x) \geq 0\}$$

$$S_2 = \{x \in \mathbb{R}^n : g_2(x) \geq 0\}$$

If there exists a polynomial  $s(x) : \mathbb{R}^n \rightarrow \mathbb{R}$  such that:

$$(1) \quad s(x) \geq 0 \quad \forall x$$

$$(2) \quad g_1(x) - s(x)g_2(x) \geq 0 \quad \forall x$$

then  $S_2 \subseteq S_1$ .

Note that the S-procedure provides a sufficient constraint. The feasibility of the problem proves the set containment constraint.

## 2.5 Summary

This chapter presented a summary of the background materials that are used throughout the thesis. The chapter discussed the Lyapunov and the dissipation inequality conditions, heavily used in the subsequent chapters, for estimating the ROA and the induced I/O gain of nonlinear systems. The chapter also reviewed materials for the SOS polynomials and SOS optimization framework. Available softwares for formulating and solving SOS optimization problems are discussed. Finally, a generalized S-procedure for handling set containment conditions is reviewed. Readers are encouraged to consult the suggested references for a more detailed treatment of all these topics.

# Chapter 3

## Polynomial Modeling of Aircraft Dynamics

This chapter provides an ad-hoc procedure to generate a polynomial description of the dynamics of an aircraft given its nonlinear mathematical model. The procedure is demonstrated by applying it on a scaled experimental aircraft model, known as the Generic Transport Model (GTM), developed by NASA. The nonlinear mathematical model of the GTM dynamics is provided by NASA. This chapter develops a polynomial description of the nonlinear GTM dynamics. Finally, the polynomial description is validated against the nonlinear model of the GTM dynamics.

### 3.1 Motivation

The thesis focuses on assessing stability and performance of nonlinear flight control systems. It turns out that the stability and performance of nonlinear systems can be inferred by checking non-negativity of certain conditions associated with the nonlinear systems. Unfortunately, for a generic nonlinear system (not necessarily polynomial), checking non-negativity is “undecidable” [38]. The work of [38] develops SOS optimization tool for deciding non-negativity of polynomial nonlinearities. This thesis utilizes the SOS-based tools for assessing stability and performance of flight control systems. Hence, it is an important step to formulate a polynomial description of the nonlinear aircraft systems.

Unfortunately, there is no systematic procedure available for generating a polynomial description of a nonlinear system. Polynomial description of nonlinear systems is often

problem specific. In practice, knowledge of the nonlinear dynamics can help result in an accurate polynomial description of the nonlinear system. This is particularly true for dynamical systems like aircrafts. For example, the nonlinearities in the aircraft dynamics primarily arise from (i) the equations of motion describing aircraft’s rigid body dynamics, and (ii) the aerodynamic characteristics (e.g., lift/drag etc.) of the aircraft. Hence, the knowledge of the nonlinear characteristics of the flight dynamics can help generate an accurate polynomial description of the nonlinear aircraft. Next, we focus on generating a polynomial description of the nonlinear Generic Transport Model (GTM) Aircraft developed by NASA.

## 3.2 Polynomial Model Formulation of Generic Transport Model (GTM) Aircraft

This section provides an engineering approach to approximate the nonlinear aircraft dynamics to polynomial description. The approach taken in this section is demonstrated by applying it to the NASA Generic Transport Model (GTM) aircraft. For simplicity, we will focus on generating a polynomial description of the longitudinal GTM dynamics. Similar approach can be taken for formulating polynomial description of the lateral dynamics.

### 3.2.1 Longitudinal Dynamics of GTM

The NASA Generic Transport Model (GTM) describes a remote-controlled 5.5 percent scale commercial aircraft [9, 37]. The GTM aircraft parameters are provided in Table 3.1. NASA constructed a high fidelity 6 degree-of-freedom Simulink model of the GTM with the aerodynamic coefficients described as look-up tables. This section describes the construction of polynomial description of the GTM longitudinal dynamics based on the look-up table data.

Wing Area, $S$	5.902 ft <sup>2</sup>
Mean Aerodynamic Chord, $\bar{c}$	0.9153 ft
Mass, $m$	1.542 slugs
Pitch Axis Moment of Inertia, $I_{yy}$	4.254 lbf-ft <sup>2</sup>
Air Density, $\rho$	0.002375 slugs/ft <sup>3</sup>
Gravity Constant, $g$	32.17 ft/s <sup>2</sup>

The longitudinal dynamics of the GTM are described by a four-state longitudinal

model [45]:

$$\dot{V} = \frac{1}{m} (-D - mg \sin(\theta - \alpha) + T_x \cos \alpha + T_z \sin \alpha) \quad (3.1a)$$

$$\dot{\alpha} = \frac{1}{mV} (-L + mg \cos(\theta - \alpha) - T_x \sin \alpha + T_z \cos \alpha) + q \quad (3.1b)$$

$$\dot{q} = \frac{(M + T_m)}{I_{yy}} \quad (3.1c)$$

$$\dot{\theta} = q \quad (3.1d)$$

where  $V$  is the air speed (ft/s),  $\alpha$  is the angle-of-attack (rad),  $q$  is the pitch rate (rad/s) and  $\theta$  is the pitch angle (rad). The control inputs are the elevator deflection  $\delta_{elev}$  (rad) and engine throttle  $\delta_{th}$  (percent).

The drag force  $D$  (lbf), lift force  $L$  (lbf), and aerodynamic pitching moment  $M$  (lbf-ft) are given by:

$$D = \bar{q} S C_D(\alpha, \delta_{elev}, \hat{q}) \quad (3.2)$$

$$L = \bar{q} S C_L(\alpha, \delta_{elev}, \hat{q}) \quad (3.3)$$

$$M = \bar{q} S \bar{c} C_m(\alpha, \delta_{elev}, \hat{q}) \quad (3.4)$$

where  $\bar{q} := \frac{1}{2} \rho V^2$  is the dynamic pressure (lbf/ft<sup>2</sup>) and  $\hat{q} := \frac{\bar{c}}{2V} q$  is the normalized pitch rate (unitless).  $C_D$ ,  $C_L$ , and  $C_m$  are unitless drag, lift and pitching moment coefficients, respectively. The coefficients are computed from look-up tables provided by NASA.

The GTM (Figure 3.1) has one engine each on the port and starboard sides of the airframe. Equal thrust settings for both engines are assumed. The thrust from a single engine  $T$  (lbf) is a function of the throttle setting  $\delta_{th}$  (percent).  $T(\delta_{th})$  is a given cubic-order polynomial in NASA's high fidelity GTM simulation model.  $T_x$  (lbf) and  $T_z$  (lbf) denote the projection of the total engine thrust along the body x and body z axes, respectively.  $T_m$  (lbf-ft) denotes the pitching moment due to both engines.  $T_x$ ,  $T_z$  and  $T_m$  are given by:

$$T_x(\delta_{th}) = n_{ENG} T(\delta_{th}) \cos(\epsilon_2) \cos(\epsilon_3) \quad (3.5)$$

$$T_z(\delta_{th}) = n_{ENG} T(\delta_{th}) \sin(\epsilon_2) \cos(\epsilon_3) \quad (3.6)$$

$$T_m(\delta_{th}) = r_z T_x(\delta_{th}) - r_x T_z(\delta_{th}) \quad (3.7)$$



Figure 3.1: GTM Aircraft developed by NASA

$n_{ENG} = 2$  is the number of engines,  $\epsilon_2 = 0.0375$  rad and  $\epsilon_3 = -0.0294$  rad are angles specifying the rotation from engine axes to the airplane body axes.  $r_x = 0.4498$  ft and  $r_z = 0.2976$  ft specify the thrust moment arm.

For convenience, we will introduce the compact notation:

$$\dot{x} = \mathcal{F}_{\mathcal{G}\mathcal{T}\mathcal{M}}(x, u) \quad (3.8a)$$

$$y = x \quad (3.8b)$$

where  $x := [V(\text{ft/s}), \alpha(\text{rad}), q(\text{rad/s}), \theta(\text{rad})]$  indicates states,  $u := [\delta_{elev}(\text{rad}), \delta_{th}(\%)]$  indicates inputs and  $y$  indicates the outputs. Input-output description of the systems is denoted as  $\mathcal{S}_{\mathcal{G}}$ .

### 3.2.2 Approach to Polynomial Model Formulation

The following terms of the longitudinal model presented in Section 3.2.1 are approximated by low-order polynomial functions:

1. Trigonometric functions:  $\sin(\alpha)$ ,  $\cos(\alpha)$ ,  $\sin(\theta - \alpha)$ ,  $\cos(\theta - \alpha)$
2. Engine model:  $T(\delta_{th})$
3. Rational dependence on speed:  $\frac{1}{V}$
4. Aerodynamic coefficients:  $C_D$ ,  $C_L$ ,  $C_m$

Constructing polynomial approximations of the trigonometric functions, engine model, and rational dependence on speed is relatively straight-forward. The trigonometric functions are approximated by Taylor series expansions:  $\sin z \approx z - \frac{1}{6}z^3$  and  $\cos z \approx 1 - \frac{1}{2}z^2$  for  $z$  in units of radians. For  $|z| \leq \frac{\pi}{4}$  rad the maximum approximation error for the sine and cosine functions is 0.35% and 2.2%, respectively. For the engine model, a least squares technique is used to approximate the ninth order polynomial function  $T(\delta_{th})$  by the following third order polynomial:

$$T(\delta_{th}) \approx -1.967 \times 10^{-6} \delta_{th}^3 + 1.150 \times 10^{-3} \delta_{th}^2 + 8.258 \times 10^{-2} \delta_{th} + 1.085 \quad (3.9)$$

The maximum approximation error is 1.3% over the full range throttle inputs  $\delta_{th} \in [0\%, 100\%]$ . The least squares technique is also used to compute a linear fit to  $\frac{1}{V}$  over the desired range of interest from 100 ft/s to 200 ft/s:

$$\frac{1}{V} \approx -4.774 \times 10^{-5} V + 0.01409 \quad (3.10)$$

The maximum approximation error is 9% over the specified velocity range. The linear fit for  $\frac{1}{V}$  is used in both the  $\dot{\alpha}$  equation and the equation for the normalized pitch rate  $\hat{q}$ .

Derivation of polynomial function approximations for the aerodynamic coefficients requires a more detailed explanation. NASA provides raw look-up table data for the aerodynamic coefficients in the airframe body axes, i.e. the raw data is provided for  $C_X$ ,  $C_Z$ , and  $C_m$ .<sup>1</sup> In addition, each aerodynamic coefficient is computed as a sum of three terms which model the aerodynamic effects of the basic airframe, elevator inputs, and pitch rate. For example,  $C_X(\alpha, \delta_{elev}, \hat{q})$  is a sum of three terms each of

---

<sup>1</sup>The notation refers to standard aircraft body axis conventions [45].  $x$  is directed to the front along the longitudinal axis of the aircraft and  $z$  is directed down.  $X$  and  $Z$  are the aerodynamic forces along the  $x$  and  $z$  axes, respectively.

which is computed from a look-up table:

$$C_X(\alpha, \delta_{elev}, \hat{q}) = C_{X,\alpha}(\alpha) + C_{X,\delta_{elev}}(\alpha, \delta_{elev}) + C_{X,\hat{q}}(\alpha, \hat{q}) \quad (3.11)$$

$C_{X,\alpha}$  models the basic airframe dependence of the body-X force on the angle of attack.  $C_{X,\delta_{elev}}$  and  $C_{X,\hat{q}}$  model the aerodynamic effects of the elevator input and pitch rate, respectively. For ease of approximation, all body-axis look-up tables were transformed into lift and drag coordinates via a rotation:

$$\begin{bmatrix} C_D \\ C_L \end{bmatrix} = - \begin{bmatrix} \cos(\alpha) & \sin(\alpha) \\ -\sin(\alpha) & \cos(\alpha) \end{bmatrix} \begin{bmatrix} C_X \\ C_Z \end{bmatrix} \quad (3.12)$$

Accurate, low-order polynomial fits could be obtained for all look-up tables after rotating into the lift and drag coordinates. For example, Figure 3.2 shows the look-up table data and cubic polynomial fits for  $C_{L,\alpha}$ ,  $C_{D,\alpha}$  and  $C_{m,\alpha}$ . A least squares technique is used to fit the lift and drag look-up table data. Specifically, a weighted least square technique is applied to capture the low angle-of-attack characteristics more accurately. The polynomial function approximations for all aerodynamic coefficient look-up tables are provided in Appendix A. For ease of interpretation, plots of  $\alpha$ ,  $q$  and  $\delta_{elev}$  are shown in units of degs, degs/s, and degs, respectively. There are two important issues associated with the fitting procedure. First, note that the  $C_L/C_D$  data is fit rather than the raw  $C_X/C_Y$ . This can be justified by considering the structure of the dynamic equations. For example,  $-D$  enters directly into the equation for  $\dot{V}$  (Equation 3.1a).  $\dot{V}$  can be alternatively expressed in terms of  $X$  and  $Z$  forces via the substitution  $-D = X \cos(\alpha) + Z \sin(\alpha)$ . Fitting the raw aerodynamic look-up data for  $C_X$  and  $C_Z$  would introduce approximation errors in  $X$  and  $Z$ . Approximation errors would also be introduced by the polynomial fits for  $\cos(\alpha)$  and  $\sin(\alpha)$ . Directly fitting the look-up data for  $C_D$  only leads to one lumped approximation error in the  $-D$  term as opposed to errors in both  $X$  and  $Z$  while fitting  $C_X$  and  $C_Z$ . Second, the least squares solutions for the lift/drag/pitching moment data were weighted to obtain extremely accurate fits at low angles of attack ( $-5^\circ \leq \alpha \leq 15^\circ$ ) and less accurate fits at higher angles of attack ( $\alpha \geq 15^\circ$ ). This weighting ensures that the polynomial model retains trim characteristics that are similar to those of the original nonlinear model. Note that the polynomial functions fail to capture important characteristics of the look-up table data of  $C_{L,\alpha}$  and  $C_{m,\alpha}$  for angles of attack between  $15^\circ \leq \alpha \leq 40^\circ$ . The mismatch between the raw data and the polynomial fitting causes the polynomial and look-up table models to have different trim characteristics for angles of attack in

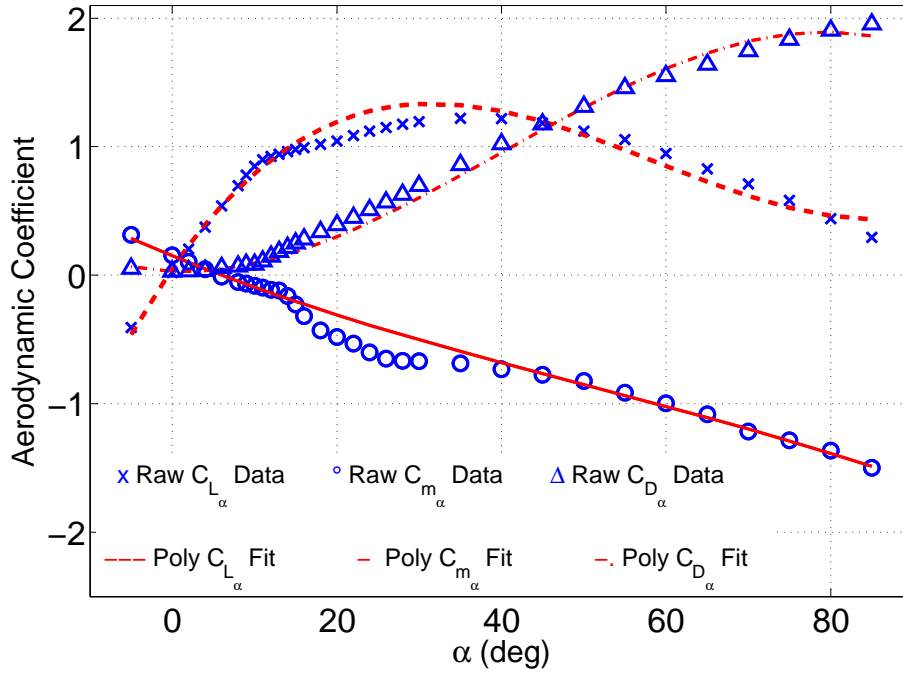


Figure 3.2: Look-up table data and polynomial fit for  $C_{L,\alpha}$ ,  $C_{m,\alpha}$ ,  $C_{D,\alpha}$

this range. Both models were simulated with numerous doublet and step inputs. The qualitative characteristics of both the trajectories are similar.

A degree seven polynomial model of the GTM is obtained after replacing all non-polynomial terms with their polynomial approximations. The polynomial system, denoted as  $\mathcal{S}_{\mathcal{P}}$  is provided below:

$$\dot{x} = \mathcal{P}_{GTM}(x, u) \quad (3.13a)$$

$$\tilde{y} = x \quad (3.13b)$$

where  $x := [V(\text{ft/s}), \alpha(\text{rad}), q(\text{rad/s}), \theta(\text{rad})]$ , and  $u := [\delta_{elev}(\text{rad}), \delta_{th}(\%)]$ . The degree seven polynomial model  $\mathcal{P}_{GTM}(x, u)$  is provided in Appendix A.

### 3.3 Polynomial Model Validation

This section compares the polynomial description of the GTM model  $\mathcal{S}_{\mathcal{P}}$  against the model  $\mathcal{S}_{\mathcal{G}}$  provided by NASA.

The polynomial function of the GTM involves approximations due to the polynomial least-squares fits. The polynomial approximation to the “original nonlinear model” is only valid within a certain state-space region. The term “original nonlinear model” refers to the high-fidelity simulation model provided by NASA,  $\mathcal{S}_G$  in Equation 3.8. The polynomial approximations of the trigonometric function ( $\sin(\alpha)$ ,  $\cos(\alpha)$  etc.) are valid up to approximately  $\pm 50$  deg for the corresponding angle. This provides an upper bound on the range of validity for the polynomial model in the  $\alpha$  direction. The look-up table data for the basic airframe aerodynamic coefficients is within the range of  $5 \text{ deg} \leq \alpha \leq 85 \text{ deg}$ , providing a lower bound on the region of validity in the  $\alpha$  direction. Hence, the polynomial model is valid for  $5 \text{ deg} \leq \alpha \leq 50 \text{ deg}$ . The least-square approximation to the rational dependence on speed ( $\frac{1}{V}$ ) is valid over the range from 100 ft/s to 200 ft/s with a maximum error of approximately 9%. The least-square approximation of the look-up table data to the rate derivative terms, i.e.  $C_{L,\dot{q}}$ ,  $C_{D,\dot{q}}$ ,  $C_{m,\dot{q}}$ , is valid for  $-70 \text{ deg/s} \leq q \leq 70 \text{ deg/s}$ . This limits the range of validity in the pitch rate direction.

The ranges mentioned above provide insight on the “size” of the state-space region the polynomial approximation is valid for. The ranges, however, do not indicate if the polynomial model captures the right dynamic characteristics of the original model. Numerical tools do not exist to rigorously perform this comparison and hence the validation performed in this section will rely on heuristic procedures. However, the validation provides some confidence that the polynomial model provides, for engineering purposes, a sufficiently accurate approximation.

### 3.3.1 Comparisons of Trim Conditions & Simulation Responses

The trim conditions for level flight across the range of velocities  $V \in [100, 200]$  ft/s are computed to assess the quality of the polynomial approximation. The trim conditions assume level flight ( $\alpha = \theta$ ) and no pitch rate ( $q = 0 \text{ deg/s}$ ). Figure 3.3 shows the trim angle-of-attack  $\alpha$  and trim inputs ( $\delta_{elev}$ ,  $\delta_{th}$ ) versus trim speed for both the original nonlinear model and the polynomial approximation. The trim behavior is similar for both models.

The response of both models were simulated with a variety of pulse, step and doublet inputs to the elevator and throttle channels. The time-domain responses are similar for both the polynomial and original model. Figure 3.4 provides a particular simulation response between the two models. This particular simulation is performed by

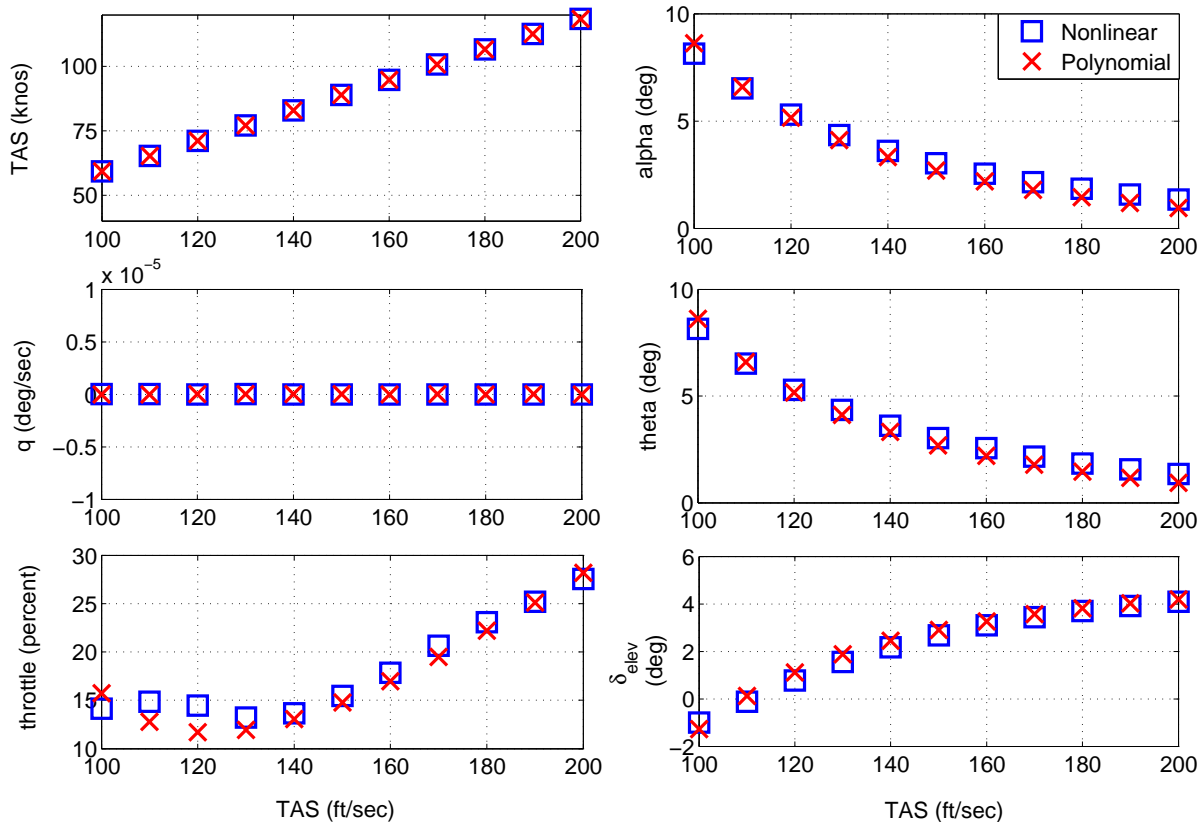


Figure 3.3: Trim states and inputs vs. trim speed for both polynomial and original nonlinear model.

perturbing the elevator and throttle channels with a pulse input of  $-3^\circ$  and 15%. Figure 3.4 shows there is excellent qualitative agreement between the trajectories of the two models. Similar results were obtained at many other simulation scenarios.

Unfortunately, neither simulation responses nor trim condition comparisons qualify as rigorous approaches for validating the approximated polynomial model. Nonetheless, they provide an useful metric to model validation for engineering purposes.

### 3.4 Summary

This chapter presents an ad-hoc approach to describe the nonlinear longitudinal flight dynamics in terms of polynomial functions. The approach is demonstrated on the GTM's longitudinal dynamics. The polynomial description of the GTM flight dynamics is then validated against the original nonlinear GTM dynamics provided by NASA. The validation procedures used are heuristic as rigorous and computable metrics of the approximation error between a generic nonlinear (non-analytic) model and

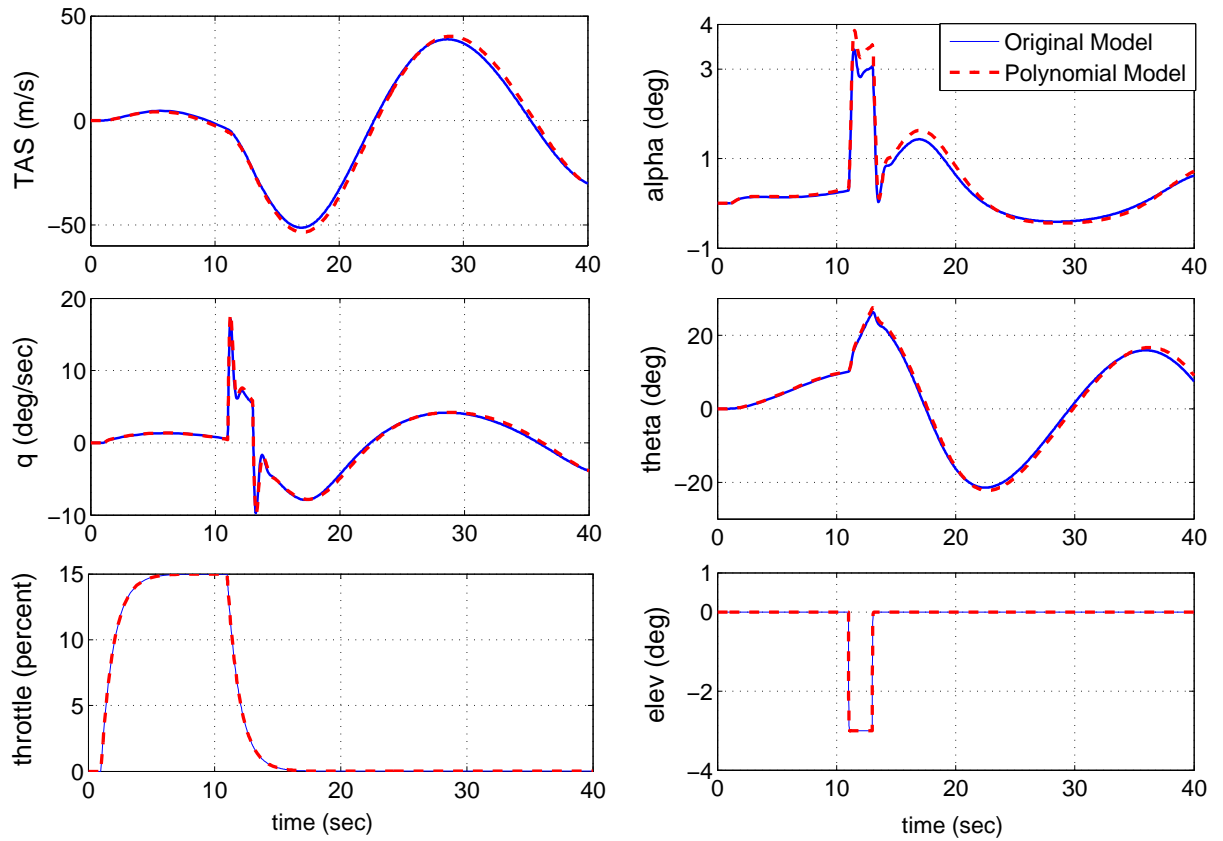


Figure 3.4: Simulation Comparison

a polynomial model is still an open problem.

# Chapter 4

## Local Stability and Performance Analysis of Polynomial Systems

This chapter discusses SOS techniques for estimating both the ROA and the local induced  $L_2$  gain of nonlinear dynamics described by smooth polynomial vector field. The techniques are then applied on the GTM flight control system to assess its stability and performance.

Computing the ROA and the induced  $L_2$  gain of nonlinear flight control systems is challenging and is typically not included in the standard flight control certification process. The current certification process can certainly be enriched by including SOS techniques for estimating the ROA and the induced  $L_2$  gain of nonlinear flight control systems [6]. The SOS estimation techniques rely on Lyapunov/Dissipation theory and the connection between the SOS optimization and the semidefinite programming. This connection has been investigated in detail in [26–28, 48, 49, 55, 56] and numerical examples are also provided in the mentioned references.

Unfortunately, the SOS estimation techniques have been proven to be computationally challenging [3]. The computational burden for SOS optimization problem grows rapidly with the state dimension and the degree of polynomial nonlinearities. Due to the computational challenges the SOS techniques have not been applied to moderately large-scale (usually at least 4 – 5 states and/or cubic nonlinearities) engineering problem, e.g. flight control systems. Moreover, SOS optimization techniques may suffer from numerical conditioning issue and hence fail to produce sensible results. In practice, numerical conditioning issue in SOS techniques is very typical in flight

control problems.

The main contribution of this chapter is in the application of both the ROA and the  $L_2$  gain estimation technique to a moderately large-scale, real engineering problem. Particularly, the techniques are applied on the polynomial longitudinal GTM model, formulated in Section 3.2. The GTM model contains 4 states and up to fifth order nonlinearities. Hence, solving the SOS optimization problem turns out to be computationally challenging. This chapter provides insights on solving moderately large-scale problems like the GTM. Section 4.1 and 4.2 describe the techniques for estimating the ROA and the induced  $L_2$  gain, respectively. The techniques are applied to NASA’s 4-state longitudinal GTM model in Section 4.1.3 and 4.2.1 to estimate stability and performance metrics of the nonlinear flight control system. Note that the techniques are not applicable to (polynomial) systems with actuator saturation and/or rate limit.

## 4.1 Technical Approach to the Region-of-Attraction (ROA) Estimation

This section describes the technical approach to estimate the region of attraction for polynomial systems. Consider an autonomous polynomial dynamic system of the form:

$$\dot{x} = f(x), \quad x(0) = x_0 \tag{4.1}$$

where  $x \in \mathbb{R}^n$  is the state vector,  $f : \mathbb{R}^n \rightarrow \mathbb{R}^n$  is a multivariable polynomial and  $x(0) = x_0$  is the initial state of the system. Assume that the origin ( $x = 0$ ) is a locally asymptotically stable equilibrium point. This assumption is without loss of generality because state coordinates can always be redefined to shift an equilibrium point to the origin. We are interested in computing the ROA ( $\mathcal{R}$ ) of the origin of the system 4.1. Recall the ROA ( $\mathcal{R}$ ) is defined as:

$$\mathcal{R} = \left\{ x_0 \in \mathbb{R}^n : \text{If } x(0) = x_0 \text{ then } \lim_{t \rightarrow \infty} x(t) = 0 \right\} \tag{4.2}$$

Computing the exact ROA for polynomial dynamical systems is difficult. There has been significant research devoted to estimating invariant subsets of the ROA [7, 10, 16–18, 38, 51, 52, 58]. The approach taken in this chapter is to restrict the ROA computation to ellipsoidal approximations of the ROA. Given an  $n \times n$  matrix  $N = N^T > 0$ , define the shape function  $p(x) := x^T N x$  and level set  $\Omega(p, \beta) := \{x \in$

$\mathbb{R}^n : p(x) \leq \beta$ .  $p(x)$  defines the shape of the ellipsoid and  $\beta$  determines the size of the ellipsoid  $\Omega(p, \beta)$ . The choice of  $p(x)$  or  $N$  is problem dependent and reflects dimensional scaling information as well as the importance of certain directions in the state space.  $N$  can typically be chosen to be diagonal with  $N_{i,i} := 1/x_{i,max}^2$ . With this choice,  $\Omega(p, \beta = 1)$  is a coordinate-aligned ellipsoid whose extreme points along the  $i^{th}$  state direction are  $\pm x_{i,max}$ . In this form, the level set value  $\beta$  provides an easily interpretable value for the size of the level set. The shape function  $p(x)$  also plays an important role in achieving better scalability properties of the optimization algorithm. Given the shape function  $p(x)$ , the ROA estimation problem reduces to finding the largest ellipsoid  $\Omega(p, \beta)$  contained in the ROA:

$$\begin{aligned} \beta^* &= \max \beta & (4.3) \\ \text{subject to: } & \Omega(p, \beta) \subset \mathcal{R} \end{aligned}$$

It is important to realize that Equation 4.3 does not provide an exact characterization of the ROA. Instead, Equation 4.3 is an optimization problem which determines the 'best' ellipsoidal ROA approximation. The lower and upper bounds for  $\beta^*$  satisfying  $\underline{\beta} \leq \beta^* \leq \bar{\beta}$  are computed. If the lower and upper bounds are close then the largest ellipsoid level set, defined by Equation (4.3), has been effectively computed.

#### 4.1.1 Upper Bound Computation

This section focuses on estimating the upper bound  $\bar{\beta}$  of the ellipsoidal ROA approximation. The upper bound is computed via a search for initial conditions leading to divergent trajectories. Recall the initial condition of the system is denoted by  $x(0)$ . Assume the trajectory of the system is divergent starting from  $x(0) = x_{0,div}$ . In other words,  $\lim_{t \rightarrow \infty} x(t) = +\infty$  when starting from  $x(0) = x_{0,div}$ . This implies that  $x_{0,div} \notin \mathcal{R}$ . Define  $\bar{\beta}_{div} := p(x_{0,div})$  and  $\Omega(p, \bar{\beta}_{div}) = \{x \in \mathbb{R}^n : p(x) \leq \bar{\beta}_{div}\}$  then  $\Omega(p, \bar{\beta}_{div}) \not\subset \mathcal{R}$  which implies  $\beta^* \leq \bar{\beta}_{div}$  and  $\Omega(p, \beta^*) \subseteq \Omega(p, \bar{\beta}_{div})$ . An exhaustive Monte Carlo search is used to find the tightest possible upper bound on  $\beta^*$ . Specifically, random initial conditions are chosen starting on the boundary of a large ellipsoid. For example, choose  $x_0$  satisfying  $p(x_0) = \beta_{try}$  where  $\beta_{try}$  is sufficiently large such that  $\beta_{try} \gg \beta^*$ . If a divergent trajectory is found, the initial condition is stored and an upper bound on  $\beta^*$  is computed.  $\beta_{try}$  is then decreased by a factor of 0.995 and the search continues until a maximum number of simulations is reached.  $\bar{\beta}_{MC}$  denotes the smallest upper bound computed with this Monte Carlo search. Figure 4.1 demonstrates the concept of the ROA upper bound on a 2-state problem. The

blue solid line indicates stable trajectories while the red dashed line indicates unstable trajectories. The green solid ellipse is the estimated upper bound, since an initial condition (marked as rectangle) on this ellipse will result in a divergent trajectory.

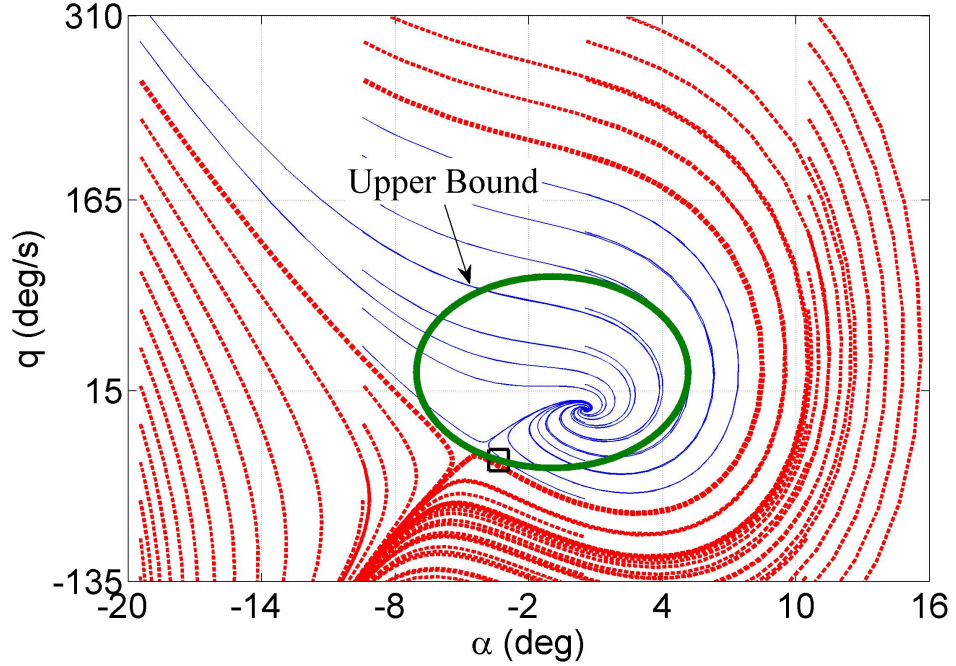


Figure 4.1: Upper Bound Estimate of ROA. Red (dashed) curves indicate unstable trajectories and blue (solid) curve indicate stable trajectories.

#### 4.1.2 Lower Bound Computation

This section focuses on estimating the lower bound  $\underline{\beta}$  of the ellipsoidal ROA approximation. The lower bound is computed using Lyapunov functions and the recent results connecting SOS polynomial optimization to semi-definite programming mentioned in Section 2.3. The algorithm to compute a lower bound using SOS optimizations is briefly described here. The full algorithmic details are described in the references [26–28, 48, 49, 55, 56].

Formally, Lemma 2 states the main Lyapunov theorem that will be used to quantify an invariant region. The proof of the lemma can be found in [48] and also in textbooks, e.g. in [59]. Given  $V$  and dynamics  $f(x)$ , define  $D(V, f) := \{x \in \mathbb{R}^n : \nabla V(x)f(x) < 0\} \cup \{0\}$ .

**Lemma 2.** *If there exists a real scalar  $\gamma > 0$  and a continuously differentiable function*

$V : \mathbb{R}^n \rightarrow \mathbb{R}$  such that:

$$V(0) = 0 \text{ and } V(x) > 0 \forall x \neq 0 \quad (4.4)$$

$$\Omega(V, \gamma) := \{x \in \mathbb{R}^n : V(x) \leq \gamma\} \text{ is bounded.} \quad (4.5)$$

$$\Omega(V, \gamma) \subset D(V, f) \quad (4.6)$$

then for all  $x_0 \in \Omega(V, \gamma)$ , the solution of Equation (4.1) exists, satisfies  $x(t) \in \Omega(V, \gamma)$  for all  $t \geq 0$ , and  $\Omega(V, \gamma) \subset \mathcal{R}$ .

A function  $V$ , satisfying the conditions in Lemma 2, is a Lyapunov function and  $\Omega(V, \gamma)$  provides an estimate of the ROA. Given any Lyapunov function  $V$ , it is desirable to find the largest sublevel set  $\Omega(V, \gamma)$  that is provably contained within the ROA. If  $\Omega(V, \gamma)$  is bounded  $\forall \gamma > 0$  then this problem can be formulated as:

$$\begin{aligned} \gamma^* &:= \sup_{\gamma} \gamma \\ &\text{subject to: } \Omega(V, \gamma) \subset D(V, f) \end{aligned} \quad (4.7)$$

For a given Lyapunov function  $V$ , the sublevel set  $\Omega(V, \gamma^*)$  is the largest provably invariant subset of the ROA. Technically, it can be shown by a continuity argument that there will be a point  $x_0$  on the boundary of  $\Omega(V, \gamma^*)$  such that  $\nabla V(x_0)f(x_0) = 0$ . Thus a more precise statement is  $\Omega(V, \gamma^*) \subset \mathcal{R}$  for all  $\gamma < \gamma^*$ .

If  $x = 0$  is asymptotically stable, a linearization can be used to compute a Lyapunov function [22]. Let  $A := \left. \frac{\partial f}{\partial x} \right|_{x=0}$  be the linearization of the nonlinear dynamics about the origin and compute  $P > 0$  that solves the Lyapunov equation  $A^T P + P A = -I$ .  $V_{LIN}(x) := x^T P x$  is a quadratic Lyapunov function that satisfies the conditions of Lemma 2 for sufficiently small  $\gamma > 0$ .  $V_{LIN}$  can be used to compute a lower bound on  $\beta^*$  by solving two maximization:

$$\begin{aligned} \gamma^* &:= \max \gamma \\ &\text{subject to: } \Omega(V, \gamma) \subset D(V_{LIN}, f) \end{aligned} \quad (4.8)$$

$$\begin{aligned} \underline{\beta} &:= \max \beta \\ &\text{subject to: } \Omega(p, \beta) \subset \Omega(V, \gamma^*) \end{aligned} \quad (4.9)$$

The first maximization finds the largest level set  $\Omega(V, \gamma^*)$  of  $V_{LIN}$  such that Lemma 2

can be used to verify  $\Omega(V, \gamma^*) \subseteq \mathcal{R}$ . The second maximization finds the largest ellipsoid  $\Omega(p, \beta)$  contain within  $\Omega(V, \gamma^*)$ .

Figure 4.2 demonstrates the concept of lower bound estimate to the ROA. The axis represents the state-space. The outermost (red) solid curve in Figure 4.2 indicates the region where  $\nabla V(x)f(x) < 0$ . The dashed (green) curve denotes the sublevel set of Lyapunov function,  $\Omega(V, \gamma)$ . This is an invariant subset of the ROA.

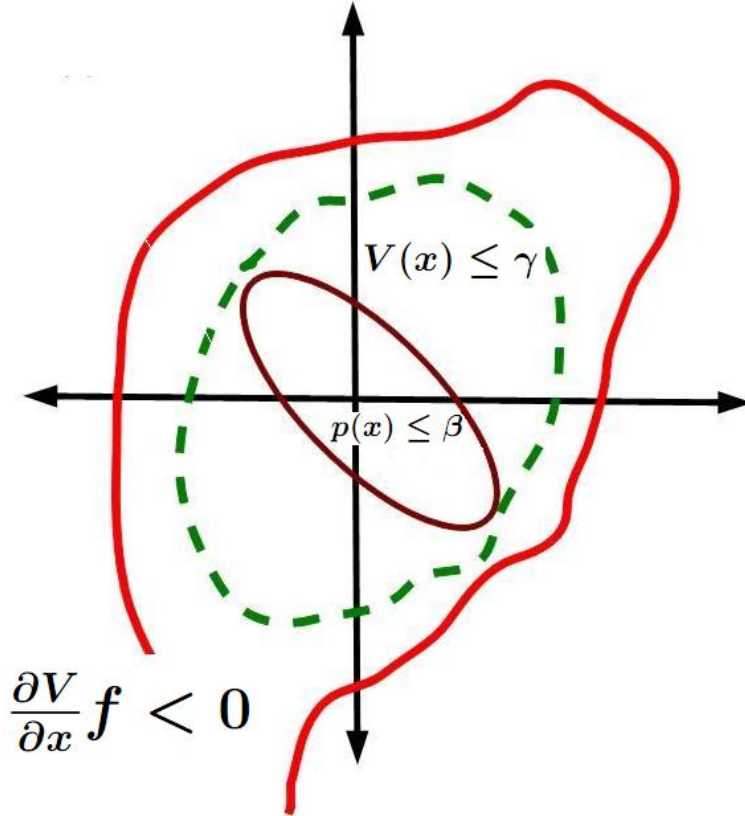


Figure 4.2: Lower Bound Estimate of ROA. The maroon ellipse  $p(x) \leq \beta$  indicates the lower bound estimate of the invariant set  $V(x) \leq \gamma$ .

The shape function  $p(x)$  reflects a cost function on the direction in the state-space. In other words,  $p(x)$  skews the analysis direction according to the analyst's choice. The choice of the shape function  $p(x)$  dictates the growth direction of the Lyapunov sublevel set  $V(x) \leq \gamma$ . It is important to realize that  $p(x) \leq \beta$  is not an invariant region, rather it is an inner estimate of an invariant sublevel set  $V(x) \leq \gamma$ .

The computational algorithm used in the analysis replaces the set containment constraints in Equation 4.8 and 4.9 with a sufficient S-procedure condition involving non-negative functions. For example,  $\Omega(p, \beta) \subset \Omega(V, \gamma^*)$  in Equation (4.9) is replaced

by

$$\begin{aligned} \underline{\beta} &:= \max_{\beta, s(x)} \beta & (4.10) \\ \text{subject to: } & s(x) \geq 0 \quad \forall x \\ & -(\beta - p(x))s(x) + (\gamma^* - V_{LIN}(x)) \geq 0 \quad \forall x \end{aligned}$$

The function  $s(x)$  is a decision variable of the optimization, i.e. it is found as part of the optimization. The function  $s(x)$  arises from the generalized S-procedure, which is discussed in Chapter 2.4.

It is straight-forward to show that the two non-negativity conditions in Equation (4.10) are a sufficient condition for the set containment condition in Equation (4.9). If  $s(x)$  is restricted to be a polynomial then both constraints involve the non-negativity of polynomial functions. Finally, replacing the non-negativity conditions in Equation (4.10) with SOS constraints, the SOS optimization problem is as follows:

$$\begin{aligned} \underline{\beta} &:= \max \beta & (4.11) \\ \text{subject to: } & s(x) \text{ is SOS} \\ & -(\beta - p(x))s(x) + (\gamma^* - V_{LIN}(x)) \text{ is SOS} \end{aligned}$$

There is software available to set up and solve these SOS problems [3,35,41,47].  $\underline{\beta}_{LIN}$  will denote the lower bound obtained from Optimization (4.11) using the quadratic Lyapunov function obtained from linearized analysis.

Unfortunately,  $\underline{\beta}_{LIN}$  is usually orders of magnitude smaller than the upper bound  $\bar{\beta}_{MC}$ . Several methods to compute better Lyapunov functions exist, including  $V$ - $s$  iterations [26–28, 49], bilinear optimization [48], and the use of simulation data [55, 56]. In this thesis, the  $V$ - $s$  iteration is used. The Lyapunov function  $V(x)$  in the iteration is initialized with  $V_{LIN}$ . The iteration also uses functions  $l_1(x) = -\epsilon_1 x^T x$  and  $l_2(x) = -\epsilon_2 x^T x$  where  $\epsilon_1$  and  $\epsilon_2$  are small positive constants on the order of  $10^{-6}$  to enforce strict positivity of the solution obtained from the SOS optimization framework. The  $V$ - $s$  iteration algorithm steps are:

1.  **$\gamma$  Step:** Hold  $V$  fixed and solve for  $s_2$  and  $\gamma^*$

$$\gamma^* := \max_{s_2 \in \text{SOS}, \gamma} \gamma \quad \text{s.t.} \quad -(\gamma - V)s_2 - \left( \frac{\partial V}{\partial x} f + l_2 \right) \in \text{SOS} \quad (4.12)$$

2.  $\beta$  Step: Hold  $V$ ,  $\gamma^*$  fixed and solve for  $s_1$  and  $\underline{\beta}$

$$\underline{\beta} := \max_{s_1 \in \text{SOS}, \beta} \beta \quad \text{s.t.} \quad -(\beta - p)s_1 + (\gamma^* - V) \in \text{SOS} \quad (4.13)$$

3.  $V$  step: Hold  $s_1$ ,  $s_2$ ,  $\underline{\beta}$ ,  $\gamma^*$  fixed and solve for  $V$  satisfying:

$$\begin{aligned} -(\gamma^* - V)s_2 - \left( \frac{\partial V}{\partial x} f + l_2 \right) &\in \text{SOS} \\ -(\underline{\beta} - p)s_1 + (\gamma^* - V) &\in \text{SOS} \\ V - l_1 &\in \text{SOS}, V(0) = 0 \end{aligned}$$

4. Repeat as long as the lower bound  $\underline{\beta}$  continues to increase.

**Remark 1:** The iteration is initialized with the linearized Lyapunov function  $V_{LIN}$ . However, it is not obvious if the  $\gamma$  step is feasible given the linearized Lyapunov function. [54] has shown that the  $\gamma$  step is feasible for a restricted class of polynomial systems given the linearized based analysis. Specifically, the system takes the form of  $\dot{x} = Ax + f_2(x) + f_3(x)$ , where  $f_2$  and  $f_3$  are purely quadratic and cubic polynomial vector fields.

The basic issue of the  $V - s$  iteration step is that searching for a Lyapunov function  $V$  results in a bilinear term  $Vs_2$  in the  $\gamma$  step. This bilinear term can not be handled directly within the SOS programming framework because the constraints in SOS programs must be linear in the decision variables. The  $V - s$  iteration avoids the bilinearity in  $Vs_2$  by holding either  $s_2$  or  $V$  fixed. Note, both  $\beta$  and  $\gamma$  steps are still bilinear in  $\beta s_1$  and  $\gamma s_2$ . However, a bisection search on  $\beta$  and  $\gamma$  can be used for both the steps. Consequently, each step of this iteration is a linear SOS optimization that can be solved with available software. In the  $V$ - $s$  iteration, the Lyapunov functions are allowed to have polynomial degree greater than two. Increasing the degree of the Lyapunov function will improve the lower bound at the expense of computational complexity.

The  $V$  step in the  $V - s$  iteration requires additional discussion. An interior-point linear matrix inequality solver is used to find a feasible solution to the feasibility problem in the  $V$  step. The Lyapunov function  $V$  used in the  $\gamma$  and  $\beta$  steps will be feasible for the constraints in the  $V$  step. Thus it is possible for the solver to simply return the same Lyapunov function that was used in the  $\gamma$  and  $\beta$  steps. While this is possible, it is typical for the solver to return a different  $V$  that allows both  $\gamma$  and

$\beta$  to be increased at the next iteration. This step can be justified by the fact that interior point solvers try to return a solution at the analytic center of set specified by the linear matrix inequality constraints. Thus the  $V$  step typically returns a feasible  $V$  that is “pushed away” from the constraints. A more formal theory for the behavior of this feasibility step is still an open question.

#### Alternate Approach to $V - s$ Iteration

A modified  $V - s$  iteration approach is developed to reduce the computational time. We will refer to this approach as *modified  $V - s$  iteration*. To avoid confusion, we will refer to the  $V - s$  iteration approach discussed above as the *original  $V - s$  iteration*.

The *original  $V - s$  iteration* is computationally expensive due to the bisection search on both  $\beta s_2$  and  $\gamma s_1$  in the  $\beta$  and  $\gamma$  steps. The computational time can be greatly reduced by reducing the bisection search to unidirectional search on the optimization parameters. The main idea behind the *modified  $V - s$  iteration* is to hold the multipliers ( $s_2$  and  $s_1$ ) fixed and maximize  $\beta$  and  $\gamma$  respectively. This requires an initial feasible knowledge about the multipliers ( $s_2$  and  $s_1$ ). The initial feasible solution of the multipliers can be achieved by running the *original  $V - s$  iteration* for one iteration step. The *modified  $V - s$  iteration* approach is outlined below:

1. Initialization: Run  $V - s$  iteration for  $n$  steps. Usually,  $n = 1$  is sufficient.
2. Hold  $\underline{\beta}$ ,  $\gamma^*$ ,  $s_2$  fixed and solve for  $V$  and  $s_1$  by solving Equation 4.12 and 4.13.
3. Hold  $V$ ,  $\gamma^*$ ,  $s_1$  fixed and maximize  $\beta$  subject to Equation 4.12. Denote the maximum value as  $\underline{\beta}$ .
4. Hold  $V$ ,  $s_2$  fixed and maximize  $\gamma$  subject to Equation 4.13. Denote the maximum value as  $\gamma^*$ .
5. Hold  $V$ ,  $\gamma^*$  fixed and find a feasible  $s_2(x)$  subject to Equation 4.13.
6. Stopping Criteria: Repeat (2) - (5) as long as the lower bound  $\underline{\beta}$  continues to increase or maximum iteration has been reached.

Note that the steps from (2)- (5) do not involve bisection. The initialization step only requires the  $V - s$  iteration to run for one step. All other steps turn out to be a linear SOS optimization problem. This modified  $V - s$  iteration can greatly reduce the

computational time of estimating ROA compared to the previously proposed  $V - s$  iteration. The modified  $V - s$  iteration approach usually works well in practice.

Next, we focus on applying the ROA estimation technique on the GTM flight control example.

### 4.1.3 ROA Analysis of 4-State Longitudinal GTM Model

This section estimates the stability region of the 4-state longitudinal GTM dynamics with a simple proportional inner-loop control law. The stability region is defined in terms of ROA. The ROA estimation is performed for two different flight conditions, one close to the stall speed and the other one away from the stall speed. The objective of the analysis is to compare the size of ROA between the two flight conditions.

The 4-state longitudinal (polynomial) GTM dynamics have been developed in Chapter 3. An inner loop (proportional) pitch rate feedback is used to improve the damping of the longitudinal model of the GTM aircraft  $\mathcal{P}_{\mathcal{GTM}}(x, u)$ , mentioned in Equation 3.13:

$$\delta_{elev} = K_q q + \delta_{elev,t} = 0.0698q + \delta_{elev,t} \quad (4.14)$$

where  $\delta_{elev,t}$  denotes the trim value. Equations 3.13 and 4.14 describe the polynomial dynamics of the closed-loop system with the thrust being held at its trim value.

The stall speed for the GTM is known to be 90 ft/s [1,32]. The analysis is performed around the level flight conditions at (i)  $V = 100$  ft/s, close to the stall speed and (ii)  $V = 150$  ft/s, away from the stall speed. The trim points are given below:

$$\begin{bmatrix} V_t \\ \alpha_t \\ q_t \\ \theta_t \end{bmatrix} = \begin{bmatrix} 150.00 \text{ ft/s} \\ 0.04690 \text{ rad} \\ 0 \text{ rad/s,} \\ 0.04690 \text{ rad} \end{bmatrix}, \quad \begin{bmatrix} \delta_{elev,t} \\ \delta_{th,t} \end{bmatrix} = \begin{bmatrix} 14.78 \% \\ 0.0506 \text{ rad} \end{bmatrix} \quad (4.15)$$

$$\begin{bmatrix} V_t \\ \alpha_t \\ q_t \\ \theta_t \end{bmatrix} = \begin{bmatrix} 100.00 \text{ ft/s} \\ 0.1505 \text{ rad} \\ 0 \text{ rad/s,} \\ 0.1505 \text{ rad} \end{bmatrix}, \quad \begin{bmatrix} \delta_{elev,t} \\ \delta_{th,t} \end{bmatrix} = \begin{bmatrix} 15.73 \% \\ -0.0223 \text{ rad} \end{bmatrix} \quad (4.16)$$

The subscript “t” denotes a trim value.

The goal is to perform the ROA analysis for the closed loop GTM aircraft around

the mentioned flight conditions and compare the size of their stability region. This analysis will help the flight control engineer to gain insight about the safe flight envelope.

First, we focus on the ROA analysis around the level flight condition at  $V = 150$  ft/s, away from the stall speed. We employ the estimation technique mentioned in Section 4.1. Recall, the estimation require a shape function  $p(x)$ . Consider the shape function to be  $p(x) = x^T N x$  where,

$$\begin{aligned} N &:= \text{diag}(50 \text{ ft/s}, 0.3491 \text{ rad}, 0.8727 \text{ rad/s}, 0.3491 \text{ rad})^{-2} \\ &:= \text{diag}(50 \text{ ft/s}, 20 \text{ deg}, 50 \text{ deg/s}, 20 \text{ deg})^{-2} \end{aligned} \quad (4.17)$$

The shape function,  $p(x)$ , roughly scales each state by the maximum magnitude observed during the flight condition. At straight and level flight,  $\alpha$  and  $\theta$  are expected to have similar deviations. Hence, the maximum deviation for both  $\alpha$  and  $\theta$  are chosen to be of the same magnitude. The velocity is assumed to deviate at most 50 ft/s from its trim airspeed of 150 ft/s during the flight condition. Recall, the polynomial model is valid over the range of airspeed from 100 ft/s to 200 ft/s. The maximum deviation in pitch rate is chosen so that it stays within the range of model validity in the pitch rate direction. Recall that the polynomial model is valid for  $-70 \text{ deg/s} \leq q \leq 70 \text{ deg/s}$ .

The polynomial model of the longitudinal dynamics was modified in two ways to make it suitable for the computational algorithms. First the states were redefined as  $z := x - x_t := [V - V_t, \alpha - \alpha_t, q - q_t, \theta - \theta_t]^T$  to shift the trim condition to the origin of the state space. Next, all polynomial terms with degree greater than five and/or coefficients less than  $10^{-6}$  were removed from the model. The terms have negligible effect on the model but their removal greatly reduces the computation time for the lower bounds due to the computation of the  $V$ -s iteration growing rapidly with the degree of the polynomial model and the Lyapunov function.

Scaling of the model is another important issue for the numerical stability of the  $V$ -s iteration. The magnitude of the coefficients in the fifth order closed-loop polynomial model can vary greatly. For example, the magnitude of the minimum and maximum coefficients in the velocity derivative equation ( $\dot{V}$ ) are  $3.335 \times 10^{-6}$  and  $2.902 \times 10^2$ , respectively. Scaling of the closed-loop state-space dynamics is used to improve the numerical conditioning. The states are scaled as  $z_{scl} = D z$  where  $D = N^2$ . In the  $z_{scl}$  coordinates the shape function is  $p(z_{scl}) = z_{scl}^T z_{scl}$ . After scaling the magnitude of the minimum and maximum coefficients in the velocity derivative equation ( $\dot{V}$ ) are

$4.132 \times 10^{-6}$  and 0.7072, respectively. The  $V$ -s iteration is run on the scaled model and results converted back to unscaled coordinates.

The  $V$ -s iteration with a quartic Lyapunov function resulted in a lower bound estimate of  $\underline{\beta}_4 = 3.360$ . This verifies that the ellipsoid  $\Omega(p, \underline{\beta}) := \{x \in \mathbb{R}^n : p(x) \leq \underline{\beta}\}$  is a subset of the ROA. The center of the ellipsoid is at the trim condition. It has a length of  $20 \text{ deg} \cdot \sqrt{\underline{\beta}} = 36.66 \text{ deg}$  along the  $\alpha$  axis. The other axis lengths can be computed similarly. The upper bound from Monte Carlo simulation approach is computed to be  $\bar{\beta}_{MC} = 3.760$ . In other words, Monte Carlo simulation found an unstable trajectory with a point on the ellipsoid  $\Omega(p, \underline{\beta}_{MC})$ .

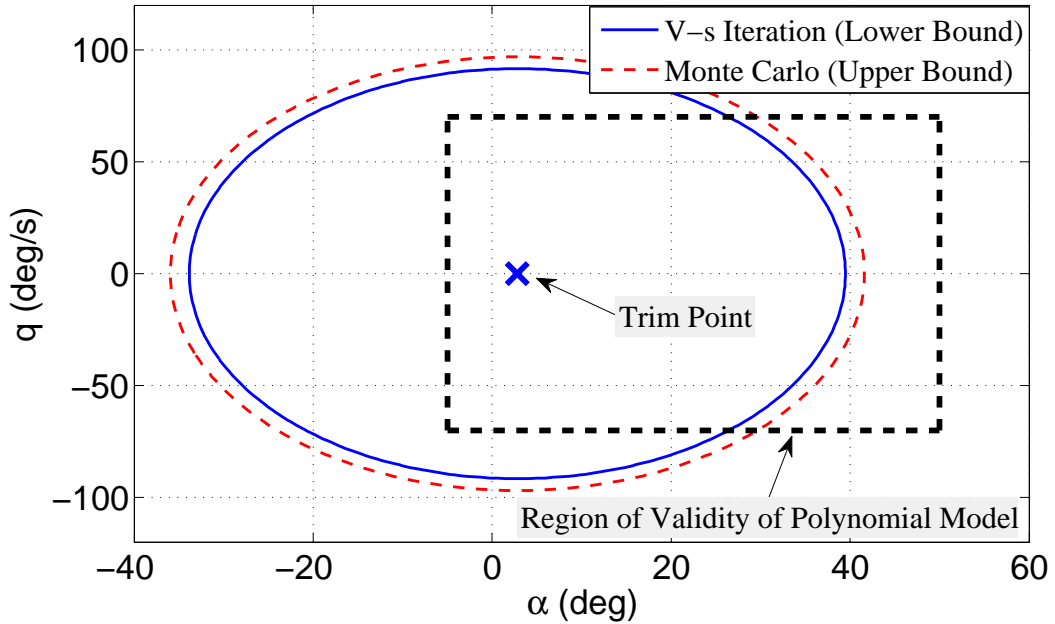


Figure 4.3: Lower and Upper Bound Estimate of ROA for the GTM longitudinal model at  $V = 150 \text{ ft/s}$ ; the rectangular region defines the validity region of the model

The ROA ellipsoidal bounds on the ROA can be visualized by plotting slices of the ellipsoids  $\Omega(p, \underline{\beta})$  and  $\Omega(p, \underline{\beta}_{MC})$ . Figure 4.3 shows slices of these ellipsoidal ROA bounds in the  $\alpha$ - $q$  plane. The solid ellipse is the slice of the  $\Omega(p, \underline{\beta})$ . Every initial condition within this ellipse will return to the trim condition (marked as an 'x'). The dashed ellipse is the slice of  $\Omega(p, \underline{\beta}_{MC})$  in the  $\alpha$ - $q$  plane. There is an unstable trajectory that touches  $\Omega(p, \underline{\beta}_{MC})$  although it may not necessarily touch the ellipse in the  $\alpha$ - $q$  plane. The Monte Carlo search returned the following initial condition

yielding an unstable trajectory.

$$\begin{aligned} x_{0,div} &:= [148.82 \text{ ft/s}, -0.62 \text{ rad}, 0.37 \text{ rad/s}, 1.19 \text{ rad}]^T \\ &:= [148.81 \text{ ft/s}, -35.70 \text{ deg}, 21.21 \text{ deg/s}, 68.51 \text{ deg}]^T \end{aligned}$$

The dotted rectangular box in Figure 4.3 shows the region of validity for the model. The region of validity for the polynomial model is explained in Section 3.2.2. The closeness of the inner and outer ellipsoids implies, for engineering purposes, that the best ROA ellipsoid problem has been solved.

Now, we focus on performing the ROA analysis around the straight level flight condition at  $V = 100 \text{ ft/s}$ , close to the stall speed of  $90 \text{ ft/s}$ . From flight dynamics perspective, the stall region is crucial and hence the flight control engineer need to investigate the stall region more closely. The stability and performance of any aircraft usually diminished at stall speed. Particularly, the aircraft possesses zero controllability at stall speed. Hence, this is region is more sensitive to disturbances.

We perform ROA analysis at  $V = 100 \text{ ft/s}$ . Figure 4.4 shows  $\alpha - q$  slices of the ellipsoidal bounds to the ROA. The  $V$ -s iteration with a quartic Lyapunov function verifies that the ellipsoid  $\Omega(p, \underline{\beta}) := \{x \in \mathbb{R}^n : p(x) \leq 1.460\}$  is a subset of the ROA. Again, the center of the ellipsoid is at the trim condition and It has a length of  $20 \text{ deg} \cdot \sqrt{\underline{\beta}} = 24.16 \text{ deg}$  along the  $\alpha$  axis. The other axis lengths can be computed similarly. The upper bound from Monte Carlo simulation approach is computed to be  $\bar{\beta}_{MC} = 1.950$ .

It is evident from comparing Figure 4.4 and Figure 4.3 that the size of ROA close to the stall speed has shrunk significantly. This is expected as discussed earlier. In fact, the reduction of the ROA size is more dramatic if the volume of the ROA estimate is considered. The volume of the ellipsoid  $\Omega(p, \underline{\beta})$  is proportional to  $\beta^{(n/2)}$  where  $n = 4$  is the state dimension. This corresponds to a volume decrease of 5.296 for the model close to the stall speed. Thus information from these two ellipsoids can be used to draw conclusions about the safe flight envelope.

Both lower ( $\underline{\beta}$ ) and upper bounds ( $\bar{\beta}_{MC}$ ) of the ROA ellipsoid provide useful information. The lower bound ellipsoid  $\Omega(p, \underline{\beta})$  defines the set of initial conditions for which the control law will bring the aircraft back to its trim point. If the aircraft is perturbed due to a wind gust or other upset condition but remains within this ellipsoid, the control law will recover the aircraft and bring it back to trim. For example, the

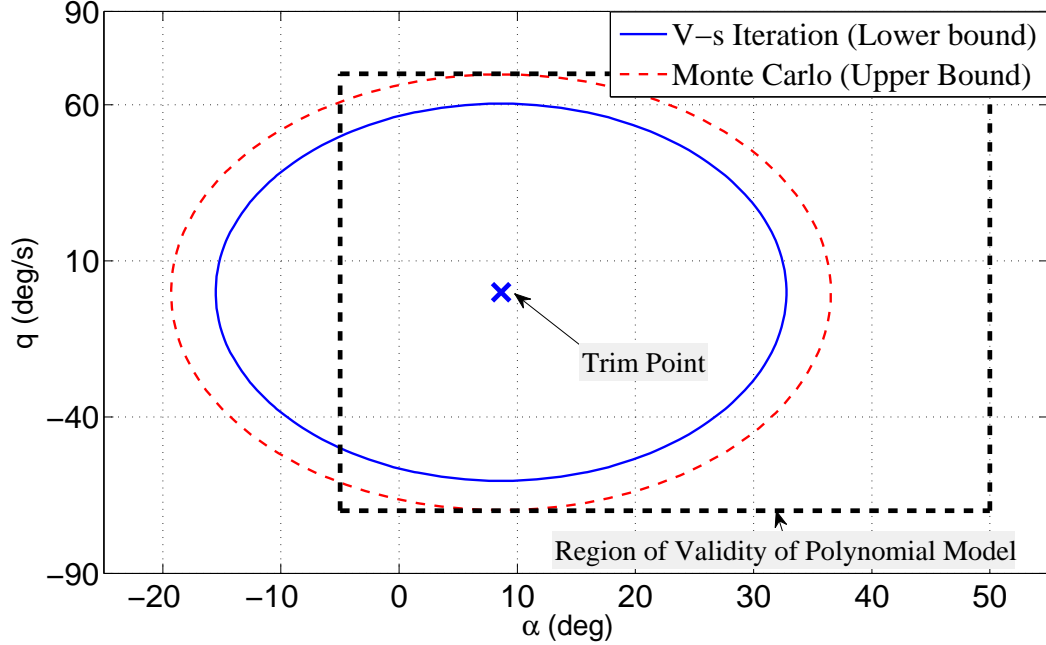


Figure 4.4: Lower and Upper Bound Estimate of ROA for the GTM longitudinal model at  $V = 100$  ft/s; the rectangular region defines the validity region of the model

state  $[V, \alpha, q, \theta]^T = [V_t, 30.00 \text{ deg}, 20.00 \text{ deg/s}, \theta_t]^T$  is inside  $\Omega(p, \underline{\beta})$  for both flight conditions. Similarly, the control law will bring the aircraft back to its trim point if a disturbance pushes the GTM aircraft to this state then. The upper bound ellipsoid  $\Omega(p, \underline{\beta}_{MC})$  contains at least one initial condition that will cause the aircraft to diverge from its trim condition. Upset conditions that push the aircraft state to this upper bound ellipsoid could lead to loss of control. In other words, information from these two ellipsoids can be used to draw conclusions about the safe flight envelope. The size of these ellipsoids measure the robustness of the flight control law to disturbances. In summary, the ellipsoids define a metric for the safe flight envelope of the GTM aircraft.

**Remark 1:**The ellipsoidal bounds in Figure 4.3 and/or Figure 4.4 are symmetric about the trim point. This is due to the choice of a shape function  $p$  centered at the trim point. The region of interest in the state space is not symmetric about the trim point. For example, the model region of validity is skewed toward positive angles of attack. It is possible to perform the ROA analysis with shape functions that are not symmetric about the trim point. However the theoretical and algorithmic details of non-symmetric shape functions have not been fully developed.

## 4.2 Induced $L_2$ ( $L_2 \rightarrow L_2$ ) Gain Estimation

Consider a polynomial dynamical system of the form:

$$\dot{x} = f(x, u) \tag{4.18a}$$

$$y = h(x) \tag{4.18b}$$

where  $x \in \mathbb{R}^n$ ,  $u \in \mathbb{R}^{n_u}$  is the state and input vector.  $f : \mathbb{R}^n \times \mathbb{R}^{n_u} \rightarrow \mathbb{R}^n$  is a multivariable polynomial describing system dynamics and  $y = h : \mathbb{R}^n \rightarrow \mathbb{R}^{n_y}$  is a multivariable polynomial denoting the output equation. Assume,  $f(0, 0) = 0$  and  $h(0) = 0$ . The polynomial system will not, in general, be globally stable. If the system is only locally stable then a sufficiently large disturbance can drive the state and the output of the system will be unbounded. Hence, it is of interest to characterize the local  $L_2$  gain where attention is restricted to “local” inputs  $u$  that satisfy  $\|u\|_2 \leq R$  where  $R \in \mathbb{R}_+$ . This section presents an approach to estimating the local (induced)  $L_2$  gain,  $\gamma_R$ , of the System 4.18 from  $u$  to  $y$ . The local  $L_2$  gain, defined in Equation 5.5, is stated here again for completeness:

$$\gamma_R := \sup_{\substack{u \in L_2, \|u\|_2 \leq R \\ x(0)=0}} \frac{\|e\|_2}{\|u\|_2} \tag{4.19}$$

Computing the exact input-to-output gain  $\gamma_R$  for nonlinear systems is a challenging problem [2]. Instead, we will be interested in estimating lower and upper bounds of the gain. Lower bounds will be computed by randomly searching for a destabilizing input. This section focuses on estimating upper bounds. Lemma 1 provides a dissipation inequality for characterizing the upper bound of the induced  $L_2$  gain for globally stable system. The dissipation inequality in Equation 2.7 can be restricted to hold only on a certain sub-level set of the state space in order to estimate the local induced  $L_2$  gain. Lemma 3 provides a local dissipation inequality to quantify how the  $L_2$  energy gain varies for different input size,  $R$ . This result is proved in [48] but very similar results are given in textbooks, e.g. by [59].

**Lemma 3.** *If there exists  $\gamma > 0$  and a polynomial  $V : \mathbb{R}^n \rightarrow \mathbb{R}$  such that:*

$$V(0) = 0 \text{ and } V(x) > 0 \ \forall x \neq 0 \tag{4.20}$$

$$\nabla V(x)f(x, u) \leq u^T u - \frac{1}{\gamma^2} y^T y \ \forall x \in \Omega_V, \mathbb{R}^2 \text{ and } u \in \mathbb{R}^{n_u}, \tag{4.21}$$

then the system in Equation 4.18 with  $x(0) = 0$  satisfies  $\|y\|_2 \leq \gamma R$  whenever  $\|u\|_2 \leq R$ .

There are two equivalent questions one may ask: (i) Given  $R$  such that  $\|u\|_2 < R$ , what is a tight upper bound for the induced  $L_2 \rightarrow L_2$  gain  $\gamma$ , or (ii) Given the upper bound  $\gamma$ , what is the largest value of  $R$  such that  $\|y\|_2 \leq \gamma R$  whenever  $\|d\|_2 < R$ ? We focus on answering the latter question.

Similar to the ROA problem, the dissipation inequality conditions provided by Lemma 3 can be turned into an SOS optimization problem. The dissipation inequality (Equation 4.21) in Lemma 3 can be expressed as the following set containment condition:

$$\Omega_{V,R^2} \subset \{(x, u) : \nabla V(x) \cdot f(x, u) \leq u^T u - \frac{1}{\gamma^2} y^T y\} \quad (4.22)$$

The set containment constraint in Equation 4.22 is replaced with a sufficient condition involving non-negative polynomials [38] by applying generalized S-procedure.

$$-[(R^2 - V)s(x, u) + \nabla V \cdot f(x, u) - u^T u + \frac{1}{\gamma^2} y^T y] \geq 0 \quad (4.23)$$

where the function  $s(x, u) \geq 0$  is a decision variable of the optimization, i.e. it is found as part of the optimization. If  $s(x, u)$  and  $V(x)$  are restricted to be polynomial, both constraints involve the non-negativity of polynomial functions. The non-negativity conditions can be replaced by sufficient SOS constraints. Finally, the dissipation inequality conditions provided in Lemma 3 are reformulated as an SOS optimization problem.

$$\bar{R} := \max R$$

subject to:

$$V(x) \text{ is SOS, } V(0) = 0 \quad (4.24a)$$

$$-[(R^2 - V)s + \nabla V \cdot f(x, u) - u^T u + \frac{1}{\gamma^2} y^T y] \text{ is SOS} \quad (4.24b)$$

$$s(x, u) \text{ is SOS} \quad (4.24c)$$

Note that the above optimization problem is bilinear in decision variables. For example, the term  $Vs(x, u)$  in Equation (4.24b) is bilinear in decision variable. If either  $V$  or  $s$  is fixed then the problem is quasiconvex and can be solved via bisection on  $R$ . Thus a  $V$ - $s$  type iteration, similar to the one proposed for estimating the ROA,

is formulated where  $V$  is solved for fixed  $s$  and vice versa. The storage function  $V$  in the iteration is initialized with the linearized storage function  $V_{LIN}$  by solving the following SOS condition.

$$-\nabla V_{LIN} \cdot f_{LIN}(x, u) - u^T u + \frac{1}{\gamma_{LIN}^2} y_{LIN}^T y_{LIN} \text{ is SOS} \quad (4.25)$$

where  $f_{LIN}$ ,  $y_{LIN}$  represents the linearization of  $f$  and  $y$ ,  $\gamma_{LIN}$  is the  $L_2$  energy gain for linearized system. Note that Equation (4.25) can be written as a Linear Matrix Inequality (LMI) in  $(x, u)$  if  $V_{LIN}$  is restricted to be quadratic,  $V_{LIN} = x^T P x$ . [4] presents the LMI formulation of the dissipation inequality.  $\gamma_{LIN}$  can be found by solving for the smallest possible  $\gamma$  that satisfies the feasibility of Equation 4.25 or the LMI formulation.

The  $V$ - $s$  iteration algorithm is applied for a given  $\gamma > \gamma_{LIN}$ . The iteration steps are:

1.  $R^2/s$  Step: Hold  $V$  fixed and solve for  $s$  and  $\bar{R}$

$$\begin{aligned} \bar{R} &:= \max R \\ &\text{subject to:} \\ &\text{Equation (4.24b) - (4.24c)} \end{aligned}$$

This step performs a bisection search on  $R$ .

2.  $V$  step: Hold  $\bar{R}$ ,  $s(x, u)$  fixed and solve for  $V$  satisfying Equation (4.24a) - (4.24c).
3. Repeat  $R^2/s$  and  $V$  step as long as the  $\bar{R}$  continues to increase.

**Remark 2:** The feasibility of the  $R^2/s$  step was established in [54] for a restricted class of polynomial system given that the linear analysis is conclusive. Specifically, the class of system takes the following form:

$$\begin{aligned} \dot{x} &= f(x, u) = Ax + Bu + f_2(x) + f_3(x) + (g_1(x) + g_2(x)) u \\ y &= h(x) = Cx + h_2(x) \end{aligned}$$

where  $A$ ,  $B$  and  $C$  are linear representation of the vector fields  $f(x, u)$  and  $h(x)$ .  $f_2$ ,  $g_2$ ,  $h_2$  are purely quadratic,  $f_3$  is cubic, and  $g_1$  is linear polynomial vector fields in  $x$ . Proof of feasibility is constructive and hence specific to the polynomial dynamics represented by  $f(x, u)$  and  $h(x)$ .

Similar to the ROA  $V - s$  iteration steps, there is no guarantee that the  $V$  step will provide a different storage function at each iteration step. It is possible to obtain the same storage function from the previous step. While this is possible, it is typical for the solver to return a different  $V$  that allows  $R$  to be increased at the next iteration. Next, we investigate the induced  $L_2$  gain behavior of the GTM flight control example.

#### 4.2.1 Induced $L_2$ Gain Analysis of 4-State Longitudinal GTM Model

This section describes the computation of the  $L_2$  gain bounds for both open and closed-loop longitudinal dynamics of the GTM. The  $L_2 \rightarrow L_2$  gain analysis is performed around the flight condition mentioned in Equation 4.15. The controller is the simple proportional pitch rate feedback control mentioned in Equation (4.14). Equations 3.13 and 4.14 describe a 4-state seven degree polynomial dynamics of the closed-loop system with the thrust being held at its trim value.

Consider an additive disturbance,  $d_{elev}$  in the elevator channel. Physically, this additive disturbance can be viewed as wind disturbances in the elevator channel. The objective is to quantify the controller's performance against the wind disturbances in the elevator channel. Particularly, this section estimates the  $L_2 \rightarrow L_2$  gain from elevator disturbances ( $d_{elev}$ ) to pitch rate ( $q$ ) for both open and closed-loop longitudinal dynamics of the GTM.

Note the SOS optimization problem for induced gain estimation of the GTM involve 5 polynomial variables (4-state and  $d_{elev}$ ) as opposed to 4 in the case of the ROA estimation problem. To reduce computational time, the induced  $L_2$  gain analysis was performed on a cubic order GTM model. The cubic order model is extracted from the 4-state seven degree polynomial model by retaining terms upto cubic order. Moreover, the cubic order model was validated against the original nonlinear GTM model by comparing numerous simulation responses. The analysis is performed on this cubic order model for both open-loop and closed-loop dynamics.

The  $V - s$  iteration is applied to estimate the induced  $L_2$  gain of the GTM. Figure 4.5 indicates how the induced gain of the system varies as the size of the elevator disturbances  $\|d_{elev}\|_2$  increases. The horizontal axis indicates the size of the elevator disturbances,  $\|d_{elev}\|_2$  around the trim input value and the vertical axis shows the estimated bounds of the induced gain from  $d_{elev}$  to  $q$ .

The linear gain is estimated by solving the LMI formulation of the dissipation in-

equality [4] for both the open-loop and closed-loop linearized system. The induced gain for the open-loop system is computed to be 23.9 and the pitch rate feedback reduces the induced gain of the closed-loop system to 16.6. Note that the induced gain for the linearized system is the same for different input sizes. Hence, computing the induced  $L_2$  gain of nonlinear systems is important in assessing how disturbances of different sizes affect the controller's performance.

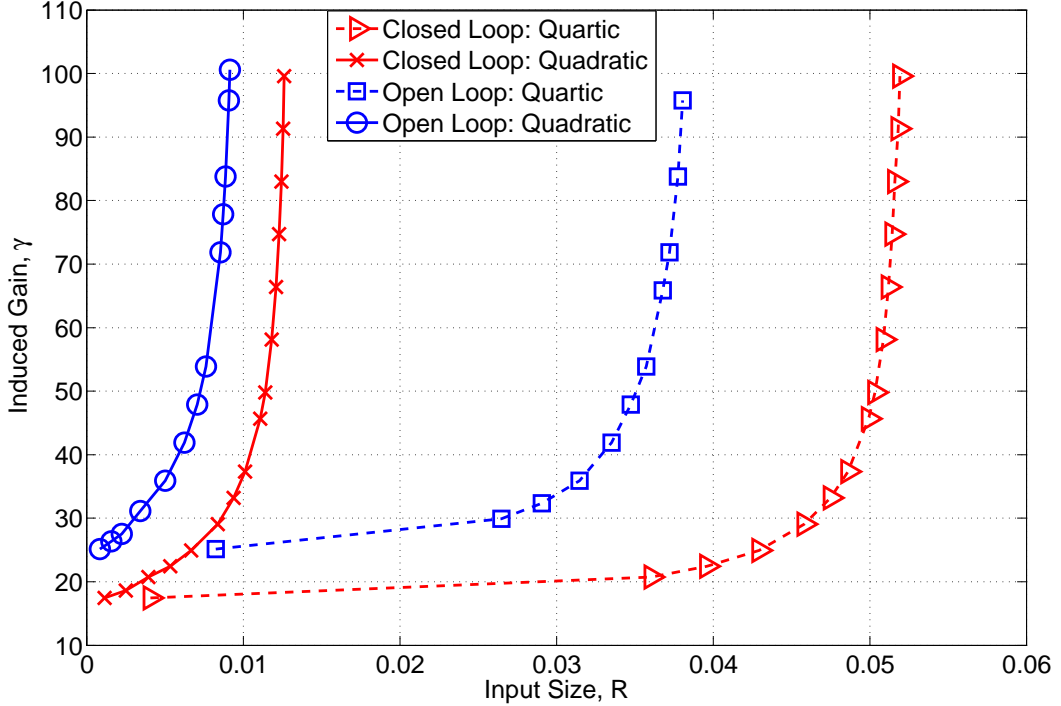


Figure 4.5: Estimation of induced  $L_2 - L_2$  gain bounds from  $d_{elev}$  to  $q$  for open-loop and closed-loop GTM model. The open-loop and the closed-loop system is found to be divergent with an input size of 0.08 and 0.11, respectively.

The upper bounds are estimated for both the open-loop and closed-loop dynamics by searching for quadratic and quartic storage function. The quadratic storage function for the open-loop (marked as -o) proves that the system can tolerate disturbance of size  $\|d_{elev}\|_2 < 9.10 \times 10^{-3}$ , while the quadratic storage for the closed-loop (marked as -x) proves the system can tolerate disturbance of size  $\|d_{elev}\|_2 < 1.26 \times 10^{-2}$ . The quartic storage function improves these bounds. The quartic storage function for the open-loop system (marked as - -□) and the closed-loop system (marked as - -▷) proves the system can tolerate an input disturbance of size  $\|d_{elev}\|_2 < 3.80 \times 10^{-2}$  and  $\|d_{elev}\|_2 < 5.20 \times 10^{-2}$ , respectively. Clearly, the pitch rate feedback improves the induced gain of the system. However, these bounds are an upper estimate of the induced gain of the system. The lower bounds are estimated by randomly searching

for inputs that cause the state trajectory to diverge. An input of size  $\|d_{elev}\|_2 = 8.00 \times 10^{-1}$  is found which causes the open-loop system to diverge. The closed-loop system is found to be divergent for an input of size  $\|d_{elev}\|_2 = 1.10 \times 10^{-1}$ . Note that the lower bounds are not shown in the Figure 4.5.

Figure 4.5 shows that the pitch rate feedback certainly improves GTM's robustness against the wind disturbance in the elevator channel. Moreover, Figure 4.5 also shows how the system performs against wind disturbances of different sizes. In contrast, the linearized analysis does not provide any insights on how disturbances of different sizes affect the system.

The upper bound results are conservative. The quadratic storage function provides a very conservative estimate. Note that the lower bound is below all gains (linearized, quadratic, and quartic). This is reasonable since the other gains are supposed to be upper bounds on the actual gain.

### 4.3 Summary

This chapter focuses on estimating the ROA and the induced  $L_2$  gain for smooth polynomial dynamical systems. Lyapunov and dissipation theory are used to estimate lower bound for the ROA and upper bound for the induced  $L_2$  gain. Sufficient set containment conditions are formulated to estimate these bounds. Iterative algorithms based on SOS optimization are formulated to solve the set containment conditions. These SOS based bounds can be very conservative. Hence, simulation based bounds are also proposed to complement the SOS based bounds. Both the ROA and the  $L_2$  gain estimation techniques are then applied to the GTM's longitudinal polynomial dynamics. The presentation of this chapter is more along the lines of discussing practical implementation issues of the SOS algorithms for moderately large scale problems, rather than a detailed description of the theory or algorithms themselves. The presentation also focused on how the SOS tools can help the flight control engineers to verify stability and performance of nonlinear flight control systems.

## Chapter 5

# Local Performance Analysis of Polynomial Systems with Actuator Saturation

This section considers the problem of estimating the local induced  $L_2$  gain of polynomial systems with actuator saturation. A majority of the research on analyzing feedback control systems with actuator saturation assumes that both the plant and the controller are linear. In practice, the Circle and the Popov criteria are two commonly used methods [31] for analyzing feedback control systems. The Circle criterion analyzes a linear time invariant (LTI) system in feedback with a memoryless, time-varying sector bounded static nonlinearity. The Popov criterion analyzes an LTI system with a memoryless, static sector-bounded nonlinearity. The Circle or the Popov criteria are used in [22, 40] to estimate Lyapunov functions for proving stability and performance bounds for linear systems with actuator saturation. The Lyapunov function is found by solving Linear Matrix Inequality (LMI) conditions. Another method, not involving Circle and Popov criteria, can be found in [13], where the saturated linear systems are analyzed by expressing the saturation function as a convex combination of piecewise linear functions.

Analyzing nonlinear systems with saturated input is still an ongoing research problem. Analysis tools for nonlinear systems in feedback with an actuator saturation are not yet well-developed. This chapter presents a method for estimating an upper bound of the local induced  $L_2$  gain for polynomial systems with hard nonlinearities, e.g., saturation and rate limits. The gain upper bound condition is formulated in terms of a

dissipation inequality that incorporates an integral quadratic constraint to model the hard nonlinearities. The dissipation inequality can be verified using sum-of-squares optimizations. This approach is applied to systems with actuator's position and rate limits. The effectiveness of the proposed method is demonstrated in two numerical examples.

## 5.1 Problem Formulation

The main goal of this chapter is to analyze performance of polynomial dynamic systems in feedback with actuator saturation. Consider the feedback interconnection

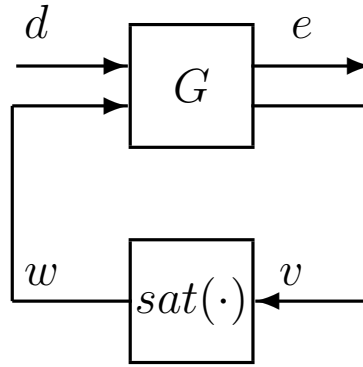


Figure 5.1: Feedback Interconnection of  $G - sat(\cdot)$

in Figure 5.1. The input-output equations associated with this interconnection are given by Equations 5.1 and 5.2.

$$\begin{bmatrix} e \\ v \end{bmatrix} = G \begin{bmatrix} d \\ w \end{bmatrix} \quad (5.1)$$

$$w = sat(v) \quad (5.2)$$

$G(x, d, w)$  is a dynamical system expressed by polynomial vector fields of the following form:

$$\dot{x} = f(x, d, w) \quad (5.3)$$

$$\begin{bmatrix} e \\ v \end{bmatrix} = \begin{bmatrix} h_1(x) \\ h_2(x) \end{bmatrix} = h(x) \quad (5.4)$$

where  $x(t) \in \mathbb{R}^n$  is the state vector,  $d(t) \in \mathbb{R}^{n_d}$  is the exogenous input,  $e(t) \in \mathbb{R}^{n_e}$  is the regulated output.  $w(t) \in \mathbb{R}^{n_w}$  and  $v(t) \in \mathbb{R}^{n_v}$  are the interconnection signals between  $G$  and  $sat(\cdot)$ . Moreover,  $f : \mathbb{R}^n \times \mathbb{R}^{n_d} \times \mathbb{R}^{n_w} \rightarrow \mathbb{R}^n$  and  $h : \mathbb{R}^n \rightarrow \mathbb{R}^{n_e+n_v}$  are both multivariable polynomials. Assume  $f(0, 0, 0) = 0$  and  $h(0) = 0$ . Note that  $h$  is not considered as a function of inputs  $w$  and  $d$ , i.e.  $G$  has no direct feedthrough from the inputs  $(d, w)$  to the outputs  $(e, v)$ .

The problem is to estimate an upper bound to the local induced  $L_2$  gain  $\gamma_R$ , as defined in Equation 5.5, of the interconnection ( Figure 5.1 ) from  $d$  to  $e$ . The local  $L_2$  gain is defined where attention is restricted to “local” inputs  $d$  that satisfy  $\|d\|_2 \leq R$  where  $R \in \mathbb{R}_+$ . The local  $L_2$  gain is formally defined in Equation 5.5.

$$\gamma_R := \sup_{\substack{d \in L_2, \|d\|_2 \leq R \\ x(0)=0}} \frac{\|e\|_2}{\|d\|_2} \quad (5.5)$$

## 5.2 Induced $L_2$ Gain Analysis

The approach is divided into three steps. First, the  $\Delta$  operator is modeled using the Integral Quadratic Constraint (IQC) framework [36]. Second, a dissipation inequality is formulated which provides a condition to estimate the local  $L_2$  energy gain bound [29]. Finally, a computational approach is proposed using the SOS framework.

### 5.2.1 Review of IQCs

IQCs, introduced in [36], provide a general framework for robustness analysis of linear dynamical systems with respect to uncertainties or nonlinearities. Assume that the uncertainties or nonlinearities are represented by  $\Delta$  in Figure 5.2. IQCs are used to constrain the input-output behavior of the uncertainties or nonlinearities. This section will focus on how to model  $\Delta$  using the IQC theory. It is required that  $\Delta$  be a bounded, causal operator which maps from  $L_2 \rightarrow L_2$ . Let  $\Pi : j\mathbb{R} \rightarrow \mathbb{C}^{(n_v+n_w) \times (n_v+n_w)}$

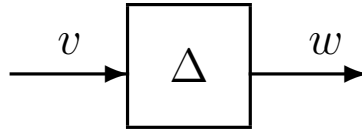


Figure 5.2: Uncertainties or nonlinearities represented by  $\Delta$

be a measurable, bounded Hermitian-valued function.  $\Delta$  is said to satisfy the IQC

defined by  $\Pi$ , if for all  $v \in L_2$ , with  $w = \Delta(v)$ , the following inequality holds [36],

$$\int_{-\infty}^{\infty} \begin{bmatrix} \hat{v}(j\omega) \\ \hat{w}(j\omega) \end{bmatrix}^* \Pi(j\omega) \begin{bmatrix} \hat{v}(j\omega) \\ \hat{w}(j\omega) \end{bmatrix} d\omega \geq 0 \quad (5.6)$$

where  $\hat{v}(j\omega)$  and  $\hat{w}(j\omega)$  are Fourier transforms of  $v$  and  $w$ , respectively. If the IQC multiplier  $\Pi$  is rational and uniformly bounded on the imaginary axis, then Equation 5.6 has an equivalent time domain expression. In that case,  $\Pi$  can be factorized as,  $\Pi(j\omega) = \Psi(j\omega)^* M \Psi(j\omega)$ , where  $M$  is a constant matrix and  $\Psi(s)$  is a stable Linear Time Invariant (LTI) filter.

**Remark:** The Laplace variable in this thesis is denoted as  $\mathbf{s}$ . This is to avoid confusion with the SOS multiplier  $s$ .

The time domain interpretation of the IQC in Equation 5.6 can be formulated as [36]:

$$\int_0^{\infty} y_{\psi}(t)^T M y_{\psi}(t) dt \geq 0 \quad (5.7)$$

where  $y_{\psi}$  is the output of the following state-space realization (See Figure 5.3).

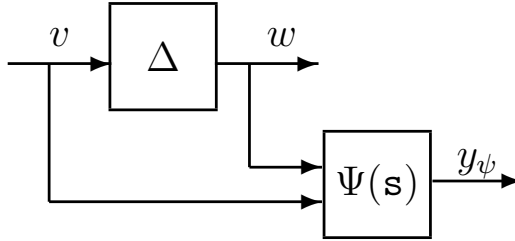


Figure 5.3: Time Domain Interpretation of IQCs

$$\dot{x}_{\Psi}(t) = A_{\Psi} x_{\Psi} + B_{\Psi 1} v + B_{\Psi 2} w \quad (5.8)$$

$$y_{\Psi}(t) = C_{\Psi} x_{\Psi} + D_{\Psi 1} v + D_{\Psi 2} w \quad (5.9)$$

$$x_{\Psi}(0) = 0 \quad (5.10)$$

Moreover,  $\Delta$  is said to satisfy the “hard” IQC defined by  $\Pi$  if,

$$\int_0^T y_{\psi}(t)^T M y_{\psi}(t) dt \geq 0 \quad \forall T < \infty \quad (5.11)$$

$\Delta$  is said to satisfy the “soft” IQC defined by  $\Pi$  if it is not “hard”, i.e. if the time domain quadratic constraint does not hold for all finite time intervals  $T$ . The

notions of “soft” and “hard” depend on the factorization of  $\Pi$  [44]. The dissipation inequality condition derived in this paper assumes that the “hard” conditions hold, i.e. the time-domain IQC condition is valid over all finite time intervals.

### 5.2.1.1 IQC Modeling of Saturation

In this chapter, we are particularly interested in analyzing feedback systems with saturation nonlinearities. Assume  $\Delta = \text{sat}(\cdot)$  denotes the normalized unit saturation function defined as:

$$\text{sat}(v) = \begin{cases} 1 & \text{if } v > 1 \\ v & \text{if } |v| \leq 1 \\ -1 & \text{if } v < -1 \end{cases} \quad (5.12)$$

The saturation nonlinearity, in this chapter, is modeled using the IQC framework. Particularly, this chapter focuses on finding a “hard” IQC factorization of saturation nonlinearity. In other words, the time domain IQC constraint of saturation should satisfy  $\int_0^T y_\psi(t)^T M y_\psi(t) dt \geq 0$ , where  $y_\psi$  is the output of the stable LTI filter  $\Psi$ , as shown in Figure 5.4, and  $M$  is a constant matrix.

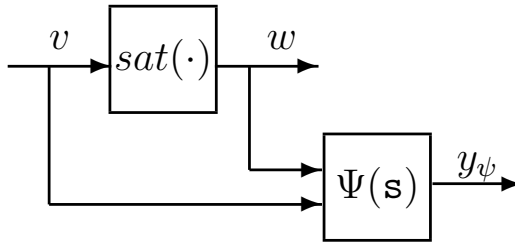


Figure 5.4: Time Domain Interpretation of IQCs

Several different multipliers are known for (amplitude) saturation in literature [29]. We will state two important IQC descriptions of saturation in terms of  $\Pi$ . Recall that  $\Pi$  can be factorized as  $\Pi(j\omega) = \Psi(j\omega)^* M \Psi(j\omega)$ .

1. In practice, saturation is often viewed as a sector bounded (slope restricted) nonlinearity. We will first derive how any nonlinearities lying inside  $[\alpha \beta]$  sector, can be represented in the IQC framework. The representation is then generalized for the saturation nonlinearities.

Consider Figure 5.3. Assume,  $\Delta$  represents  $[\alpha \beta]$  sector bounded nonlinearity as shown in Figure 5.5.

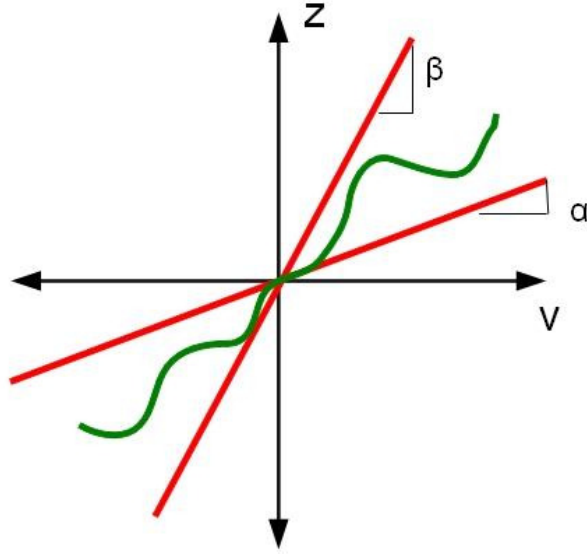


Figure 5.5:  $\alpha$  and  $\beta$  are the slopes of the straight lines. The nonlinearity (green curve) lies within these slopes and is known as sector bounded or slope-restricted nonlinearities.

Consequently,  $\Delta$  satisfies  $[w - \alpha v]^T [\beta v - w] \geq 0$ , which is equivalent to:

$$\begin{bmatrix} v \\ w \end{bmatrix}^T \begin{bmatrix} -\alpha\beta & \frac{(\alpha+\beta)}{2} \\ \frac{(\alpha+\beta)}{2} & -1 \end{bmatrix} \begin{bmatrix} v \\ w \end{bmatrix} \geq 0 \quad (5.13)$$

Assume a static description of the LTI filter  $\Psi$  in Figure 5.3. Specifically,  $\Psi = I$  and  $y_\psi = \begin{bmatrix} v \\ w \end{bmatrix}$ . Now the  $[\alpha \ \beta]$  sector bounded nonlinearity satisfies Equation 5.11 with the following constant matrix  $M$ :

$$M = \begin{bmatrix} -\alpha\beta & \frac{(\alpha+\beta)}{2} \\ \frac{(\alpha+\beta)}{2} & -1 \end{bmatrix} \quad (5.14)$$

Saturation can be viewed as  $[0, 1]$  sector bounded nonlinearity. Hence, an appropriate multiplier is:

$$\Pi_1 = \begin{bmatrix} 0 & 1 \\ 1 & -2 \end{bmatrix} \quad (5.15)$$

2. Popov IQC [29] can also be used to model actuator saturation. The multiplier

is:

$$\Pi_2(j\omega) := \pm \begin{bmatrix} 0 & j\omega \\ -j\omega & 0 \end{bmatrix} \quad (5.16)$$

However, this is not a proper IQC as it is not bounded on the imaginary axis. [36] proposes a method of circumventing this problem.

3. Any conic combination of the above two multipliers is also considered as an appropriate IQC multiplier for the saturation function:  $\Pi := \sum_{i=1}^2 c_i \Pi_i$  for any  $c_i \geq 0$  ( $i = 1, 2$ )

Next, we focus on formulating the dissipation inequality.

### 5.2.2 Local Dissipation Inequality Formulation

This section presents the dissipation inequality providing the induced  $L_2$  gain for nonlinear systems in feedback with  $\text{sat}(\cdot)$ . The dissipation inequality is formulated based on the connection between IQC theory and dissipation theory shown in [29,44]. This connection has been investigated previously in [29,44].

Figure 5.6 shows the analysis interconnection structure which is obtained by simply replacing the relation  $w = \text{sat}(v)$  with the time domain IQC constraint,  $\int_0^T y_\psi(t)^T M y_\psi(t) dt \geq 0$ . This interconnection is used to formulate the dissipation inequality provided in Theorem 5.1. For notational simplicity, let,  $\tilde{x} = \begin{bmatrix} x \\ x_\psi \end{bmatrix}$  and  $F(\tilde{x}, w, d) = \begin{bmatrix} \dot{x} \\ \dot{x}_\psi \end{bmatrix}$ .

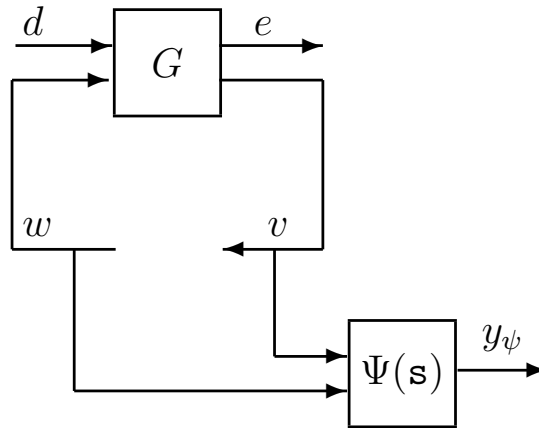


Figure 5.6: Analysis Interconnection Structure

**Theorem 5.1.** *Assume the interconnection of  $G$  and  $\text{sat}(\cdot)$  is well-posed and  $\text{sat}(\cdot)$  satisfies the hard IQC defined by  $\Pi = \Psi^* M \Psi$ . If  $\exists$  a smooth, continuously differentiable function  $V : \mathbb{R}^{n_x + n_{x_\psi}} \rightarrow \mathbb{R}$  and real numbers  $\gamma, \lambda > 0$  such that:*

$$V(0) = 0 \text{ and } V(\tilde{x}) \geq 0 \quad \forall \tilde{x} \quad (5.17)$$

$$\Omega_{V,R^2} := \{\tilde{x} : V(\tilde{x}) \leq R^2\} \text{ is bounded} \quad (5.18)$$

$$\begin{aligned} \nabla V \cdot F(\tilde{x}, w, d) &\leq d^T d - \frac{1}{\gamma^2} e^T e - \lambda (y_\psi^T M y_\psi) \\ \forall \tilde{x} \in \Omega_{V,R^2}, \forall d \in \mathbb{R}^{n_d} \text{ and } \forall w \in \mathbb{R}^{n_w} \end{aligned} \quad (5.19)$$

then  $\|d\|_2 < R$  implies  $\|e\|_2 \leq \gamma \|d\|_2$ .

*Proof.* The theorem assumes the dissipation inequality holds only over a sublevel set,  $\Omega_{V,R^2}$ . Hence, the proof first ensures that the state remains in the sublevel set for all finite time. Let  $\tilde{x}(0) = 0$  and  $d$  be any input such that  $\|d\|_2 < R$ . Since the interconnection is assumed to be well-posed, unique solutions to the ODEs exist for all finite time. Assume  $\exists$  a  $T_1 > 0$  such that  $x(T_1) \notin \Omega_{V,R^2}$ . Define  $T_2 := \inf_{x(T) \notin \Omega_{V,R^2}} T$ . By continuity of the ODE solutions,  $x(T_2) \in \partial\Omega_{V,R^2}$ , where  $\partial(\Omega_{V,R^2})$  indicates the boundary of the set  $\Omega_{V,R^2}$ . We can conclude that  $x(t) \in \Omega_{V,R^2}$  for all  $t \in [0, T_2]$ . Thus the dissipation inequality holds along the trajectory from  $[0, T_2]$ . Integrating this dissipation inequality gives:

$$\int_0^{T_2} \dot{V}(\tilde{x}) dt \leq \int_0^{T_2} (d^T d - \frac{1}{\gamma^2} e^T e) dt - \int_0^{T_2} \lambda (y_\psi^T M y_\psi) dt$$

Since the hard IQC satisfies  $\int_0^{T_2} \lambda (y_\psi^T M y_\psi) dt \geq 0$  and  $V(\tilde{x}(0)) = 0$ , this inequality gives:

$$R^2 = V(\tilde{x}(T_2)) \leq \int_0^{T_2} d^T d dt \leq \|d\|_2^2 < R^2$$

This is a contradiction and hence the assumption that  $\exists$  a  $T_1 > 0$  such that  $x(T_1) \notin \Omega_{V,R^2}$  is not true. Thus  $\|d\|_2 < R$  implies  $x(t) \in \Omega_{V,R^2}$  for all finite time. Hence the dissipation inequality holds along the trajectories of  $\tilde{x}$  for all finite time.

Integrating the dissipation inequality (Equation 5.19) from  $t = 0$  to  $t = T$  with the initial condition  $\tilde{x}(0) = 0$  and using  $V(\tilde{x}(0)) = 0$  and  $V(\tilde{x}(T)) \geq 0$  yields:

$$0 \leq \int_0^T \lambda(y_\psi^T M y_\psi) dt \leq \int_0^T (d^T d - \frac{1}{\gamma^2} e^T e) dt$$

This implies that  $\frac{1}{\gamma^2} \int_0^T e^T e dt \leq \int_0^T d^T d dt$  for all finite time  $T$  and hence  $\|e\|_2 \leq \gamma \|d\|_2$ .  $\square$

**Remark 1** Notice,  $\frac{\|e\|_2}{\|d\|_2} \leq \gamma$  implies  $\gamma_R \leq \gamma$ . Hence,  $\gamma$  provides an upper bound estimate of the local  $L_2$  gain.

**Remark 2** In the dissipation inequality formulation,  $\lambda$  is a Lagrange multiplier for the time domain constraint. It can be shown that the dissipation inequality can not be satisfied with  $\lambda = 0$ . Hence, the restriction of  $\lambda$  to be strictly positive is without loss of generality.

**Remark 3** The dissipation inequality formulated is restrictive in the sense that it is applicable only when hard factorization exists for the IQCs. Additionally, the theorem also requires the storage function to be positive definite. In [44], it was incorrectly claimed that this dissipation inequality condition is equivalent to the standard frequency domain IQC condition when  $G$  is restricted to be a linear system. The dissipation inequality condition in Theorem 5.1 is, for general multipliers, a more conservative condition than the standard frequency-domain IQC test.

**Remark 4** Theorem 5.1 remains valid if  $sat(\cdot)$  is replaced by a causal, bounded (in  $L_2$  sense) operator  $\Delta$ . In other words,  $sat(\cdot)$  can be replaced by any operator for which an IQC description is available.

**Remark 5** The operator  $sat(\cdot)$  or  $\Delta$  can be modeled as conic combinations of several multipliers. Hence, the term  $\lambda(y_\psi^T M y_\psi)$  in the dissipation inequality can be replaced by  $\sum_{i=1}^p \lambda_i(y_{\psi_i}^T M_i y_{\psi_i})$ . Less conservative bounds on the  $L_2$  gain will be computed if more IQCs are used.

Theorem 5.1 provides a dissipation inequality for nonlinear systems in feedback with actuator saturation. The dissipation inequality condition characterizes an upper bound of the induced  $L_2$  gain of such systems. In the case of polynomial systems in feedback with the saturation, SOS estimation technique can be applied to compute the upper bound of the induced  $L_2$  gain. The induced  $L_2$  gain characterization is of practical importance, particularly for flight control systems, where the actuator saturation plays an important role in affecting the performance of the system.

### 5.2.3 $L_2 \rightarrow L_2$ Gain Computation

The computational approach is similar to the  $L_2$  gain estimation technique mentioned in Chapter 4.2. The set containment constraint in the dissipation inequality, Equation 5.19, is replaced with a sufficient non-negative condition by applying generalized S-procedure. The non-negative conditions are then relaxed to be SOS inequality. The conditions provided in Theorem 5.1 are reformulated as an SOS optimization problem:

$$\bar{R} := \max R$$

subject to:

$$V(\tilde{x}) \text{ is SOS, } V(0) = 0 \quad (5.20a)$$

$$- [(R^2 - V)s(\tilde{x}, w, d) + \nabla V \cdot F(\tilde{x}, w, d) - d^T d + \frac{1}{\gamma^2} e^T e + \lambda(y_\psi^T M y_\psi)] \text{ is SOS} \quad (5.20b)$$

$$\lambda \text{ is SOS} \quad (5.20c)$$

$$s(\tilde{x}, w, d) \text{ is SOS} \quad (5.20d)$$

The storage function  $V$  in the iteration is initialized with the linearized storage function  $V_L$  by solving the following SOS condition.

$$-\nabla V_L \cdot F_L(\tilde{x}, w, d) - d^T d + \frac{1}{\gamma_L^2} e^T e + \lambda(y_\psi^T M y_\psi) \text{ is SOS} \quad (5.21)$$

where  $F_L$  represents the linearization of  $F$  and  $\gamma_L$  is the  $L_2$  energy gain with  $G = F_L$  in Figure 5.1. Now, the  $V$ - $s$  iteration algorithm is applied for a given  $\gamma > \gamma_L$ . The  $V$ - $s$  iteration steps are:

1.  $R^2/s$  Step: Hold  $V$  fixed and solve for  $s$  and  $\bar{R}$

$$\bar{R} := \max R$$

subject to:

$$\text{Equation (5.20b) - (5.20d)}$$

2.  $V$  step: Hold  $\bar{R}$ ,  $s(\tilde{x}, w, d)$  fixed and solve for  $V$  satisfying Equation (5.20a) - (5.20c).

3. Repeat  $R^2/s$  and  $V$  step as long as the  $\bar{R}$  continues to increase.

### 5.2.4 Guaranteed SOS Feasibility

The SOS optimization problem posed in Equation 5.20 provides an upper bound to the induced  $L_2$  gain of system 5.1 from  $d$  to  $e$ . Assume the linearized condition in Equation 5.21 provides a finite gain  $\gamma_L$ . However, it is not clear, given a finite gain  $\gamma_L$ , if a feasible solution to the SOS conditions in Equation 5.20 exists. Next, we investigate feasibility of the optimization problem 5.20 given that a finite gain  $\gamma_L$  exists.

The feasibility of the solution depends on the structure of the nonlinear systems. Specifically, we will consider the following structure of the polynomial dynamics:

$$\dot{x} = f(x, w, d) = Ax + B_w w + B_d d + f_{23}(x) + g_{12}(x)w + h_{01}(x)d^2 + m_{01}(x)w^2 \quad (5.22)$$

$$\begin{bmatrix} e \\ v \end{bmatrix} = \begin{bmatrix} C_1 \\ C_2 \end{bmatrix} x + \begin{bmatrix} 0 \\ D_2 \end{bmatrix} d \quad (5.23)$$

$$w = \text{sat}(v) \quad (5.24)$$

where  $f_{23}$  is quadratic and cubic in  $x$ ,  $g_{12}$  is linear and quadratic in  $x$ , and  $h_{01}(x)$ ,  $m_{01}(x)$  are affine in  $x$ .  $A$ ,  $B_w$ ,  $B_d$ ,  $C_1$ ,  $C_2$ ,  $D_2$  are matrices (of reals) of appropriate dimensions. Here,  $x$  represents the states,  $w$ ,  $d$  represents the inputs and  $e$ ,  $v$  indicates the outputs. Assume that the saturation is modeled as  $[\alpha \beta]$  sector bounded nonlinearity. Hence, an appropriate IQC description of saturation can be described by  $y_\psi^T M y_\psi$ , where

$$y_\psi = \begin{bmatrix} w \\ v \end{bmatrix}, \quad M = \begin{bmatrix} -\alpha\beta & \frac{(\alpha+\beta)}{2} \\ \frac{(\alpha+\beta)}{2} & -1 \end{bmatrix} = \begin{bmatrix} M_{11} & M_{12} \\ M_{12}^T & M_{22} \end{bmatrix}$$

Assume that the linearized dissipation inequality condition (Equation 5.21) corresponding to the dynamics of Equation 5.22 is feasible. According to the KYP-lemma, there exist  $P = P^T \succ 0$  and  $\lambda > 0$  such that the following LMI is satisfied.

$$\Lambda = \begin{bmatrix} A^T P + PA + C_1^T C_1 + \lambda C_2^T M_{11} C_2 & PB_w + \lambda C_2^T M_{12} & PB_d + \lambda C_2^T M_{11} D_2 \\ (PB_w + \lambda C_2^T M_{12})^T & \lambda M_{22} & \lambda M_{12}^T D_2 \\ (PB_d + \lambda C_2^T M_{11} D_2)^T & (\lambda M_{12}^T D_2)^T & -\gamma^2 + \lambda D_2^T M_{11} D_2 \end{bmatrix} \preceq 0 \quad (5.25)$$

**Theorem 5.2.** *Consider Equation 5.22 and a sector bounded IQC description for*

saturation. If there exist a  $P = P^T \succ 0$  and  $\lambda > 0$  such that Equation 5.25 is satisfied then the SOS constraints in Equation 5.20 are always feasible.

*Proof.* Define the storage function  $V$  in Equation 5.20 to be  $V = x^T P x$ . Let,  $s = \begin{bmatrix} x \\ w \\ d \end{bmatrix}$ , and  $r = s \otimes x$ , where  $\otimes$  denote the Kronecker product. There exists constant matrix  $Q_1, Q_2$  such that,

$$2x^T P (f_{23}(x) + g_{12}(x)w + h_{01}(x)d^2 + m_{01}(x)w^2) = r^T Q_1 r + s^T Q_2 r + r^T Q_2^T s$$

The dissipation inequality can be rewritten in the following form:

$$\nabla(V)\dot{x} - \gamma^2 d^T d + e^T e + \lambda(y_\psi^T M y_\psi) = \begin{bmatrix} s \\ r \end{bmatrix} \begin{bmatrix} \Lambda & Q_2 \\ Q_2^T & Q_1 \end{bmatrix} \begin{bmatrix} s \\ r \end{bmatrix}$$

Let,  $s_1 = \alpha(x^T x + w^T w + d^T d)$ , where  $\alpha > 0$ . Hence, the term  $V s_1 = \alpha(x^T P x)(x^T x + w^T w)$ . According to Lemma II.5 from [54], there exists a  $H \succ 0$  such that  $r^T H r = \alpha(x^T P x)(x^T x + w^T w)$ . Now we focus on the local dissipation inequality as mentioned in Equation 5.20b. Define,

$$D := -\nabla(V)\dot{x} - \gamma^2 d^T d + e^T e + \lambda(y_\psi^T M y_\psi) - (R^2 - V)s_1(x, w)$$

The dissipation inequality condition is quadratic in  $x, w, d, r$  and can be written as:

$$D := \begin{bmatrix} s \\ r \end{bmatrix} \left( \begin{bmatrix} -\Lambda & -Q_2 \\ -Q_2^T & -Q_1 \end{bmatrix} + \begin{bmatrix} -\alpha\gamma^2 R^2 I & 0 \\ 0 & \alpha H \end{bmatrix} \right) \begin{bmatrix} s \\ r \end{bmatrix} \quad (5.26)$$

With proper choice of  $\alpha$  and  $R$  the dissipation inequality can be made SOS. Since,  $H \succ 0$  and  $\Lambda \prec 0$ , there is an  $\alpha > 0$  such that,

$$\begin{bmatrix} -\Lambda & -Q_2 \\ -Q_2^T & -Q_1 \end{bmatrix} + \begin{bmatrix} 0 & 0 \\ 0 & \alpha H \end{bmatrix} \succ 0$$

With this  $\alpha$  fixed, by continuity, there exists  $R > 0$  such that,

$$\begin{bmatrix} -\Lambda & -Q_2 \\ -Q_2^T & -Q_1 \end{bmatrix} + \begin{bmatrix} -\alpha\gamma^2 R^2 I & 0 \\ 0 & \alpha H \end{bmatrix} \succ 0$$

□

The proof of Theorem 5.2 is specific for the dynamics described in Equation 5.22 and for sector bounded IQC description. The proof is constructive and hence does not apply when the dynamics are different than Equation 5.22. In that case, similar arguments can be made to prove or disprove SOS feasibility.

### 5.3 Applications

This section presents two examples involving estimation of the  $L_2$  energy gain bound. The first example investigates amplitude saturation and the second example is the GTM short period flight control system with rate saturation.

#### 5.3.1 Amplitude Saturation

Consider the feedback interconnection shown in Figure 5.1 with  $\text{sat}(\cdot)$  denoting a normalized unit amplitude saturation function. The dynamics of  $G$  are given as:

$$\dot{x}_1 = -x_1 + x_2 + \alpha x_2^2 \quad (5.27)$$

$$\dot{x}_2 = -x_2 + d + w \quad (5.28)$$

$$\begin{bmatrix} e \\ v \end{bmatrix} = \frac{1}{2} \begin{bmatrix} x_1 \\ x_1 \end{bmatrix} \quad (5.29)$$

The goal is to estimate the upper bound of the  $L_2 \rightarrow L_2$  gain from  $d$  to  $e$  for different values of  $\alpha$ . The term  $\alpha$  is a *weighting* on the nonlinearity of the dynamics. For  $\alpha = 0$ ,  $G$  reduces to a linear model. In that case, the  $L_2$  gain from  $d$  to  $e$  can be computed by using the IQC $\beta$  [30] toolbox. The saturation is modeled as a  $[0, 1]$  sector bounded nonlinearity. The  $L_2$  gain computed with the IQC $\beta$  toolbox for the linear plant ( $\alpha = 0$ ) in feedback with saturation is  $\gamma = 1.0$ . It is expected that as  $\alpha$  goes to zero, the  $L_2$  gain of the nonlinear plant in feedback with the saturation should converge to  $\gamma = 1.0$ . The purpose of this example is to understand the conservatism introduced by the dissipation inequality condition.

The first step in analyzing the problem is to model the saturation in the IQC framework. This entails replacing the precise relation  $w = \text{sat}(v)$  with the time domain IQC,  $\int_0^T y_\psi(t)^T M y_\psi(t) dt \geq 0$ . In this specific example, the  $[0 \ 1]$  sector bounded nonlinearity is considered.

The dissipation inequality condition is solved to estimate the local  $L_2$  gain for three

different values of  $\alpha$ . The  $L_2$  gain of the nonlinear plant in feedback with saturation is estimated with a quadratic storage function and the multiplier  $s$  is a quadratic function of  $[x_1; x_2; w; d]$ . Figure 5.7 shows that as  $\alpha$  goes close to zero, the dissipation inequality recovers the linear results. Hence, for this particular example, the dissipation inequality condition does not introduce any conservatism as  $\alpha$  tends to zero. This example also verifies the correctness of the dissipation inequality condition.

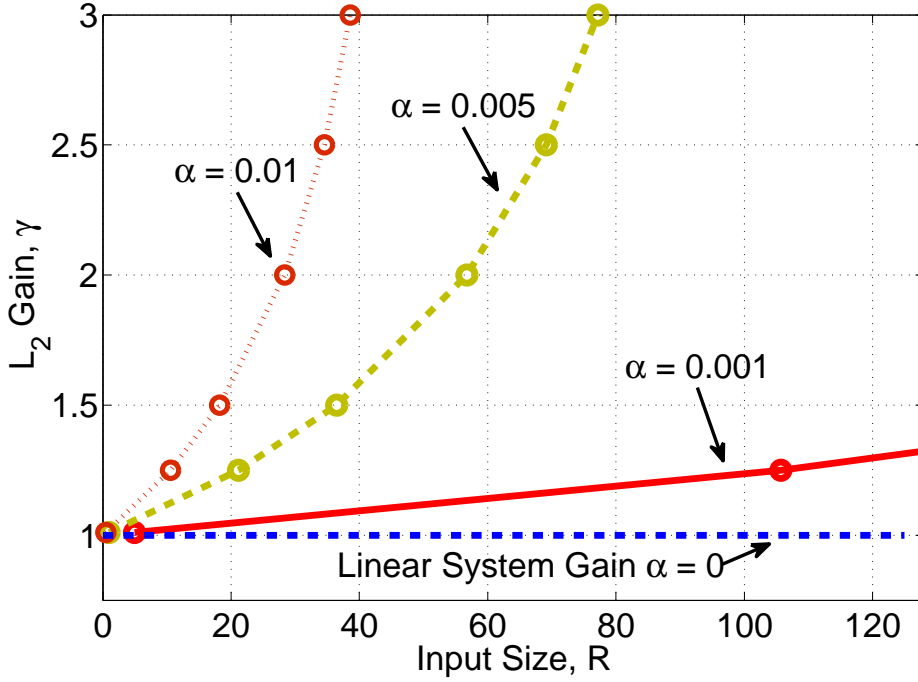


Figure 5.7:  $L_2$  gain bounds with quadratic storage function for different size of inputs and different values of  $\alpha$ .

### 5.3.2 GTM Short Period Control with Rate Saturation

Consider the longitudinal dynamics of the GTM aircraft (Equation 3.13) around the flight condition specified in Equation 5.30.

$$\begin{bmatrix} V_t \\ \alpha_t \\ q_t \\ \theta_t \end{bmatrix} = \begin{bmatrix} 150.00 \text{ ft/s} \\ 0.04690 \text{ rad} \\ 0 \text{ rad/s} \\ 0.04690 \text{ rad} \end{bmatrix}, \quad \begin{bmatrix} \delta_{elev,t} \\ \delta_{th,t} \end{bmatrix} = \begin{bmatrix} 14.78 \% \\ 0.0506 \text{ rad} \end{bmatrix} \quad (5.30)$$

The subscript “t” denotes a trim value. A polynomial short period model is extracted from the 4-state polynomial model, Equation 3.13, by holding  $V$ ,  $\theta$  and  $\delta_{th}$  at their

trim values. The short period model has two states  $x := [\alpha \ q]$  and the elevator deflection ( $\delta_e$  in radian) as the control input. The state  $\alpha$  is the angle of attack (rad) and  $q$  is the pitch rate (rad/s). The polynomial short period model is given by:

$$\begin{aligned}\dot{\alpha} &= (-1.492\alpha^2 + 4.239\alpha - 3.236)\alpha + (3.063 \times 10^{-3}\alpha + 6.226 \times 10^{-3}q + 9.227 \times 10^{-1})q \\ &\quad + (2.402 \times 10^{-1}\alpha - 6.491 \times 10^{-2}\delta_e - 3.166 \times 10^{-1})\delta_e \\ \dot{q} &= (-7.228\alpha^2 + 18.36\alpha - 45.34)\alpha - 4.372q + (41.50\alpha - 59.99)\delta_e\end{aligned}$$

Consider Figure 5.8.  $P$  is a two-state short period polynomial model provided above. The damping of the short period dynamics are improved with a proportional pitch rate ( $q$ ) feedback control and is denoted by  $K$ , where  $K = 4\frac{\pi}{180}$ . An exogenous disturbance  $d$  affects both states and enters the plant additively. The goal is to estimate an upper bound of the local  $L_2$  gain from  $d$  to  $q$  under rate limit saturation. For simplicity, the rate limit in this example is designed to have a bandwidth of 1 rad/s. In reality, the GTM rate limit bandwidth is faster than 1 rad/s.

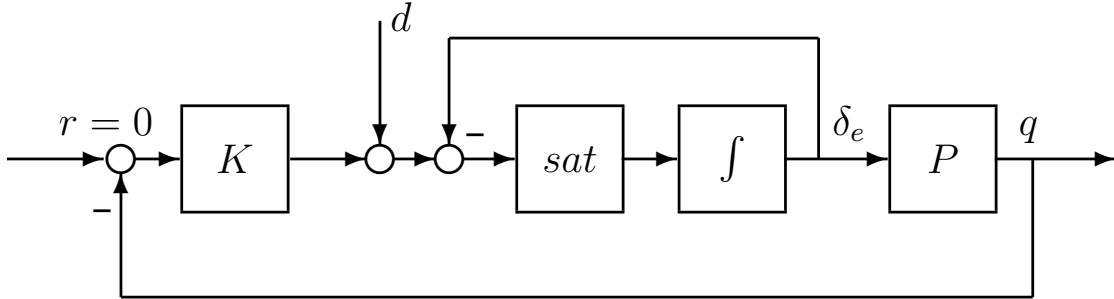


Figure 5.8: Feedback interconnection of GTM short period dynamics

*IQC Modeling of Rate Saturation:* The first step is to model the rate limit saturation within the IQC framework. In the rate limiter, an integrator appears in combination with a saturation. This interconnection is not  $L_2$  stable and hence the IQC framework cannot be used. However, [42] resolves this issue by encapsulating the nonlinearity in an artificial feedback loop, as shown in Figure 5.9. Let the feedback encapsulated rate limiter be denoted by  $\tilde{\delta}_e = \Gamma_{\text{sat}}(\delta_{e_{cmd}})$ . This is defined by the relations,

$$\begin{aligned}\dot{\delta}_e &= \text{sat}(\delta_{e_{cmd}} - \delta_e), \quad \delta_e(0) = 0 \\ \tilde{\delta}_e &= \delta_e + \text{sat}(\delta_{e_{cmd}} - \delta_e)\end{aligned}$$

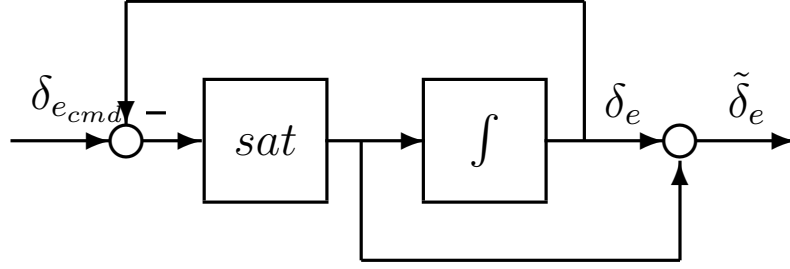


Figure 5.9: Feedback encapsulation of rate limit

The following IQC multipliers are used to model the feedback encapsulated rate limit saturation,  $\tilde{\delta}_e = \Gamma_{\text{sat}}(\delta_{e_{\text{cmd}}})$ .

1. The gain from  $\delta_{e_{\text{cmd}}}$  to  $\tilde{\delta}_e$  is shown not to exceed  $\sqrt{2}$  in [42]. This forms the basis of the following multiplier.

$$\Pi_{\Gamma_1} = \begin{bmatrix} 2 & 0 \\ 0 & -1 \end{bmatrix} \quad (5.31)$$

2. Another IQC multiplier can be derived by observing that the relation from  $(\delta_{e_{\text{cmd}}} - \delta_e)$  to  $\dot{\delta}_e$  can be modeled as a  $[0, 1]$  sector bounded nonlinearity. The corresponding IQC multiplier is:

$$\Pi_{\Gamma_2} = \begin{bmatrix} 0 & \frac{j\omega}{j\omega+1} \\ (\cdot)^* & -2\left(\frac{j\omega}{j\omega+1}\right)^* \left(\frac{j\omega}{j\omega+1}\right) \end{bmatrix} \quad (5.32)$$

3. Any conic combination of the above two multipliers is also considered an appropriate IQC multiplier for the  $\Gamma_{\text{sat}}$  operator:  $\Pi_{\Gamma} := \sum_{i=1}^2 c_i \Pi_{\Gamma_i}$  for any  $c_i \geq 0$  ( $i = 1, 2$ )

**Remark** Note that the IQCs are provided for the encapsulated rate limiter,  $\Gamma_{\text{sat}}$ . Hence to use the IQCs for the encapsulated rate limit, an  $(s+1)$  filter is introduced at the output of the rate limit and a  $\frac{1}{(s+1)}$  filter is introduced at the input of  $P$ . The feedback interconnection of  $\tilde{P} = \frac{P}{s+1}$  and the encapsulated rate limit is then analyzed. The input-to-output gain from  $d$  to  $q$  of this modified loop is equivalent to the  $d$  to  $e$  gain for the original problem.

The  $L_2 \rightarrow L_2$  gain from  $d$  to  $q$  is estimated for the GTM dynamics under rate saturation. The rate saturation is modeled with a conic combination of the multipliers

$\Pi_{\Gamma_i}$  for  $i = 1, 2$ . The multiplier  $s$  is a quadratic function of  $[\alpha; q; x_\Psi; \delta_e; d]$ .  $x_\Psi$  is the state of the  $\Psi$  filter used in the factorization of  $\Pi_{\Gamma_2}$ . Figure 5.10 indicates how the induced gain of the system varies as the size of the disturbance  $\|d\|_2$  increases. The horizontal axis indicates the size of the disturbance,  $\|d\|_2$  and the vertical axis shows the estimated bounds of the induced gain from  $d$  to  $q$ . The upper bounds are estimated for both quadratic (marked as  $-x$ ) and quartic (marked as  $-\square$ ) storage functions. The induced gain for the linearized system is also shown (marked as  $-$ ). The lower bound (marked as  $-o$ ) is estimated using the algorithm proposed in [53].

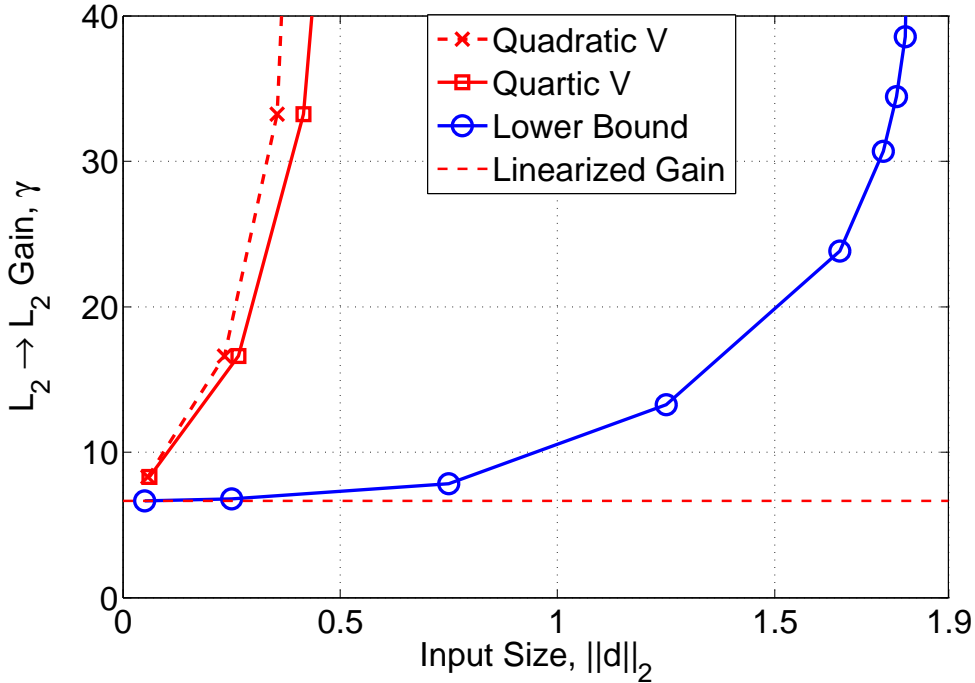


Figure 5.10: Estimation of induced  $L_2 - L_2$  gain bounds for GTM short period under rate limit

The linear gain is estimated by solving the dissipation inequality for the linearized system and is computed to be 1.65. The quadratic and quartic storage function prove that the system can tolerate a disturbance input of a size  $\|d\|_2 < 0.4$  and  $\|d\|_2 < 0.5$ , respectively. The storage function proves that the system cannot be destabilized by any input of size less than 0.5. The lower bound demonstrates that the system gain becomes unbounded for  $\|d\|_2 < 1.83$ . In other words, there exists an input of size 1.83 which will destabilize the system. Note, for small  $\|d\|_2$  the lower bound is below all three gains (linearized, quartic, quadratic). This is expected since the three gains are supposed to be upper bounds on the actual gain.

The upper bound results are conservative. The conservativeness is possibly due to the IQCs that are used for modeling rate saturation. The IQC in Equation 5.31 is constant and the other dynamic IQC in Equation 5.32 arises from modeling the saturation as sector bound nonlinearity.

## 5.4 Connection Between Dissipation Inequality to Lyapunov Function

Consider the feedback interconnection of Figure 5.1 with  $d = 0$  and  $e = 0$ . For convenience, this interconnection is presented here again in Figure 5.11.

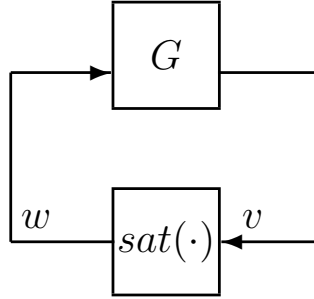


Figure 5.11: Feedback Interconnection of  $G - sat(\cdot)$

One may then ask the question: if there are no external disturbances ( $d = 0$ ) in System 5.3, does the dissipation inequality imply Lyapunov stability? In other words, can the storage function  $V$  in the dissipation inequality (Equation 5.19) be used as a Lyapunov function to conclude stability of the origin? It turns out that the storage function can be used as a Lyapunov function to prove stability of the origin if the time domain IQC constraint of saturation is satisfied point-wise in time, i.e.  $y_\psi(t)^T M y_\psi(t) \geq 0 \forall t$ . Theorem 5.3 provides conditions as to when the storage function is equivalent to a Lyapunov function.

**Theorem 5.3.** *Suppose the assumptions of the dissipation inequality of Theorem 5.1 is satisfied on a domain  $D \subset \mathbb{R}^{n+n_\psi}$  that contains the origin. Specifically,*

$$V(0) = 0 \text{ and } V(\tilde{x}) \geq 0 \quad \forall \tilde{x} \in D$$

$$\nabla V \cdot F(\tilde{x}, w) \leq -\lambda(y_\psi^T M y_\psi) \quad \forall \tilde{x} \in D, \text{ and } \forall w \in \mathbb{R}^{n_w}$$

*If the following conditions are satisfied,*

- Time domain IQC constraint of saturation is satisfied point-wise in time  $\rightarrow y_\psi^T M y_\psi \geq 0 \forall \tilde{x} \in D$ , and  $\forall w \in \mathbb{R}^{n_w}$
- No solution of  $F(\tilde{x}, w)$  can stay identically in  $S = \{\tilde{x} \in D | h_1(x) = 0\}$  other than the trivial solution  $\tilde{x}(t) = 0$ . This is also known as the zero-state observability condition.

then the origin of  $F(\tilde{x}, w)$  is asymptotically stable.

*Proof.* A brief sketch of proof is included here. The condition  $y_\psi^T M y_\psi \geq 0$  is satisfied point-wise in time and hence  $\nabla V \cdot F(\tilde{x}, w) \leq -\lambda(y_\psi^T M y_\psi) < 0 \in D - \{0\}$ . Using zero-state observability assumption, it can be shown that  $V(\tilde{x})$  is positive definite in the domain. This concludes that the system is asymptotically stable.  $\square$

#### 5.4.1 Equivalence to Circle Criterion

Assume  $G$  represents a linear system,  $G = G_{LIN}(\mathbf{s})$ . Specifically, the feedback interconnection in Figure 5.11 is represented by

$$\dot{x} = Ax + Bw \quad (5.33)$$

$$v = Cx \quad (5.34)$$

$$w = sat(v) \quad (5.35)$$

where  $A$ ,  $B$ ,  $C$  are matrices of appropriate dimensions and  $sat(\cdot)$  lies in the  $[\alpha, \beta]$  sector. The stability of the system in Equation 5.33 is provided by the well-known Circle Criteria [31]. It is convenient, for the purpose of applying the Circle Criteria, to transform the  $sat(\cdot)$  lies in  $[0, \infty]$  sector via loop transformation [31] of Figure 5.12.

After the loop transformation, the linear system, indicated as  $Z(\mathbf{s})$  in Figure 5.12, takes the following form:

$$\dot{x} = (A - \alpha BC)x + B\hat{w} \quad (5.36)$$

$$\hat{v} = (\beta - \alpha)Cx + \hat{w} \quad (5.37)$$

The saturation nonlinearity now belongs to the  $[0, \infty]$  sector, as shown in the bottom part of the Figure 5.12. Investigating stability of the original system 5.33 is now equivalent to investigating stability of the loop transformed linear system  $Z(\mathbf{s})$  in feedback

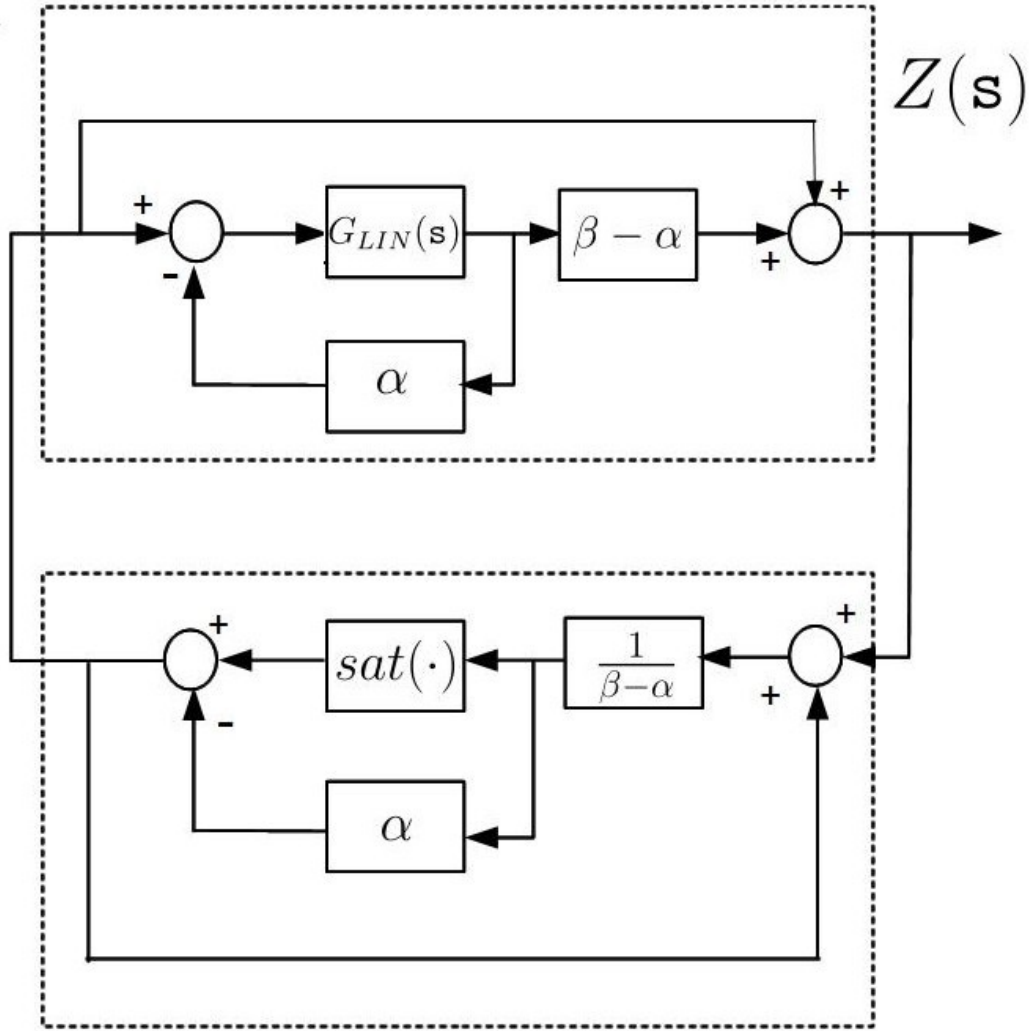


Figure 5.12: Saturation nonlinearity is transformed from  $[\alpha, \beta]$  sector to  $[0, \infty]$  sector.

with with  $sat(\cdot)$  in the  $[0, \infty]$  sector. The Circle Criteria will be applied on this transformed system. The Circle Criteria states that the loop transformed feedback interconnection in Figure 5.12 is stable if  $Z(s)$  is a positive real transfer function. Positive real transfer functions can be characterized by the Kalman-Yakuubovich-Popov (KYP) Lemma (see Lemma 6.3, [31]). The KYP lemma states that  $Z(s)$  is strictly positive real if and only if there exist matrices  $P = P^T > 0$ ,  $L$ , and  $W$  and a

scalar  $\epsilon > 0$  such that

$$(A - \alpha BC)^T P + P(A - \alpha BC) = -L^T L - \epsilon P \quad (5.38)$$

$$PB = (\beta - \alpha)C^T - L^T W \quad (5.39)$$

$$W^T W = 2 \quad (5.40)$$

Equation 5.38 provides conditions for  $Z(\mathbf{s})$  to be strictly positive real, hence, proving absolute stability of the original system 5.33. In other words, if we can find matrices  $P = P^T > 0$ ,  $L$ , and  $W$  and  $\epsilon > 0$  such that Equation 5.38 is satisfied then the original system 5.33 is stable. Equation 5.38 can be turned into the following LMI:

$$\begin{bmatrix} A - \alpha BC)^T P + P(A - \alpha BC) & (\beta - \alpha)C^T - PB \\ & -2 \end{bmatrix} = -\epsilon P \prec 0 \quad (5.41)$$

The LMI in Equation 5.41 turns out to be equivalent to applying Theorem 5.3 on the transformed system in Figure 5.12. Specifically, Theorem 5.3 states the system in Figure 5.12 is stable if we can find a storage function  $V(x) > 0$  satisfying

$$\dot{V} \leq -(y_\psi^T M y_\psi) \quad (5.42)$$

where  $y_\psi = \begin{bmatrix} \hat{w} \\ -\hat{v} \end{bmatrix}$  and  $M = \begin{bmatrix} 0 & 1 \\ 1 & 0 \end{bmatrix}$  is an appropriate multiplier for  $\text{sat}(\cdot)$  lying in  $[0, \infty]$  sector. If  $V(x)$  is taken to be a quadratic storage function, specifically  $V(x) = x^T P x$ , then Equation 5.42 can be written as the LMI in Equation 5.41.

Theorem 5.3 is shown to be equivalent to the Circle Criteria for linear systems in feedback with saturation nonlinearity. Next, we show the application of Theorem 5.3.

#### 5.4.2 Application

*Linear System with Saturation* [Example 7.4 in [31]]

Consider the linear system in feedback with saturation nonlinearity presented in Equa-

tion 5.43.

$$\dot{x} = \begin{bmatrix} 0 & 1 \\ 1 & 0 \end{bmatrix} x + \begin{bmatrix} 0 \\ 1 \end{bmatrix} w \quad (5.43)$$

$$y = \begin{bmatrix} 2 & 1 \end{bmatrix} x \quad (5.44)$$

$$w = -\text{sat}(y) \quad (5.45)$$

where  $\text{sat}(y)$  belongs globally to the sector  $[0 \ 1]$ . The objective of this example is to study the stability of the system using Theorem 5.3. The stability of this system has previously been studied in [31] using the Circle Criteria. The linear system under study is not Hurwitz and hence the Circle Criteria showed that the system is absolutely stable if the saturation belongs to the sector  $[\alpha 1]$ , where  $\alpha > 0.5359$ . Here we will apply Theorem 5.3 to recover the results obtained in [31].

Next, Theorem 5.3 is applied to search for an optimal sector  $\alpha^*$  such that the system in Equation 5.43 remains absolutely stable for nonlinearities lying between  $[\alpha^* 1]$ . Assume that a quadratic Lyapunov function,  $V(x) = x^T P x$  is used to solve the condition  $\dot{V} \leq -(y_\psi^T M y_\psi)$  provided by Theorem 5.3. Here,  $y_\psi = \begin{bmatrix} y \\ -w \end{bmatrix}$  and  $M = \begin{bmatrix} -2\alpha^* & 1 + \alpha^* \\ 1 + \alpha^* & -2 \end{bmatrix}$ . This condition can be relaxed to be SOS constraint. The SOS framework can then be used to maximize  $\alpha^*$  satisfying the condition  $\dot{V} \leq -(y_\psi^T M y_\psi)$ . The SOS optimization returns an optimal  $\alpha^*$  to be 0.536. Hence, Theorem 5.3 recovers the results obtained by the Circle Criteria.

Theorem 5.3 also provides a Lyapunov function. The ROA can be characterized by the sub-level set of the Lyapunov function,  $\Omega_c = \{x \in \mathbb{R}^2 | V(x) \leq c\}$ , where  $c$  needs to be computed. The ROA can then be approximated by solving for maximum  $c$  subject to the set containment condition  $\Omega_c \subset \{|y| \leq \frac{1}{\alpha}\}$ . Figure 5.13 shows the ROA for the system obtained by the Lyapunov function from Theorem 5.3. Theorem 5.3 can be viewed as a process which has automated the conditions provided by the Circle Criteria.

## 5.5 Summary

This chapter presents a method for estimating the upper bound of the induced  $L_2$  gain for polynomial dynamical systems in feedback with saturation. The method

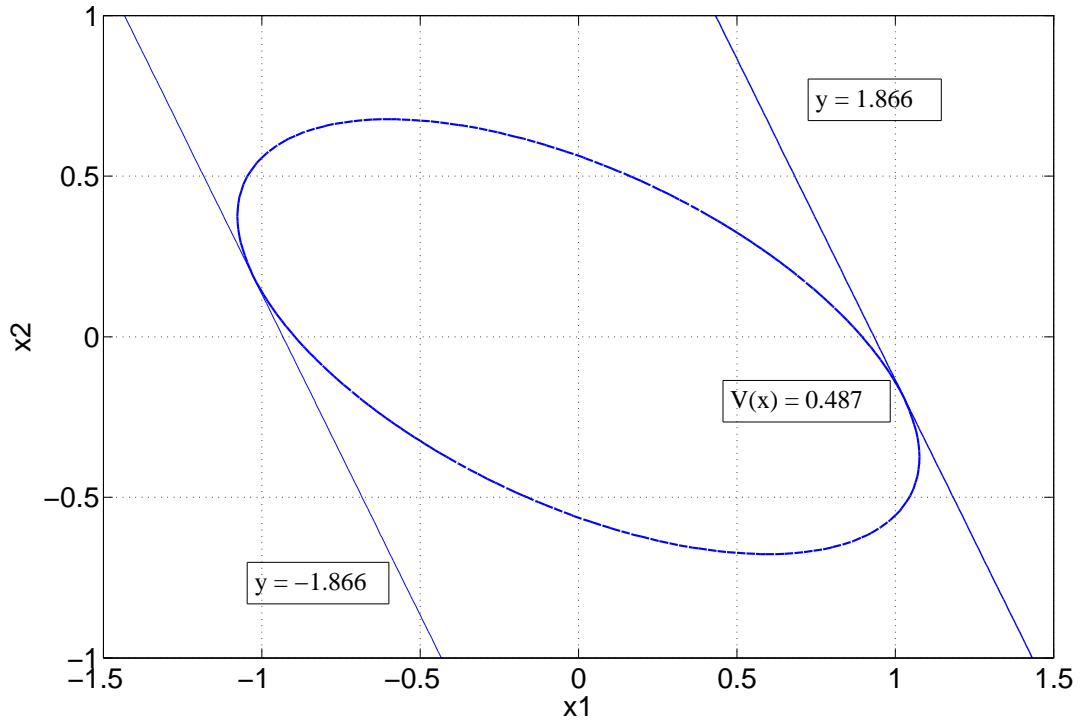


Figure 5.13: Region of attraction obtained by the Lyapunov function from Theorem 5.3.

relies on merging the dissipation theory with the IQC framework. The SOS optimization framework has been used for computing the bounds. The conservativeness of the results are quantified by estimating the lower bound of the induced gain. The technique has been applied to the short period model of the GTM dynamics. A possible future direction of research will be to reduce the conservativeness of this method by including a rich description of IQCs. The framework can also be extended to handle uncertainty. This requires further investigation.

The storage function from the dissipation inequality is shown to be a Lyapunov function under certain (restrictive) assumptions. This connection results in a condition for inferring the stability of polynomial systems in feedback with saturation. For linear systems, this stability condition is equivalent to the well known Circle Criteria. The condition introduces an absolute stability framework for polynomial type “Lure” systems.

# Chapter 6

## Local Stability Analysis of Polynomial Systems with Actuator Saturation

This chapter considers the local stability analysis of polynomial systems in feedback with actuator saturation. The work presented in this chapter is motivated by the stability results in [23]. Polytopic set invariance conditions are formulated in [23] for estimating the ROA of linear systems in feedback with actuator saturation. The key idea in formulating the set invariance conditions relies on representing the saturation as a convex hull of a group of linear (possibly nonlinear) feedbacks. In the case of linear systems, quadratic Lyapunov functions can be computed by turning the stability conditions into LMI conditions.

This chapter focuses on extending the invariance conditions in [23] to a polynomial system in feedback with actuator saturation. For polynomial systems, the invariance conditions can be verified using SOS optimizations. An iterative algorithm is provided to solve the optimization problem. Finally, the algorithm is applied to a polynomial system with actuator saturation.

### 6.1 Problem Formulation

Consider the feedback interconnection in Figure 6.1.

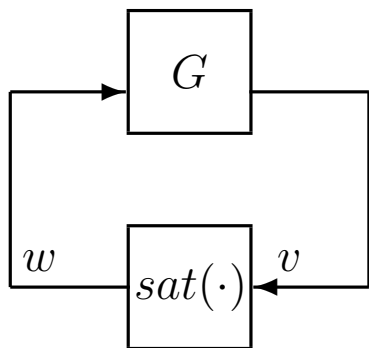


Figure 6.1: Feedback Interconnection of  $G - sat(\cdot)$

$G$  is a dynamical system expressed by a polynomial vector field of the following form:

$$\dot{x} = f(x) + g(x)w \quad (6.1a)$$

$$v = h(x) \quad (6.1b)$$

$$w = sat(v) \quad (6.1c)$$

where  $x \in \mathbb{R}^n$  is the state vector,  $w \in \mathbb{R}^{n_w}$  and  $v \in \mathbb{R}^{n_v}$  are the interconnection signals between  $G$  and  $sat$ . Moreover,  $f : \mathbb{R}^n \rightarrow \mathbb{R}^n$ ,  $g : \mathbb{R}^n \rightarrow \mathbb{R}^{n_w}$  and  $h : \mathbb{R}^n \rightarrow \mathbb{R}^{n_v}$  are multivariable polynomials. Assume  $f(0, 0) = 0$  and  $h(0) = 0$ . Note that  $G$  is affine in input. This assumption is required for the set invariance conditions presented later. Assume  $sat(\cdot)$  denotes the normalized unit saturation function defined in Equation 5.12. System 6.1 can be compactly written as:

$$\dot{x} = f(x) + g(x)sat(h(x)) \quad (6.2)$$

The objective of this chapter is to estimate the ROA ( $\mathcal{R}$ ) for the polynomial system defined by Equation 6.2. The approach involves the following steps. First, appropriate invariance conditions for polynomial system are derived by extending the ideas presented in [23]. Second, these invariance conditions are relaxed to be non-negative polynomials and formulated as an SOS optimization problem. Finally, an iterative algorithm is proposed for solving the SOS optimization problem.

From here onwards, we will present results for single input systems for simplicity. These results are also applicable for multiple input systems, unless otherwise noted.

## 6.2 Polytopic Set Invariance Conditions

This section focuses on deriving invariance conditions to estimate  $\mathcal{R}$  for Equation 6.2. In other words, we are interested in estimating the largest sublevel sets of Lyapunov function  $\Omega(V, \gamma) = \{x \in \mathbb{R}^n | V(x) \leq \gamma\}$  such that Equation 6.3 is satisfied. Define,  $D(V(x), r(x)) := \{x \in \mathbb{R}^n : \nabla V(x)r(x) < 0\} \cup \{0\}$ .

$$\begin{aligned} \gamma^* &:= \sup_{\gamma} \gamma \\ \text{subject to: } &\Omega(V, \gamma) \subset D(V, f(x) + g(x)\text{sat}(h(x))) \end{aligned} \quad (6.3)$$

We review previous works on actuator saturation analysis by [12, 23, 24] and presents the main invariance results. The previous works focus on estimating the ROA for linear systems in feedback with saturation. Consider the linear representation of  $G$ :

$$\dot{x}_{LIN} = Ax + Bw \quad (6.4a)$$

$$v_{LIN} = Hx \quad (6.4b)$$

Define the linear system in feedback with saturation:

$$\dot{x}_{LIN} = Ax + B\text{sat}(Hx) = \mathcal{G}_{LIN} \quad (6.5)$$

The key idea in [23] is based on the following property of the saturation function: For any  $p \in \mathbb{R}$  and  $q \in [-1, 1]$ , there exists  $\phi \in [0, 1]$  such that:

$$\text{sat}(p) = \phi p + (1 - \phi)q \quad (6.6)$$

In other words,  $\text{sat}(p)$  can be expressed as a convex combination of  $p$  and any  $q \in [-1, 1]$ . See Lemma 7.3.2 in [23] for an extension of this property for multi-input systems.

The next theorem uses this property to develop a sufficient condition for the set containment constraint in Equation 6.3. For  $l : \mathbb{R}^n \rightarrow \mathbb{R}$ , define  $\mathcal{W}(l) := \{x \in \mathbb{R}^n : |l(x)| \leq 1\}$ .

**Theorem 6.1.** *[ [12, 23, 24] ] Assume there exists a continuously differentiable function  $V : \mathbb{R}^n \rightarrow \mathbb{R}$  such that  $V(0) = 0$ ,  $V(x) > 0 \forall x \neq 0$ ,  $\Omega(V, \gamma_L)$  is bounded, and*

$$\Omega(V, \gamma_L) \subset D(V, (A + BH)x) \quad (6.7)$$

If there exists  $l : \mathbb{R}^n \rightarrow \mathbb{R}$  such that:

$$\Omega(V, \gamma_L) \subset D(V, Ax + Bl(x)) \quad (6.8)$$

$$\Omega(V, \gamma_L) \subset \mathscr{W}(l) \quad (6.9)$$

then  $\Omega(V, \gamma_L) \subset \mathcal{R}$ .

*Proof.* By Equation 6.9,  $|l(x)| \leq 1$  for all  $x \in \Omega(V, \gamma_L)$  and hence for each  $x \in \Omega(V, \gamma_L)$  there is  $\phi(x) \in [0, 1]$  such that

$$\text{sat}(Hx) = \phi(x)Hx + (1 - \phi(x))l(x) \quad (6.10)$$

It follows that  $\forall x \in \Omega(V, \gamma_L)$

$$\nabla V(x)(Ax + B\text{sat}(Hx)) = \phi(x)\nabla V(x)(A + BH)x + (1 - \phi(x))\nabla V(x)(Ax + Bl(x)) \quad (6.11)$$

By Equations 6.7 and 6.8, both terms on the right side are strictly negative  $\forall x \in \Omega(V, \gamma_L)$ . Thus  $\Omega(V, \gamma_L) \subset D(V, \mathcal{G}_{\mathcal{L}IN})$ .  $\Omega(V, \gamma_L) \subset \mathcal{R}$  follows from Lemma 2 (See Chapter 4).  $\square$

Theorem 6.1 is a restatement of the results in [12, 23, 24], e.g. Theorem 7.4.1 in [23]. The main result of the chapter is an extension to Theorem 6.1. Theorem 6.1 can be trivially extended for systems with nonlinear dynamics. The proof is straightforward and similar to the proof presented for Theorem 6.1. Hence, the proof is omitted. The theorem is stated next:

**Theorem 6.2.** *Assume there exists a continuously differentiable function  $V : \mathbb{R}^n \rightarrow \mathbb{R}$  such that  $V(0) = 0$ ,  $V(x) > 0 \forall x \neq 0$ ,  $\Omega(V, \gamma)$  is bounded, and*

$$\Omega(V, \gamma) \subset D(V, f(x) + g(x)h(x)) \quad (6.12)$$

If there exists  $l : \mathbb{R}^n \rightarrow \mathbb{R}$  such that:

$$\Omega(V, \gamma) \subset D(V, f(x) + g(x)l(x)) \quad (6.13)$$

$$\Omega(V, \gamma) \subset \mathscr{W}(l) \quad (6.14)$$

then  $\Omega(V, \gamma) \subset \mathcal{R}$ .

Both Theorem 6.1 and 6.2 provide conditions for a sublevel set of  $V$  to be inside the ROA. The theorems are simplified for single input systems but can be generalized for systems with multiple inputs. The assumption in Equation 6.12 means that  $V$  is a Lyapunov function for the closed-loop dynamics. This is a necessary condition for  $V$  to be a Lyapunov function for dynamics with actuator saturation. The remaining two assumptions in Equations 6.13 and 6.14 are sufficient conditions for the set containment constraint in Equation 6.3. The essential step of the proof is to express the closed-loop dynamics with saturation as a convex combination of the dynamics and dynamics with the auxiliary feedback  $l(x)$ . Thus this result can be interpreted as a common Lyapunov condition for polytopic systems [4].

### 6.3 Estimation of Region of Attraction

This section focuses on formulating an optimization algorithm to estimate the ROA. Theorem 6.2 provides conditions for a sublevel set of  $V$  to be inside the ROA. A function  $V$  that satisfies the conditions in Theorem 6.2 is a Lyapunov function and  $\Omega(V, \gamma)$  provides an estimate of the ROA. Another optimization can be formulated to determine the largest estimate of the ROA:

$$\gamma_{NL} := \sup_{l, \gamma} \gamma$$

subject to:

$$\Omega(V, \gamma) \subset D(V, f(x) + g(x)h(x)) \quad (6.15a)$$

$$\Omega(V, \gamma) \subset D(V, f(x) + g(x)l(x)) \quad (6.15b)$$

$$\Omega(V, \gamma) \subset \mathcal{W}(l) \quad (6.15c)$$

The subscript  $NL$  indicates that the optimization problem provides an ROA estimate of the polynomial dynamics mentioned in Equation 6.2. This section focuses on formulating optimization algorithm to find optimal  $\gamma_{NL}$  of 6.15.

Optimization 6.15 implicitly assumes that  $V$  satisfies the other conditions in Theorem 6.2. The sublevel set  $\Omega(V, \gamma)$  is a provable subset of the ROA for any  $\gamma < \gamma_{NL}$ . The constraints in this optimization are sufficient conditions for the set containment constraint in Equation 6.3. Hence  $\gamma_{NL} \leq \gamma^*$ , i.e. the optimization in Equation 6.15 may give conservative results relative to the optimization in Equation 6.3.

Previous works [23] have focused on estimating ROA for linear systems in feedback with saturation (Equation 6.5). Specifically, [23] provides a Semi-definite programming (SDP) formulation for Theorem 6.1 when  $l$  is restricted to be a linear function:  $l(x) = Lx$  for some  $L \in \mathbb{R}^{n_w \times n}$ . In particular, let  $\gamma_{LIN}$  denote the solution of this optimization. The conversion to an SDP requires the additional assumption that  $V$  be a quadratic function. Let  $V(x) = x^T P x$  where  $P > 0$  and  $(A+BH)^T P + P(A+BH) < 0$  and assume that  $P$  is known. Given these restrictions, the optimization in Equation 6.15 is equivalent to [12]:

$$\begin{aligned} \gamma_{LIN}^{-1} &= \inf_{\tau, L} \tau \\ &\text{subject to:} \\ &(A + BL)^T P + P(A + BL) < 0 \\ &\begin{bmatrix} \tau & L \\ L^T & P \end{bmatrix} \geq 0 \end{aligned} \tag{6.16}$$

where  $\tau := 1/\gamma$ . SDPs such as this one can be efficiently solved for systems of moderate state dimensions ( $< 100$ ) [4]. The two constraints are referred to as linear matrix inequalities (LMIs). Next, we focus on formulating an algorithm to solve the optimization problem 6.15 for polynomial systems..

For a given polynomial Lyapunov function  $V$ , Theorem 6.2 provides appropriate conditions for a set to be invariant. With all the Lyapunov functions satisfying the conditions, it is desirable to choose the “best” one to obtain a least conservative estimate of the ROA. Next, we introduce the notion of shape function to quantify “best”. Given an  $n \times n$  matrix  $N = N^T > 0$ , define the shape function  $p(x) := x^T N x$  and level set  $\mathcal{E}(N, \beta) := \{x \in \mathbb{R}^n : p(x) \leq \beta\}$ .  $p(x)$  defines the shape of the ellipsoid and  $\beta$  determines the size of the ellipsoid  $\mathcal{E}(N, \beta)$ . The choice of  $N$  is problem dependent and reflects dimensional scaling information as well as the importance of certain directions in the state space.  $N$  can typically be chosen to be diagonal with  $N_{i,i} := 1/x_{i,max}^2$ . With this choice,  $\mathcal{E}(N, \beta = 1)$  is a coordinate-aligned ellipsoid whose extreme points along the  $i^{th}$  state direction are  $\pm x_{i,max}$ . In this form, the level set value  $\beta$  provides an easily interpretable value for the size of the level set.

Given the shape function  $N$ , the problem is to find the largest ellipsoid  $\mathcal{E}(N, \beta)$

contained in the ROA:

$$\begin{aligned} \beta^* &= \max \beta & (6.17) \\ \text{subject to: } & \mathcal{E}(N, \beta) \subset \mathcal{R} \end{aligned}$$

As discussed in Chapter 4.1, determining the best ellipsoidal approximation to the ROA is still a challenging computational problem. We focus on estimating a lower bound for  $\beta^*$  satisfying  $\underline{\beta} \leq \beta^*$ . Estimating a lower bound  $\underline{\beta}$  can be posed as the following optimization problem which entails solving the set containment conditions:

$$\begin{aligned} \underline{\beta} &:= \sup_{V>0, l, \gamma, \beta} \beta & (6.18) \\ \text{subject to:} & \\ & \mathcal{E}(N, \beta) \subset \Omega(V, \gamma) \\ & \text{Equations (6.12) – (6.14)} \end{aligned}$$

The above optimization problem provides an estimate to the lower bound  $\beta^*$ . The optimization grows the shape function contained within the sublevel set of Lyapunov function  $\Omega(V, \gamma)$ . The following section discusses the computational issue of this optimization problem.

### 6.3.1 SOS Iteration Algorithm

This section turns the set invariance conditions provided by Theorem 6.2 into a Sum-of-Squares (SOS) [33, 38] optimization problem. Similar to the approach taken in previous chapters, all the set containment constraints in the optimization problem

6.18 are reformulated as an SOS optimization problem:

$$\underline{\beta} := \max_{V>0, l, \gamma, \beta} \beta$$

subject to:

$$V(x) \text{ is SOS, } V(0) = 0 \quad (6.19)$$

$$- [s_1(x)(\beta - x^T N x) - (\gamma - V)] \text{ is SOS} \quad (6.20)$$

$$- [\nabla V \cdot (f(x) + g(x)h(x)) + s_2(x)(\gamma - V)] \text{ is SOS} \quad (6.21)$$

$$- [\nabla V \cdot (f(x) + g(x)l(x)) + s_3(x)(\gamma - V)] \text{ is SOS} \quad (6.22)$$

$$- [s_4(x)(\gamma - V) - (-l(x) + 1)] \text{ is SOS} \quad (6.23)$$

$$- [s_5(x)(\gamma - V) - (l(x) + 1)] \text{ is SOS} \quad (6.24)$$

$$s_i(x) \text{ is SOS } \forall i = 1, 2, 3, 4, 5 \quad (6.25)$$

Note that the optimization problem is bilinear in the decision variables. Hence, an iterative approach needs to be taken. The iteration steps are very similar to the  $V - s$  iterations as discussed in Chapter 4.

The Lyapunov function  $V$  in the iteration is initialized with the linearized Lyapunov function  $V_{LIN} = x^T P x$  by solving the linear matrix inequality  $A^T P + P A < 0$ .

1. Initialization Step: Set  $V = V_{LIN}$  and solve for  $\gamma$  and a feasible  $s_2$  satisfying Equation (6.21).
2.  $l$  Step: Hold  $V$  and  $\gamma$  fixed and solve for  $l(x)$ ,  $s_i(x)$  satisfying Equation (6.21) - (6.25).
3.  $\beta$  Step: Hold  $V$ ,  $\gamma$  fixed and solve for  $s_1$  and  $\beta$

$$\beta^* := \max \beta$$

subject to:

$$\text{Equation (6.20)}$$

4.  $V$  step: Hold  $\bar{\beta}$ ,  $l(x)$ ,  $s_i$  fixed and solve for  $V$  and  $\gamma$  such that

$$\gamma^* := \max \gamma$$

subject to:

$$\text{Equation (6.19) - (6.24)}$$

5. Repeat  $l$  Step,  $\beta$  Step and  $V$  Step as long as the  $\beta^*$  continues to increase.

Note that the initialization step computes a feasible  $\gamma$  for polynomial dynamics  $f(x) + g(x)h(x)$  by solving Equation (6.21) while holding  $V = V_{LIN}$ . The solution results in an initial sublevel set  $\Omega(V_{LIN}, \gamma)$  which is then used to seed the iteration. Specifically,  $\Omega(V_{LIN}, \gamma)$  is guaranteed to produce a feasible solution for the  $l$  Step. For example, Equation (6.22) in  $l$  Step is trivially satisfied by setting  $l(x) = h(x)$  and Equation (6.23) -(6.24) are satisfied by setting  $s_j = \frac{1}{\gamma}$  for  $j = 4, 5$  and using the fact that  $|l(x)| \leq 1$ . Next we focus on the application of the algorithm.

## 6.4 Application: F/A-18 Longitudinal Flight Control System with Saturation

Consider the feedback interconnection of Figure 6.2.  $P$  represents the polynomial dynamics of the F/A-18 aircraft's longitudinal direction. The input to the plant  $P$  is the elevator deflection,  $\delta_{elev}$  and pitch rate  $q$  denotes the output of the plant. The controller  $K_q$  is a proportional pitch rate feedback gain. The controller generates the elevator deflection command  $\delta_{elev_{cmd}}$ , which passes through the saturation block and produces the input to the plant  $P$ . The goal of this section is to estimate the ROA of the feedback system shown in Figure 6.2.

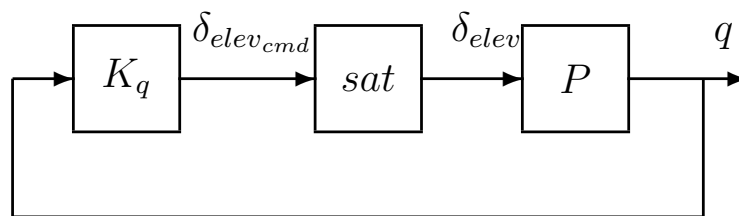


Figure 6.2: Feedback Interconnection of the F/A-18 Longitudinal Direction

Consider the longitudinal dynamics of the F/A-18 aircraft, which can be found in [6]. We generate a polynomial description of the longitudinal F/A-18 dynamics as presented in [6]. Denote the polynomial description as  $\mathcal{F}_{long}$ . The details of generating the polynomial description are omitted here. The polynomial description  $\mathcal{F}_{long}$  is

presented in Appendix B. The plant  $P$  then takes the following input-output form:

$$\dot{x} = \mathcal{F}_{long}(x, u) \quad (6.26a)$$

$$y = q \quad (6.26b)$$

where  $x := [V(\text{ft/s}), \alpha(\text{rad}), q(\text{rad/s}), \theta(\text{rad})]^T$ , and  $u := \delta_{elev}(\text{rad})$ . Moreover, the pitch rate feedback gain is  $K_q = 0.1$ .

We consider a steady wing level flight condition around  $260 \text{ ft/s}$  for the purpose of analysis. Equation 6.27 provides the flight condition:

$$\begin{bmatrix} V_t \\ \alpha_t \\ q_t \\ \theta_t \end{bmatrix} = \begin{bmatrix} 260.00 \text{ ft/s} \\ 0.6095 \text{ rad} \\ 0 \text{ rad/s} \\ 0.6095 \text{ rad} \end{bmatrix}, \quad \delta_{elev,t} = -0.3038 \text{ rad} \quad (6.27)$$

The subscript “t” denotes a trim value. Next we estimate the ROA of the feedback system shown in Figure 6.2 using the SOS estimation procedure presented in Section 6.3.1. We first apply the estimation technique on the short period dynamics of the polynomial plant  $\mathcal{F}_{long}$ . The short-period dynamics involve two states,  $x_{SP} = [\alpha(\text{rad}), q(\text{rad/s})]^T$  and the ROA estimated by the SOS algorithm can be verified against the phase plane simulation. Finally, the SOS estimation technique is applied on the 4-state longitudinal dynamics presented in Equation 6.26.

#### 6.4.1 Analysis of Short Period Model

This section focuses on the ROA estimation of the short period model. A polynomial short period model is extracted from the 4-state polynomial model ( $\mathcal{F}_{long}$ ) by holding  $V$  and  $\theta$  at their trim values and considering the  $\dot{\alpha}$  and the  $\dot{q}$  equation of  $\mathcal{F}_{long}$ . In this case, the plant  $P$  in Figure 6.2 takes the following form:

$$\dot{x}_{SP} = \mathcal{F}_{SP}(x_{SP}, u) \quad (6.28a)$$

$$y = q \quad (6.28b)$$

Figure 6.3 shows the phase plane for the short period model. The solid trajectories are stable, while the dashed trajectories grow unbounded. The ROA consists of all the points that lie on the stable trajectories.

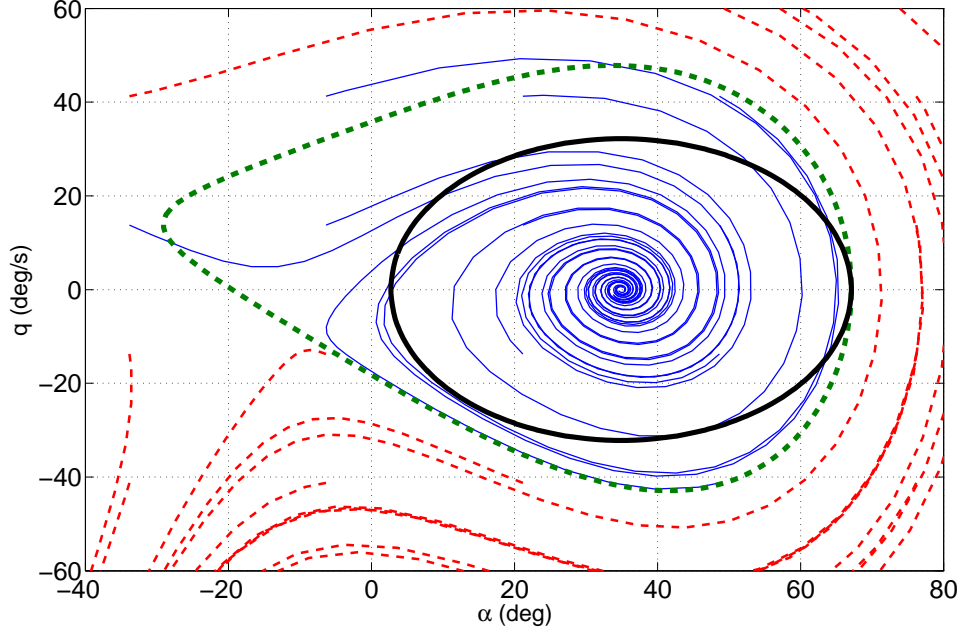


Figure 6.3: Phase plane simulation for polynomial short period model with lower bound estimation of ROA; Stable trajectories are denoted by solid and dashed denotes the unstable trajectories

Next, the  $V$ - $s$  iteration technique is applied on the short period model. We employ the  $V$ - $s$  iteration procedure for a quartic Lyapunov function. The shape function is chosen to be  $p(z) = z^T z$  where  $z := [\alpha - \alpha_t, q - q_t]^T$ . The (black) solid ellipse in Figure 6.3 shows the ellipsoidal estimate of the ROA for the shape function  $p(z)$  and lies within the stable region. The level set of the quartic Lyapunov function found by the  $V$ - $s$  iteration procedure is also plotted in Figure 6.3 a (cyan) dotted curve. The sublevel set of the Lyapunov function lies within the stable region and provides a better (in terms of conservativeness) estimate of the ROA. Note that the (black) solid ellipse provides an under approximation to the invariant region certified by the quartic Lyapunov sublevel set. Unfortunately, the sublevel set of the Lyapunov function cannot be visualized for higher-dimensional (more than 2-states) systems. Hence, the shape function is useful for plotting the ROA estimates.

The short period analysis provided confidence on the correctness of the  $V$ - $s$  iteration technique. Additionally, the Lyapunov sublevel set provided a non-conservative estimate of the ROA. Hence, it is possible to get tighter ellipsoidal estimate of the ROA by choosing the shape function  $p(z)$  appropriately. Next, we focus on applying the  $V$ - $s$  iteration technique on the 4-state polynomial dynamics as presented in Equation 6.26.

### 6.4.2 ROA Analysis of 4-State Longitudinal F/A-18 Model

ROA analysis is performed for the F/A-18 aircraft around the steady, wing level flight condition at  $V = 260$  ft/s. The shape function is  $p(x) = x^T N x$  where

$$\begin{aligned} N &:= \text{diag}(100 \text{ ft/s}, 0.3491 \text{ rad}, 0.8727 \text{ rad/s}, 0.3491 \text{ rad})^{-2} \\ &:= \text{diag}(100 \text{ ft/s}, 20 \text{ deg}, 50 \text{ deg/s}, 20 \text{ deg})^{-2} \end{aligned} \quad (6.29)$$

The polynomial model of the longitudinal F/A-18 dynamics is modified in two ways to make it suitable for the computational algorithms. First, the states are redefined as  $z := x - x_t := [V - V_t, \alpha - \alpha_t, q - q_t, \theta - \theta_t]^T$  to shift the trim condition to the origin of the state space. Next, we perform scaling of the model, which is another important issue for the numerical stability of the  $V$ -s iteration. The states are scaled as  $\hat{z} = D z$  where  $D = N^2$ . In the  $\hat{z}$  coordinates the shape function is  $p(\hat{z}) = \hat{z}^T \hat{z}$ .

The  $V$ -s iteration with a quartic Lyapunov function resulted in a lower bound estimate of  $\underline{\beta} = 0.630$ . This verifies that the ellipsoid  $\mathcal{E}_{\underline{\beta}} := \{x \in \mathbb{R}^n : p(x) \leq \underline{\beta}\}$  is a subset of the ROA. The center of the ellipsoid is at the trim condition. It has a length of  $20 \text{ deg} \cdot \sqrt{\underline{\beta}_4} = 15.88 \text{ deg}$  along the  $\alpha$  axis. The other axis lengths can be computed similarly. The upper bound, denoted as  $\mathcal{E}_{\bar{\beta}}$ , is computed by the Monte Carlo simulation approach as described in Section 4.1.1. The upper bound is found to be  $\bar{\beta} = 0.748$ . The ellipsoid  $\mathcal{E}_{\bar{\beta}} := \{x \in \mathbb{R}^n : p(x) \leq \bar{\beta}\}$  is an over approximation of the ROA. The ROA ellipsoidal bounds on the ROA can be visualized by plotting slices of the ellipsoids  $\mathcal{E}_{\underline{\beta}}$  and  $\mathcal{E}_{\bar{\beta}}$ . Figure 6.4 shows slices of these ellipsoidal ROA bounds in the  $\alpha$ - $q$  plane. The solid ellipse is the slice of the  $\mathcal{E}_{\bar{\beta}}$ . There is an unstable trajectory that touches  $\mathcal{E}_{\bar{\beta}}$  although it may not necessarily touch the ellipse in the  $\alpha$ - $q$  plane. The Monte Carlo search returned the following initial condition yielding an unstable trajectory.

$$x_{0,div} := [236.66 \text{ ft/s}, 0.5745 \text{ rad}, -0.7203 \text{ rad/s}, 0.6313 \text{ rad}]^T$$

The dotted ellipse is the slice of the  $\mathcal{E}_{\underline{\beta}}$ . Every initial condition within this ellipsoid will return to the trim condition (marked as an 'x'). The closeness of the upper and the lower bound indicates that the best ellipsoidal ROA approximation problem has been solved for engineering purposes.

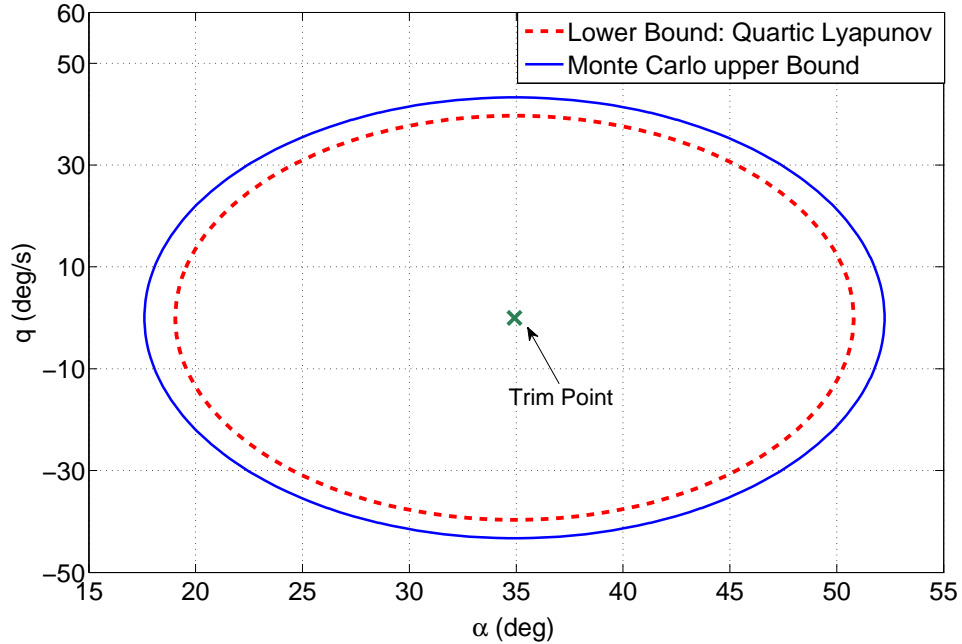


Figure 6.4: Lower and Upper Bound Estimate of ROA for the F/A-18 4-state longitudinal model with actuator saturation

## 6.5 Summary

This chapter presents a method for estimating a lower bound of the ROA for polynomial dynamical systems in feedback with saturation. The actuator saturation is expressed as a convex combination of linear feedbacks. This idea is the key to formulating a polytopic set invariance condition for estimating the bound on the ROA. The SOS optimization framework has been used for computing the bound. The conservativeness of the results are quantified by estimating the upper bound of the ROA via a Monte Carlo search for a divergent trajectory. The technique has been applied to the short period model and the 4-state longitudinal model of the F/A-18 dynamics.

# Chapter 7

## Peak Gain Analysis

This chapter analyzes the performance of nonlinear systems in terms of  $L_\infty$  norm. In other words, the size of the signals, in this chapter, are measured using the  $L_\infty$  norm. Particularly, the chapter computes the  $L_\infty$  gain function as a performance metric of the nonlinear systems. The technique is then applied on the 4-state longitudinal GTM dynamics.

The previous chapters have focused on computing the induced  $L_2$  gain of nonlinear systems. The induced  $L_2$  gain computation requires the assumption that the signals of interest belong to the  $L_2$  signal space. In other words, the signals must have finite energy when integrated over time. This assumption seems trivial for nonpersistent signals. From a practical standpoint, engineers are often interested to analyze the effect of the system when the peak value (in time) of the signals is given. In other words, the signals of interest are measured in  $L_\infty$  norm. Analyzing system's performance in terms of  $L_\infty$  norm, also known as peak gain analysis, can provide a lot of insight to the worst case behaviors of the system. This is particularly true for flight control systems. For example, flight control engineers are often interested to know how far the aircraft can be pushed when the pilot gives a certain size of pulse input to the elevator channel. Peak gain analysis turns out to be a natural framework to answer this question.

## 7.1 $L_\infty$ Gain Function Estimation

Consider a polynomial (time-invariant) dynamical system of the form:

$$\dot{x} = f(x, d) \quad (7.1a)$$

$$y = h(x) \quad (7.1b)$$

where  $x \in \mathbb{R}^n$ ,  $d \in \mathbb{R}$ ,  $y \in \mathbb{R}$  denote the state vector, exogenous input, and output of the system, respectively. The dynamics of the system is described by a multivariable polynomial function denoted by  $f : \mathbb{R}^n \times \mathbb{R} \rightarrow \mathbb{R}^n$ . The output equation is represented by a multivariable polynomial function  $h(x) : \mathbb{R}^n \rightarrow \mathbb{R}$ . Also assume that  $f(0, 0) = 0$  and  $h(0) = 0$ .

**Remark** We consider SISO system for simplicity purpose. The results presented in this chapter are also applicable for MIMO systems unless otherwise noted.

$L_\infty$ -norm (in time), denoted as  $\|\cdot\|_\infty$ , is used to measure the signal size. For any continuous signal  $e(t)$ , the  $L_\infty$ -norm is defined as:

$$\|e\|_\infty := \sup_{t \geq 0} |e(t)| \quad (7.2)$$

The input  $d$  is viewed as a norm-bounded disturbance signal such that  $\|d\|_\infty \leq R$ , where  $R \in \mathbb{R}_+$ . Define the set of admissible disturbance  $\mathcal{D} = \{d \in \mathbb{R}^m : d \in L_\infty \text{ and } \|d\|_\infty \leq R\}$ . We are interested in investigating the worst case effect of the disturbance signal  $d \in \mathcal{D}$ , on the system as the disturbance size  $R$  varies. The worst case behavior of nonlinear systems is usually quantified by the *induced  $L_\infty$  gain* or the  *$L_\infty$  gain function* of the system [14]. These two metrics are defined below.

The induced  $L_\infty$  gain, denoted as  $\gamma_\infty(R)$ , is defined as:

$$\gamma_\infty(R) := \sup_{d \in \mathcal{D}, x(0)=0} \frac{\|y\|_\infty}{\|d\|_\infty} \quad (7.3)$$

The  $L_\infty$  gain function, denoted as  $\Sigma_\infty(R)$ , is defined as:

$$\Sigma_\infty(R) := \sup\{\|y\|_\infty : d \in \mathcal{D}, x(0) = 0\} \quad (7.4)$$

The subscript  $\infty$  in both equations indicates that the signals are measured in the  $L_\infty$  norm.

The goal of this chapter is to compute the  $L_\infty$  gain function,  $\Sigma_\infty(R)$ , given the input size  $R$ . The characterization of  $\Sigma_\infty(R)$  can be thought of as a two-step process. The first step involves characterizing a reachable set of the system with disturbance  $d \in \mathcal{D}$ . The reachable set  $\mathbf{R}_\infty(x)$  represents the set of points that can be reached in finite time by a trajectory generated by Equation 7.1a with some admissible disturbance input  $d \in \mathcal{D}$ . For a fixed time  $T \geq 0$ , the reachable set is formally defined as [4]:

$$\mathbf{R}_\infty(x) := \{x(T) \mid x, d \text{ satisfies Equation 7.1a, } x(0) = 0, d \in \mathcal{D}, T \geq 0\} \quad (7.5)$$

The second step performs a maximization of the output direction  $h(x)$  on the reachable set  $\mathbf{R}_\infty(x)$ . The peak gain function can now be rewritten as:

$$\Sigma_\infty(R) := \sup\{\|h(\xi)\|_\infty : \xi \in \mathbf{R}_\infty(x)\} \quad (7.6)$$

The first step in computing the  $L_\infty$  gain function  $\Sigma_\infty(R)$  involves characterizing the reachable set  $\mathbf{R}_\infty(x)$ . Unfortunately, exact characterization of the reachable set  $\mathbf{R}_\infty(x)$  is challenging and hence, we focus on estimating an upper bound of the set  $\mathbf{R}_\infty(x)$ .

Lyapunov arguments are typically used to bound reachable sets. Lemma 4 provides a local inequality condition to quantify an upper bound of the reachable set  $\mathbf{R}_\infty(x)$ . A brief sketch of proof is also provided.

**Lemma 4.** *If there exists  $\epsilon > 0$  and a polynomial  $V : \mathbb{R}^n \rightarrow \mathbb{R}$  such that:*

$$\nabla V(x)f(x, d) \leq -\epsilon \text{ whenever } V(x) = 1 \text{ and } d \in \mathcal{D}, \quad (7.7)$$

*and define the sublevel set  $\Omega(V, 1) = \{x : V(x) \leq 1\}$  then, if  $\dot{x} = f(x, d)$ ,  $x(0) \in \Omega(V, 1)$ , and  $d \in \mathcal{D}$ , we have  $x(t) \in \Omega(V, 1)$  for  $0 \leq t \leq T$ .*

*Proof.* This is a proof by contradiction. Suppose  $\dot{x} = f(x, d)$ ,  $x(0) \in \Omega(V, 1)$ , and  $d \in \mathcal{D}$  for  $0 \leq t \leq T$ . Also assume that  $V$  satisfies Equation 7.7. Now, suppose that  $x(T) \notin \Omega(V, 1)$ . This implies that  $V(x(0)) \leq 1$  and  $V(x(T)) > 1$ . Hence,  $\exists$  a  $t_0 \in [0, T]$  such that  $V(x(t_0)) = 1$ ,  $\nabla V(x(t_0))f(x, d) \geq 0$ . However, it is assumed that  $\nabla V(x)f(x, d) \leq -\epsilon < 0$ ,  $\forall t \in [0, T]$ . This gives us a contradiction.  $\square$

Note that the positive scalar  $\epsilon$  guarantees strict negativity of the gradient of the Lyapunov function  $V$ . Lemma 4 states that every trajectory that starts in  $\Omega(V, 1)$

will stay there in future with disturbance  $d \in \mathcal{D}$ . This implies  $\mathbf{R}_\infty(x) \subset \Omega_{V,1}$  given  $0 \in \Omega(V, 1)$ . Hence, the Lyapunov sublevel set  $\Omega(V, 1)$  of Lemma 4 gives an over approximation of the reachable set  $\mathbf{R}_\infty(x)$ . The set  $\Omega(V, 1)$  also provides an conservative estimate of the reachable set and in turn measuring the worst case effect of the disturbance  $d$  on the state  $x$ .

The second step in computing the  $L_\infty$  gain function  $\Sigma_\infty(R)$  involves solving for Equation 7.6. Equation 7.6 relies on maximizing the size of the output  $h(x)$  on the reachable set. However, only an upper bound estimate of the reachable set is available. Consequently, computing the  $L_\infty$  gain function  $\Sigma_\infty(R)$  is restricted to an upper bound estimate of  $\Sigma_\infty(R)$ . Denote this upper bound estimate of  $\Sigma_\infty(R)$  as  $\bar{\Sigma}_\infty(R)$ . Equation 7.6 is relaxed to compute  $\bar{\Sigma}_\infty(R)$ :

$$\bar{\Sigma}_\infty(R) := \sup\{\|h(x)\|_\infty : x \in \Omega(V, 1)\} \quad (7.8)$$

If  $\Omega(V, 1)$  is bounded then this problem can be formulated as:

$$\begin{aligned} \bar{\Sigma}_\infty(R) &:= \sup_{\beta} \beta \\ &\text{subject to: } \Omega(V, 1) \subset \{x \in \mathbb{R}^n : \|h(x)\|_\infty \leq \beta\} \end{aligned} \quad (7.9)$$

The two step procedure discussed above gives an upper bound estimate of the  $L_\infty$  gain function  $\Sigma_\infty(R)$ . Specifically, the conditions provided by Lemma 4 and Equation 7.9 can be combined to provide characterize an upper bound estimate of the  $L_\infty$  gain function. Formally, the characterization is given in the following Lemma. This result can also be found in [57] (See Lemma 6.1.1)

**Lemma 5.** *For any  $\epsilon > 0$ , if  $\exists$  a real scalar  $\beta > 0$  and a continuously differentiable function  $V : \mathbb{R}^n \rightarrow \mathbb{R}$  such that  $\Omega(V, 1)$  is bounded and*

$$\nabla V(x)f(x, d) \leq -\epsilon \quad \forall x \in \{x \in \mathbb{R}^n : V(x) = 1\} \text{ and } d \in \mathcal{D}, \quad (7.10)$$

$$\Omega(V, 1) \subset \{x \in \mathbb{R}^n : \|h(x)\|_\infty \leq \beta\} \quad (7.11)$$

*then for system in Equation 7.1  $\|y\|_\infty \leq \beta$  whenever  $d \in \mathcal{D}$ .*

Lemma 5 contains set containment arguments for estimating an upper bound  $\bar{\Sigma}_\infty(R)$  of the gain function. The conditions in Lemma 5 can be turned into the following

optimization problem.

$$\bar{\Sigma}_\infty(R) := \sup_{\beta, V} \beta$$

subject to:

$$\{x : V(x) = 1, d \in \mathcal{D}\} \subset \{x : \nabla V(x)f(x, d) \leq -\epsilon\} \quad (7.12a)$$

$$\Omega(V, 1) \subset \{x : \|h(x)\|_\infty \leq \beta\} \quad (7.12b)$$

The positive scalar  $\epsilon$  is a small positive number that ensures the strict negativity of the term  $\nabla V(x)f(x, d)$  on the set  $\{x \in \mathbb{R}^n : V(x) = 1\}$  and  $d \in \mathcal{D}$ .

The computational algorithm used in the analysis replaces the set containment constraints in Equation 7.12 with a sufficient S-procedure condition involving non-negative functions. Consequently, the non-negative functions can be replaced by SOS constraints. Hence, estimating  $\bar{\Sigma}_\infty(R)$ , given an input size  $R$ , can be formulated as an SOS optimization problem.

$$\bar{\Sigma}_\infty(R) := \sup_{\beta, V, r, s_0, s_1} \beta$$

subject to:

$$-\epsilon - \nabla V(x)f(x, d) - r(x)(1 - V(x)) - s_1(x, d)(R^2 - d^2) \text{ is SOS} \quad (7.13a)$$

$$(\beta^2 - h^2) - s_0(x)(1 - V) \text{ is SOS} \quad (7.13b)$$

$$s_0(x), s_1(x, d) \text{ is SOS} \quad (7.13c)$$

The functions  $s_0(x)$ ,  $s_1(x, d)$ ,  $r(x)$  arise from the generalized S-procedure and are decision variables of the optimization. The function  $r(x)$  is not necessary to be non-negative as the constraint  $\nabla V(x)f(x, d) \leq -\epsilon$  needs to hold on the set  $\{x : V(x) = 1\}$ . Note that the positive scalar  $\epsilon$  is not a decision variable of the optimization and is typically chosen by the analyst.

Equation 7.13 provides an upper bound to the gain function given an input size  $R$ . Another equivalent question can be asked: given an upper bound  $\beta$ , what is the largest value of  $R$  such that  $\|d\|_\infty \leq R$  whenever  $\|h(x)\|_\infty \leq \beta$ ? We can formulate an SOS optimization problem, similar to the one in Equation 7.13, to find the largest

value of  $R$  given an upper bound  $\beta$ .

$$\bar{R} := \sup_{V, r, s_0, s_1} R$$

subject to:

$$-\epsilon - \nabla V(x)f(x, d) - r(x)(1 - V(x)) - s_1(x, d)(R^2 - d^2) \text{ is SOS} \quad (7.14a)$$

$$(\beta^2 - h^2) - s_0(x)(1 - V) \text{ is SOS} \quad (7.14b)$$

$$s_0(x), s_1(x, d) \text{ is SOS} \quad (7.14c)$$

Note that both the optimization problem as mentioned in Equation 7.13 and Equation 7.14 are bilinear in decision variables. For example, the term  $V(x)r(x)$  is bilinear in decision variable. A  $V$ - $s$  type iteration technique, where  $r$  is solved for fixed  $V$  and vice versa, is proposed to solve the SOS optimization problem. Hence, we require an initial  $V$  to seed the iteration. The Lyapunov function  $V$  is initialized with the linearized Lyapunov function  $V_{LIN} = x^T P x$ ,  $P > 0$  by solving the following SOS condition.

$$-\epsilon - \nabla V_{LIN}(x) \cdot f_{LIN}(x, d) - r(x)(1 - V_{LIN}(x)) - s_1(x, d)(R^2 - d^2) \text{ is SOS} \quad (7.15)$$

where  $f_{LIN}$  represents the linearization of  $f$ . Consider,  $f_{LIN} = Ax + Bd$ , where  $A$ ,  $B$  are matrices of appropriate dimensions. For linear system,  $r(x)$  and  $s_1(x, d)$  can be set to constant value of  $r_c$  and  $s_c$ , respectively. Equation (7.15) represents the condition for estimating reachable sets for peak inputs. Equation (7.15) is presented in [4] for  $R = 1$ . Equation (7.15) can be formulated as an LMI in  $(x, d)$ :

$$\begin{bmatrix} -(A^T P + PA) + r_c P & -PB & 0 \\ -(PB)^T & s_c & 0 \\ 0 & 0 & -\epsilon - s_c - r_c \end{bmatrix} \succeq 0 \quad (7.16)$$

By setting  $\epsilon = 0$  and  $r_c = -s_c$  Equation 7.17 reduces to the following LMI:

$$\begin{bmatrix} -(A^T P + PA) - s_c P & -PB \\ -(PB)^T & s_c \end{bmatrix} \succeq 0 \quad (7.17)$$

Note that Equation 7.17 is bilinear in  $s_c$  and  $P$ . Equation 7.17 can be solved by holding  $s_c$  to a fixed value and searching for a feasible  $P > 0$ . The linearized Lyapunov function  $V_{LIN} = x^T P x$  can be used to seed the  $V$ - $s$  iteration. Next, the  $V$ - $s$  iteration

steps are given for the optimization problem mentioned in Equation 7.14.

1.  $R^2/s$  Step: Hold  $V$  fixed and solve for  $s$  and  $\bar{R}$

$$\begin{aligned} \bar{R} &:= \max R \\ &\text{subject to:} \\ &\text{Equation (7.14a) - (7.14c)} \end{aligned}$$

This step performs a bisection search on  $R$ .

2.  $V$  step: Hold  $\bar{R}$ ,  $s_0(x)$ ,  $s_1(x, d)$  fixed and solve for  $V$  satisfying Equation (7.14a) - (7.14c).
3. Repeat  $R^2/s$  and  $V$  step as long as the  $\bar{R}$  continues to increase.

**Remark 1:** The iteration is initialized with the linearized Lyapunov function  $V_{LIN}$ . However, it is not obvious if the  $R^2/s$  step is feasible given the linearized Lyapunov function. In practice, we have found another initialization technique that may work. For example, one can use the quadratic Lyapunov function that proves the ROA of the corresponding autonomous dynamics, i.e.,  $\dot{x} = f(x, d = 0)$ .

## 7.2 Application

This section describes the computation of upper and lower bounds on the  $L_\infty$  gain function for the closed-loop longitudinal dynamics of the GTM. The analysis is performed around the flight condition mentioned in Equation 4.15. The controller is the simple proportional pitch rate feedback control mentioned in Equation (4.14). Equations 3.13 and 4.14 describe a 4-state seven degree polynomial dynamics of the closed-loop system with the thrust being held at its trim value.

Consider an additive disturbance,  $d_{elev}$  in the elevator channel for the purpose of analysis. Assume that the disturbance is norm bounded such that  $\|d_{elev}\|_\infty \leq R$ . Physically, this additive disturbance can be viewed as wind disturbances in the elevator channel. The objective is to quantify the worst case behavior of the pitch rate state against the wind disturbances in the elevator channel. In other words, we are interested in estimating the maximum value of  $\|q\|_\infty$  as the size of the elevator disturbances  $\|d_{elev}\|_\infty$  varies. The proposed problem is equivalent to computing an  $L_\infty$  gain function as mentioned in Equation 7.4. However, the problem can be solved

by asking an equivalent question. Given the maximum value of  $\|q\|_\infty$  what is the maximum size of the elevator disturbance  $\|d_{elev}\|_\infty$ ? An upper bound on the maximum size of the input can be extracted by employing the SOS based  $V$ - $s$  iteration technique for solving Equation 7.14.

The analysis is performed on a cubic order GTM model to reduce the computational time. The cubic order model is extracted from the 4-state seven degree polynomial model by retaining terms upto cubic order.

Figure 7.1 indicates how the worst case behavior of the pitch rate state varies as the size of the elevator disturbances  $R$  increases. The horizontal axis indicates the size of the elevator disturbances  $R$  and the vertical axis shows the size of the pitch rate state  $\beta$ . The upper bounds (marked as blue x) are found by searching for a quartic Lyapunov function to solve Equation 7.14 using the  $V$ - $s$  iteration technique. Different values of  $\beta$  are assumed and the maximum value of  $R$  is computed for each  $\beta$ . The upper bound results indicate that the GTM can tolerate a disturbance of size  $\|d_{elev}\|_\infty \leq 5.7 \times 10^{-3}$ . This bound is an upper estimate of the worst case behavior of the pitch rate direction. The lower bounds are estimated by randomly searching for inputs that cause the state trajectory to diverge or maximize the gain in the pitch rate direction. The lower bound (marked as red o) indicates the system can tolerate a disturbance of size  $\|d_{elev}\|_\infty \leq 5.7 \times 10^{-3}$ . An input of size  $\|d_{elev}\|_\infty = 0.014$  is found which causes the GTM trajectory to diverge.

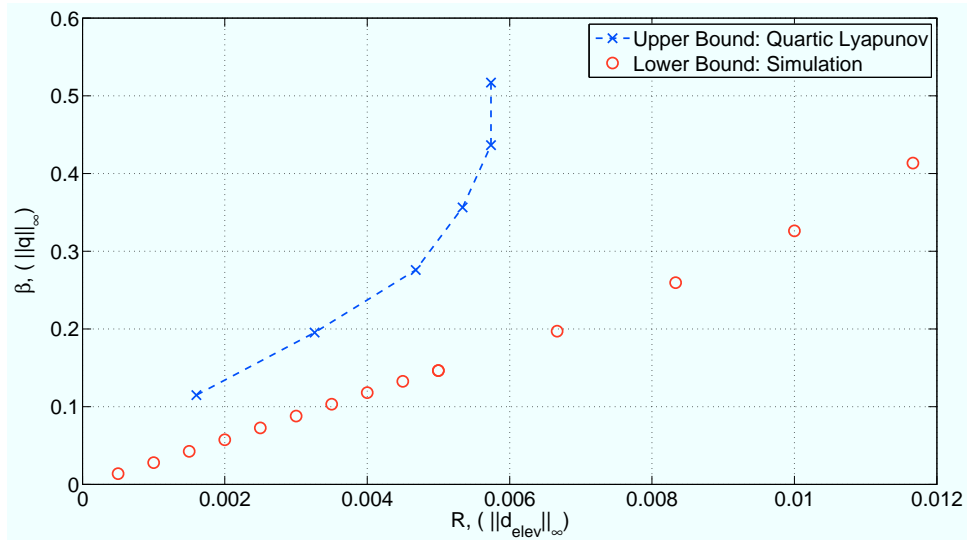


Figure 7.1: Estimation of peak gain function of the 4-state longitudinal GTM dynamics.

### 7.3 Summary

This chapter presents the peak gain function analysis of polynomial systems. The analysis problem is divided into two steps. First, an upper bound of the reachable set is characterized given the peak value of the input. Second, the output of interest is maximized on the reachable set. This two step process provides an upper bound on the peak gain function. The problem is solved using the SOS optimization framework. The technique is then applied to the 4-state longitudinal GTM dynamics.

# Chapter 8

## Conclusion

This chapter summarizes the main contribution of this thesis and discusses some future research directions.

### 8.1 Contributions

This thesis developed quantitative nonlinear analysis tools for the purpose of analytical certification of nonlinear flight control laws. The analytical certification relied on computing the ROA and the induced gain as stability and performance metrics, respectively. Computation of the ROA and the induced gain of nonlinear flight control laws relied on utilizing the SOS optimization framework. The main contributions of this thesis are outlined below:

1. This thesis proposes a framework for analyzing local performance properties of polynomial systems in feedback with actuator saturation. In particular, we formulated a dissipation inequality condition for estimating the local induced  $L_2$  gain for polynomial systems in feedback with actuator saturation. The formulation of the dissipation inequality relies on modeling the saturation in the IQC framework and analytically expressing the saturation constraint. The dissipation inequality condition is then formulated by merging the SOS and the IQC framework.
2. This thesis proposes a method for estimating the ROA of polynomial systems in feedback with actuator saturation. We formulated set invariance conditions for ROA estimation. The key idea in formulating the set invariance conditions

relies on placing the saturation in a convex hull of a group of linear (possibly nonlinear) feedbacks. This idea has its origin in the work of [23]. This thesis extends the stability conditions proposed in [23] for polynomial systems.

3. The SOS based nonlinear analysis tools developed in this thesis are known to be computationally challenging and often suffer from numerical scalability issues for moderately large-scale systems. One of the main contributions of this thesis is in applying this SOS based nonlinear analysis techniques to a moderately large-scale (usually at least 4–5 states and/or cubic nonlinearities) engineering problem, e.g. flight control systems. In particular, we apply the SOS based techniques to the longitudinal GTM and to the longitudinal F/A-18 plant.

## 8.2 Future Research

There are some interesting research directions that were not pursued in this thesis. They are discussed below:

1. In this thesis, we have not discussed the computation of reachable sets for polynomial systems in feedback with actuator saturation. The reachable sets under input constraint provide insights to the determination of safe flight envelope and hence, an important aspect in flight control law certification process.
2. Theorem 5.1, presented in this thesis, remains valid if for any causal, bounded (in  $L_2$  sense) operator  $\Delta$  in place of  $sat(\cdot)$ . This indicates that Theorem 5.1 can be used to answer performance questions for uncertain polynomial systems. This introduces a notion of robust performance analysis of polynomial systems. It will be interesting to apply Theorem 5.1 to such case.
3. The SOS based analysis techniques rely on expressing the nonlinear dynamics via polynomial description. Hence, it is important to quantify the accuracy of the polynomial description of the original nonlinear dynamics. This thesis presents an ad-hoc approach to compare the polynomial description to the original nonlinear system. However, a formal approach is needed to quantify if the polynomial dynamics is a true description of the original nonlinear systems. This is an open research problem.
4. Throughout the thesis, we implemented SOS based  $V$ - $s$  iteration technique for estimating stability and performance metrics. The numerical aspects of the

iteration steps are not analyzed in this thesis. For example, it is not clear why the  $V$  step in the iteration typically returns a different  $V$  in each iteration. Moreover, the thesis does not emphasize on formulating an “efficient” iteration technique rather the thesis simply develops an iteration procedure that provides feasible results. Specifically, one can envision formulating a different estimation technique which minimizes the computational time.

# Bibliography

- [1] R.C. Allen and H.G. Kwatny. Maneuverability and envelope protection in the prevention of aircraft loss of control. In *Control Conference (ASCC), 2011 8th Asian*, pages 381–386. IEEE, 2011.
- [2] J.P. Aubin. *Viability theory*. Springer, 2009.
- [3] G.J. Balas, A. Packard, P. Seiler, and U. Topcu. Robustness analysis of nonlinear systems. <http://www.aem.umn.edu/~AerospaceControl/>.
- [4] Stephen Boyd, Laurent El Ghaoui, Eric Feron, and V. Balakrishnan. *Linear Matrix Inequalities in System and Control Theory*. SIAM Studies in Applied Mathematics, 1994.
- [5] Philip Butterworth-Hayes. Gripen crash raises canard fears. *Aerospace America*, 32:10–11, February 1994.
- [6] A. Chakraborty. Linear and nonlinear analysis of susceptibility of F/A-18 flight control laws to the falling leaf mode. Master’s thesis, University of Minnesota, Twin Cities, 2010.
- [7] H.-D. Chiang and J.S. Thorp. Stability regions of nonlinear dynamical systems: A constructive methodology. *IEEE Trans. on Automatic Control*, 34(12):1229–1241, 1989.
- [8] M.D. Choi, T.Y. Lam, and B. Reznick. Sums of squares of real polynomials. *Proceedings of Symposia in Pure Mathematics*, 58(2):103–126, 1995.
- [9] Dave Cox. *The GTM DesignSim v0905*, 2009.
- [10] E.J. Davison and E.M. Kurak. A computational method for determining quadratic Lyapunov functions for nonlinear systems. *Automatica*, 7:627–636, 1971.

- [11] M.A. Domheim. Report pinpoints factors leading to yf-22 crash. *Aviation Week and Space Technology*, pages 53–54, November 1992.
- [12] Haijun Fang, Zongli Lin, and Tingshu Hu. Analysis of linear systems in the presence of actuator saturation and  $L_2$  disturbances. *Automatica*, 40:1229 – 1238, 2004.
- [13] Haijun Fang, Zongli Lin, and Tingshu Hu. Analysis of linear systems in the presence of actuator saturation and  $L_2$  disturbances. *Automatica*, 40:1229 – 1238, 2004.
- [14] I.J. Fialho and T.T. Georgiou. Worst case analysis of nonlinear systems. *Automatic Control, IEEE Transactions on*, 44(6):1180–1196, 1999.
- [15] K. Gatermann and P. Parrilo. Symmetry groups, semidefinite programs, and sums of squares. *Journal of Pure and Applied Algebra*, 192:95–128, 2004.
- [16] R. Genesio, M. Tartaglia, and A. Vicino. On the estimation of asymptotic stability regions: State of the art and new proposals. *IEEE Trans. on Automatic Control*, 30(8):747–755, 1985.
- [17] O. Hachicho and B. Tibken. Estimating domains of attraction of a class of nonlinear dynamical systems with LMI methods based on the theory of moments. In *Proc. of the IEEE Conference on Decision and Control*, pages 3150–3155, 2002.
- [18] J. Hauser and M.C. Lai. Estimating quadratic stability domains by nonsmooth optimization. In *Proc. of the American Control Conference*, pages 571–576, 1992.
- [19] M. Heller, R. David, and J. Holmberg. Falling leaf motion suppression in the F/A-18 Hornet with revised flight control software. In *AIAA Aerospace Sciences Meeting*, number AIAA-2004-542, 2004.
- [20] M. Heller, R. Niewoehner, and P. K. Lawson. High angle of attack control law development and testing for the F/A-18E/F Super Hornet. In *AIAA GNC Conf.*, number AIAA-1999-4051, pages 541–551, 1999.
- [21] M. Heller, R. Niewoehner, and P. K. Lawson. On the validation of safety critical aircraft systems, Part I: An overview of analytical & simulation methods. In *AIAA Guidance, Navigation, and Control Conference*, number AIAA 2003-5559, 2003.

- [22] H. Hindi and S. Boyd. Analysis of linear systems with saturation using convex optimization. In *Proceedings of the 37th IEEE Conference on Decision and Control*, pages 903 – 908, 1998.
- [23] T. Hu and Z. Lin. *Control Systems with Actuator Saturation - Analysis and Design*. Birkhauser, 2001.
- [24] Tingshu Hu, Zongli Lin, and Ben M. Chen. An analysis and design method for linear systems subject to actuator saturation and disturbances. *Automatica*, 38:351 – 359, 2002.
- [25] P. T. Jaramillo and J. N. Ralston. Simulation of the F/A-18D falling leaf. In *AIAA Atmos. Flight Mechanics Conf.*, pages 756–766, 1996.
- [26] Z. Jarvis-Wloszek. *Lyapunov Based Analysis and Controller Synthesis for Polynomial Systems using Sum-of-Squares Optimization*. PhD thesis, University of California, Berkeley, 2003.
- [27] Z. Jarvis-Wloszek, R. Feeley, W. Tan, K. Sun, and A. Packard. Some controls applications of sum of squares programming. In *Proc. of the IEEE Conference on Decision and Control*, volume 5, pages 4676–4681, 2003.
- [28] Z. Jarvis-Wloszek, R. Feeley, W. Tan, K. Sun, and A. Packard. *Positive Polynomials in Control*, volume 312 of *Lecture Notes in Control and Information Sciences*, chapter Controls Applications of Sum of Squares Programming, pages 3–22. Springer-Verlag, 2005.
- [29] U. Jonsson. *Robustness analysis of uncertain and nonlinear systems*. PhD thesis, Lund Institute of Technology, 1996.
- [30] U. Jonsson, C. Y. Kao, A. Megretski, and A. Rantzer. *A Guide To IQC $\beta$  : A MATLAB Toolbox for Robust Stability and Performance Analysis*, 2004.
- [31] H.K. Khalil. *Nonlinear Systems*. Prentice Hall, 3rd edition, 1996.
- [32] H.G. Kwatny, J.E.T. Dongmo, B.C. Chang, G. Bajpai, M. Yasar, and C. Belcastro. Aircraft accident prevention: Loss-of-control analysis, 2009.
- [33] J.B. Lasserre. Global optimization with polynomials and the problem of moments. *SIAM Journal on Optimization*, 11(3):796–817, 2001.

- [34] C. D. Lluch. Analysis of the out-of-control falling leaf motion using a rotational axis coordinate system. Master's thesis, Virginia Polytechnic Institute and State University, 1998.
- [35] J. Lofberg. Yalmip : A toolbox for modeling and optimization in MATLAB. In *Proc. of the CACSD Conf.*, Taipei, Taiwan, 2004.
- [36] Alexander Megretski and Anders Rantzer. System analysis via integral quadratic constraints. *IEEE Transactions on Automatic Control*, 42:819 – 830, 1997.
- [37] A.M. Murch and J.V. Foster. Recent NASA research on aerodynamic modeling of post-stall and spin dynamics of large transport airplanes. In *45th AIAA Aerospace Sciences Meeting*, 2007.
- [38] P. Parrilo. *Structured Semidefinite Programs and Semialgebraic Geometry Methods in Robustness and Optimization*. PhD thesis, California Institute of Technology, 2000.
- [39] P. Parrilo. Semidefinite programming relaxations for semialgebraic problems. *Mathematical Programming Ser. B*, 96(2):293–320, 2003.
- [40] C. Pittet, S. Tarbouriech, and C. Burgat. Stability regions for linear systems with saturating controls via circle and Popov criteria. In *Proceedings of the 36th IEEE Conference on Decision and Control*, pages 4518 – 4523, 1997.
- [41] S. Prajna, A. Papachristodoulou, P. Seiler, and P. A. Parrilo. *SOSTOOLS: Sum of squares optimization toolbox for MATLAB*, 2004.
- [42] Anders Rantzer and Alexander Megretski. Analysis of rate limiters using integral quadratic constraints. In *Proceedings of IFAC Nonlinear Control Systems Design Symposium*, pages 696–700, Enschede, Netherlands, 1998.
- [43] B. Reznick. Extremal PSD forms with few terms. *Duke Mathematical Journal*, 45(2):363–374, 1978.
- [44] Pete Seiler, Andrew Packard, and Gary Balas. A dissipation inequality formulation for stability analysis with integral quadratic constraints. In *Proceedings of the 2010 Conference on Decision and Control*, 2010.
- [45] B.L. Stevens and F.L. Lewis. *Aircraft Control and Simulation*. John Wiley & Sons, 1992.

- [46] J. Sturm. SeDuMi version 1.05. <http://fewcal.kub.nl/sturm/software/sedumi.html>, 2001.
- [47] J.F. Sturm. Using SeDuMi 1.02, a MATLAB toolbox for optimization over symmetric cones. *Optimization Methods and Software*, pages 625–653, 1999.
- [48] W. Tan. *Nonlinear Control Analysis and Synthesis using Sum-of-Squares Programming*. PhD thesis, University of California, Berkeley, 2006.
- [49] W. Tan and A. Packard. Searching for control Lyapunov functions using sums of squares programming. In *Allerton Conf. on Comm., Control and Computing*, pages 210–219, 2004.
- [50] W. Tan, U. Topcu, P. Seiler, G. Balas, and A. Packard. Simulation-aided reachability and local gain analysis for nonlinear dynamical systems. In *Proc. of the IEEE Conference on Decision and Control*, pages 4097–4102, 2008.
- [51] B. Tibken. Estimation of the domain of attraction for polynomial systems via LMIs. In *Proc. of the IEEE Conference on Decision and Control*, pages 3860–3864, 2000.
- [52] B. Tibken and Y. Fan. Computing the domain of attraction for polynomial systems via BMI optimization methods. In *Proc. of the American Control Conference*, pages 117–122, 2006.
- [53] J. Tierno, R. Murray, and J. C. Doyle. An efficient algorithm for performance analysis of nonlinear control systems. In *Proceedings of the American Control Conference*, pages 2717–2721, 1995.
- [54] U. Topcu and A. Packard. Linearized analysis versus optimization-based nonlinear analysis for nonlinear systems. In *American Control Conference, 2009. ACC '09.*, pages 790–795, june 2009.
- [55] U. Topcu, A. Packard, and P. Seiler. Local stability analysis using simulations and sum-of-squares programming. *Automatica*, 44(10):2669–2675, 2008.
- [56] U. Topcu, A. Packard, P. Seiler, and T. Wheeler. Stability region analysis using simulations and sum-of-squares programming. In *Proc. of the American Control Conference*, pages 6009–6014, 2007.
- [57] Ufuk Topcu. *Quantitative Local Analysis of Nonlinear Systems*. PhD thesis, University of California, Berkeley, 2008.

- [58] A. Vannelli and M. Vidyasagar. Maximal Lyapunov functions and domains of attraction for autonomous nonlinear systems. *Automatica*, 21(1):69–80, 1985.
- [59] M. Vidyasagar. *Nonlinear Systems Analysis*. Prentice Hall, 2nd edition, 1993.

# Appendix A

## Polynomial Longitudinal GTM Model

The longitudinal model of the GTM dynamics is presented in this chapter.

### A.1 Physical Parameters of GTM

The GTM aircraft parameters were provided in Table 3.1. For convenience and completeness, the physical parameters are presented below again.

Wing Area, $S$	5.902 ft <sup>2</sup>
Mean Aerodynamic Chord, $\bar{c}$	0.9153 ft
Mass, $m$	1.542 slugs
Pitch Axis Moment of Inertia, $I_{yy}$	4.254 lbf-ft <sup>2</sup>
Air Density, $\rho$	0.002375 slugs/ft <sup>3</sup>
Gravity Constant, $g$	32.17 ft/s <sup>2</sup>

### A.2 Longitudinal Aerodynamic Model

This section provides closed-form polynomial expression for the aerodynamic model of the GTM's longitudinal dynamics. The aerodynamics model presented here characterizes the lift force, drag force and pitching moment. The forces and the moment are modeled based on the contribution from (i) the bare airframe, denoted as  $C_{(\cdot)\alpha}$ , (ii) the elevator deflection, denoted as  $C_{(\cdot)\delta_{elev}}$ , and (iii) the normalized pitch rate,

denoted as  $C_{(\cdot)_q}$ . The notation  $(\cdot)$  can be replaced by  $L$ ,  $D$ ,  $M$  to indicate lift, drag and pitching moment, respectively. The aerodynamic coefficients are computed from look-up tables provided by NASA.

### A.2.1 Lift Coefficient, $C_L$

The lift coefficients are presented below:

$$C_{L_\alpha} = 2.141\alpha^3 - 6.575\alpha^2 + 5.299\alpha + 5.337 \times 10^{-2} \quad (\text{A.1a})$$

$$C_{L_{\delta_{elev}}} = 3.750\alpha^2 - 3.438 \times 10^{-1}\alpha\delta_{elev} + 2.831 \times 10^{-5}\delta_{elev}^2 - 2.004\alpha \\ + 8.0474 \times 10^{-3}\delta_{elev} + 2.543 \times 10^{-3} \quad (\text{A.1b})$$

$$C_{L_q} = -4.089 \times 10^{-7}V^2q^2 + 2.970 \times 10^{-5}V\alpha q + 2.415 \times 10^{-4}Vq^2 \\ - 7.512 \times 10^{-4}Vq + 2.297 \times 10^{-2}\alpha^2 - 8.771 \times 10^{-3}\alpha q \\ - 3.566 \times 10^{-2}q^2 - 1.673 \times 10^{-2}\alpha + 2.219 \times 10^{-1}q + 3.703 \times 10^{-3} \quad (\text{A.1c})$$

The total lift force coefficient is:

$$C_L = C_{L_\alpha} + C_{L_{\delta_{elev}}} + C_{L_q} \quad (\text{A.2})$$

### A.2.2 Drag Coefficient, $C_D$

The drag coefficients are presented below:

$$C_{D_\alpha} = -1.477\alpha^3 + 3.110\alpha^2 - 1.303 \times 10^{-1}\alpha + 3.064 \times 10^{-2} \quad (\text{A.3a})$$

$$C_{D_{\delta_{elev}}} = -195.1\alpha^2 + 1.435 \times 10^{-1}\alpha\delta_{elev} + 1.818 \times 10^{-5}\delta_{elev}^2 + 1.525\alpha \\ + 4.770 \times 10^{-4}\delta_{elev} - 1.904 \times 10^{-3} \quad (\text{A.3b})$$

$$C_{D_q} = -7.206 \times 10^{-8}V^2q^2 - 7.336 \times 10^{-4}V\alpha q + 4.256 \times 10^{-5}Vq^2 \\ + 2.117 \times 10^{-5}Vq - 2.197 \times 10^{-2}\alpha^2 + 2.166 \times 10^{-1}\alpha q \\ - 6.285 \times 10^{-3}q^2 - 3.023 \times 10^{-3}\alpha - 6.253 \times 10^{-3}q \\ + 2.210 \times 10^{-4} \quad (\text{A.3c})$$

The total drag force coefficient is:

$$C_D = C_{D_\alpha} + C_{D_{\delta_{elev}}} + C_{D_q} \quad (\text{A.4})$$

### A.2.3 Pitching Moment Coefficient, $C_m$

The pitching moment coefficients are presented below:

$$C_{m_\alpha} = -2.199 \times 10^{-1} \alpha^3 + 5.912 \times 10^{-1} \alpha^2 - 1.498 \alpha + 1.516 \times 10^{-1} \quad (\text{A.5a})$$

$$C_{m_{\delta_{elev}}} = 1.263 \alpha \delta_{elev} - 3.294 \times 10^{-2} \delta_{elev} \quad (\text{A.5b})$$

$$C_{m_q} = 9.010 \times 10^{-4} V q - 2.661 \times 10^{-1} q \quad (\text{A.5c})$$

The total pitching moment coefficient is:

$$C_m = C_{m_\alpha} + C_{m_{\delta_{elev}}} + C_{m_q} \quad (\text{A.6})$$

## A.3 Engine Model

The GTM has one engine each on the port and starboard sides of the airframe. Equal thrust settings for both engines are assumed. The thrust from a single engine  $T$  (lbf) is a function of the throttle setting  $\delta_{th}$  (percent).  $T(\delta_{th})$  is a given cubic-order polynomial in NASA's high fidelity GTM simulation model.  $T_x$  (lbf) and  $T_z$  (lbf) denote the projection of the total engine thrust along the body x and body z axes, respectively.  $T_m$  (lbf-ft) denotes the pitching moment due to both engines.  $T_x$ ,  $T_z$  and  $T_m$  are given by:

$$T_x(\delta_{th}) = n_{ENG} T(\delta_{th}) \cos(\epsilon_2) \cos(\epsilon_3) \quad (\text{A.7})$$

$$T_z(\delta_{th}) = n_{ENG} T(\delta_{th}) \sin(\epsilon_2) \cos(\epsilon_3) \quad (\text{A.8})$$

$$T_m(\delta_{th}) = r_z T_x(\delta_{th}) - r_x T_z(\delta_{th}) \quad (\text{A.9})$$

$n_{ENG} = 2$  is the number of engines,  $\epsilon_2 = 0.0375$  rad and  $\epsilon_3 = -0.0294$  rad are angles specifying the rotation from engine axes to the airplane body axes.  $r_x = 0.4498$  ft and  $r_z = 0.2976$  ft specify the thrust moment arm.  $T(\delta_{th})$  is given by the following polynomial expression:

$$T(\delta_{th}) \approx -1.967 \times 10^{-6} \delta_{th}^3 + 1.150 \times 10^{-3} \delta_{th}^2 + 8.258 \times 10^{-2} \delta_{th} + 1.085 \quad (\text{A.10})$$

## A.4 Polynomial Longitudinal Model Formulation

The drag force  $D$  (lbf), lift force  $L$  (lbf), and aerodynamic pitching moment  $M$  (lbf-ft) are given by:

$$D = \bar{q}SC_D(\alpha, \delta_{elev}, \hat{q}) \quad (\text{A.11})$$

$$L = \bar{q}SC_L(\alpha, \delta_{elev}, \hat{q}) \quad (\text{A.12})$$

$$M = \bar{q}S\bar{c}C_m(\alpha, \delta_{elev}, \hat{q}) \quad (\text{A.13})$$

where  $\bar{q} = \frac{1}{2}\rho V^2$ . The longitudinal dynamics of the GTM presented in Equation 3.1 contain the rational term  $\frac{1}{V}$  and the trigonometric terms e.g.,  $\sin(\theta - \alpha)$ ,  $\cos(\theta - \alpha)$ ,  $\cos\alpha$ , and  $\sin\alpha$ . The trigonometric functions are approximated by Taylor series expansions:  $\sin z \approx z - \frac{1}{6}z^3$  and  $\cos z \approx 1 - \frac{1}{2}z^2$  for  $z$  in units of radians. The rational term  $\frac{1}{V}$  is replaced by a linear fit, denoted as  $V_{inv}$ , over the desired range of interest from 100 ft/s to 200 ft/s, provided by Equation 3.10. This approximation is provided below for completeness:

$$\frac{1}{V} \approx V_{inv} = -4.774 \times 10^{-5}V + 0.01409 \quad (\text{A.14})$$

With the approximation, the polynomial longitudinal GTM model is presented:

$$\dot{V} = \frac{1}{m} \left( -D - mg((\theta - \alpha) - \frac{1}{6}(\theta - \alpha)^3) + T_x(1 - \frac{1}{2}\alpha^2) + T_z(\alpha - \frac{1}{6}\alpha^3) \right) \quad (\text{A.15a})$$

$$\dot{\alpha} = \frac{V_{inv}}{m} \left( -L + mg(1 - \frac{1}{2}\alpha^2) - T_x(\alpha - \frac{1}{6}\alpha^3) + T_z(1 - \frac{1}{2}\alpha^2) \right) + q \quad (\text{A.15b})$$

$$\dot{q} = \frac{(M + T_m)}{I_{yy}} \quad (\text{A.15c})$$

$$\dot{\theta} = q \quad (\text{A.15d})$$

# Appendix B

## Polynomial Longitudinal F/A-18 Model

The longitudinal model of the F/A-18 dynamics is presented in this chapter. For a more detailed and full 6-DoF F/A-18 model development, refer to [6]. The longitudinal F/A-18 model is presented below.

### B.1 Physical Parameters of the F/A-18

The F/A-18 aircraft parameters related to the longitudinal direction are provided in Table B.1.

Wing Area, $S$	400 ft <sup>2</sup>
Mean Aerodynamic Chord, $\bar{c}$	11.52 ft
Mass, $m$	1034.5 slugs
Pitch Axis Moment of Inertia, $I_{yy}$	151293 lbf-ft <sup>2</sup>
Air Density, $\rho$	0.001066 slugs/ft <sup>3</sup>
Gravity Constant, $g$	32.17 ft/s <sup>2</sup>

### B.2 Longitudinal Aerodynamic Model

This section provides closed-form polynomial expression for the aerodynamic model of the F/A-18's longitudinal dynamics. The aerodynamics model presented here characterizes the lift force, drag force and pitching moment. Details on the aerodynamic

coefficients can be found in [6] and the references mentioned therein.

### B.2.1 Lift Coefficient, $C_L$

The lift coefficients are presented below:

$$C_{L\alpha} = 1.1645\alpha^3 - 5.4246\alpha^2 + 5.6770\alpha - 2.0400 \times 10^{-2} \quad (\text{B.1a})$$

$$C_{L\delta_{stab}} = 2.1852\alpha^3 - 2.6975\alpha^2 + 0.4055\alpha - 5.7250 \times 10^{-1} \quad (\text{B.1b})$$

The total lift force coefficient is:

$$C_L = C_{L\alpha} + C_{L\delta_{stab}} \cdot \delta_{stab} \quad (\text{B.2})$$

### B.2.2 Drag Coefficient, $C_D$

The drag coefficients are presented below:

$$C_{D\alpha} = 1.4610\alpha^4 - 5.7341\alpha^3 + 6.3971\alpha^2 - 0.1995\alpha + 4.2000 \times 10^{-3} \quad (\text{B.3a})$$

$$C_{D\delta_{stab}} = -3.8578\alpha^3 + 4.2360\alpha^2 - 0.2739\alpha - 3.6600 \times 10^{-2} \quad (\text{B.3b})$$

The total drag force coefficient is:

$$C_D = C_{D\alpha} + C_{D\delta_{stab}} \cdot \delta_{stab} \quad (\text{B.4})$$

### B.2.3 Pitching Moment Coefficient, $C_m$

The pitching moment coefficients are presented below:

$$C_{m\alpha} = -1.2897\alpha^2 + 0.5110\alpha - 8.6600 \times 10^{-2} \quad (\text{B.5a})$$

$$C_{m\delta_{stab}} = 0.9338\alpha^2 - 0.3245\alpha - 9.0510 \times 10^{-1} \quad (\text{B.5b})$$

$$C_{m_q} = 64.7190\alpha^3 - 68.5641\alpha^2 + 10.9921\alpha - 4.1186 \quad (\text{B.5c})$$

The total pitching moment coefficient is:

$$C_m = C_{m\alpha} + C_{m\delta_{stab}} \cdot \delta_{stab} + C_{m_q} \cdot \left( \frac{\bar{c}}{2V} \right) q \quad (\text{B.6})$$

### B.3 Polynomial Longitudinal Model Formulation

The drag force  $D$  (lbf), lift force  $L$  (lbf), and aerodynamic pitching moment  $M$  (lbf-ft) are given by:

$$D = \bar{q}SC_D(\alpha, \delta_{stab}) \quad (\text{B.7})$$

$$L = \bar{q}SC_L(\alpha, \delta_{stab}) \quad (\text{B.8})$$

$$M = \bar{q}S\bar{c}C_m(\alpha, \delta_{stab}, q) \quad (\text{B.9})$$

where  $\bar{q} = \frac{1}{2}\rho V^2$ . Similar to the polynomial GTM formulation, we will approximate the rational term  $\frac{1}{V}$  and the trigonometric terms e.g.,  $\sin(\theta - \alpha)$ ,  $\cos(\theta - \alpha)$ ,  $\cos \alpha$ , and  $\sin \alpha$ .

The rational term  $\frac{1}{V}$  is replaced by a linear fit, denoted as  $V_{inv}$ , over the desired range of interest from 240 ft/s to 300 ft/s, provided by Equation 3.10.

$$\frac{1}{V} \approx V_{inv} = 5.1359 \times 10^{-8}V^2 - 4.1556 \times 10^{-5}V + 1.1180 \times 10^{-2} \quad (\text{B.10})$$

With the approximation, the polynomial longitudinal F/A-18 model is presented:

$$\dot{V} = \frac{1}{m} \left( -D - mg((\theta - \alpha) - \frac{1}{6}(\theta - \alpha)^3) + \frac{T}{m}(1 - \frac{1}{2}\alpha^2) \right) \quad (\text{B.11a})$$

$$\dot{\alpha} = \frac{V_{inv}}{m} \left( -L + mg(1 - \frac{1}{2}\alpha^2) - T(\alpha - \frac{1}{6}\alpha^3) \right) + q \quad (\text{B.11b})$$

$$\dot{q} = \frac{(M + l_t T)}{I_{yy}} \quad (\text{B.11c})$$

$$\dot{\theta} = q \quad (\text{B.11d})$$